

CELLULAR AND SYNAPTIC CORRELATES  
OF LEARNING AND MEMORY AND THEIR IMPAIRMENT  
IN A MOUSE MODEL OF ALZHEIMER'S DISEASE

Dissertation zur Erlangung  
des Doktorgrades (Dr. rer. nat.)  
der Mathematisch-Naturwissenschaftlichen Fakultät  
der Rheinischen Friedrich-Wilhelms Universität Bonn

Vorgelegt von

**Stefanie Poll**

aus Marl

Bonn 2017

Angefertigt mit Genehmigung der Mathematisch-Naturwissenschaftlichen Fakultät der Rheinischen Friedrich-Wilhelms Universität Bonn

1. Gutachter: Prof. Dr. Stefan Remy

2. Gutachter: Prof. Dr. Michael Pankratz

Tag der Promotion: 19.10.2017

Erscheinungsjahr: 2017

# ERKLÄRUNG

Hiermit erkläre ich, dass ich die vorliegende Dissertation selbstständig angefertigt habe. Es wurden nur die in der Arbeit ausdrücklich benannten Quellen und Hilfsmittel benutzt. Wörtlich oder sinngemäß übernommenes Gedankengut habe ich als solches kenntlich gemacht.

---

Ort, Datum

---

Unterschrift

# ZUSAMMENFASSUNG

Die Alzheimer-Krankheit (AD) ist durch synaptische Fehlfunktionen, eine Dysregulation des neuronalen Netzwerkes und darauf folgende Gedächtnisstörungen gekennzeichnet. Der Hippocampus ist für Lern- und Gedächtnisfunktionen unverzichtbar und sehr früh von der charakteristischen Pathologie der Krankheit betroffen. Wie genau die Bildung oder auch das Abrufen von Gedächtnisinhalten gestört wird, wurde noch nicht hinreichend geklärt. Die vorliegende Studie untersuchte die Beteiligung individueller Nervenzellen an der Bildung und dem Abrufen von Erinnerungen und eruiert mögliche Fehlfunktionen in einem präklinischen AD Model. Die Zwei-Photonen Intravitalmikroskopie wurde benutzt um repetitiv die Aktivität individueller Nervenzellen während einer hippocampus-abhängigen Lern- und Gedächtnisaufgabe zu verfolgen. Die untersuchte CA1-Region des Hippocampus wies hierbei zwei unterschiedliche Nervenzellpopulationen auf. Diese unterschieden sich hinsichtlich ihrer stabilen beziehungsweise wechselhaften Einbindung in das aktive Netzwerk. Nervenzellen letzterer Population wurden während des Lernens und Erinnerns in das aktive Netzwerk rekrutiert und somit als Träger der Erinnerung identifiziert, als sogenanntes Engramm. In einem Mausmodell, das Aspekte der Alzheimer-Krankheit repräsentiert (APP/PS1 Mäuse), wies die generelle Aktivität der CA1 Pyramidenzellen sowie das für den Erinnerungsprozess wichtige Engramm keine Abweichungen auf. Jedoch wurden im Erinnerungsnetzwerk der APP/PS1 Tiere zusätzlich aktivierte Nervenzellen identifiziert, die zu einer Überlagerung der Erinnerung und einer damit verbundenen Gedächtnisstörung führten. Durch künstliches Erzeugen dieser überlagernden Aktivität in experimentell gesunden Mäusen konnte ihre Gedächtnisfähigkeit vermindert und die Hypothese der Erinnerungsüberlagerung bestätigt werden. Des Weiteren wurde die Bedeutung von hippocampalen PV-positiven (PV<sup>+</sup>) Interneuronen bei Lern- und Gedächtnisprozessen bewiesen. Eine mögliche Unterfunktion ihrer hemmenden Leistung auf CA1 Pyramidenzellen könnte der vorher beschriebenen Überlagerung zugrunde liegen. Abschließend wurde ein durch Lernen induzierter Verlust von dendritischen Dornenfortsätzen im *Stratum Radiatum* der CA1 Pyramidenzellen gesunder Mäuse untersucht. Diese strukturelle Veränderung stellt einen potentiellen Selektionsmechanismus dar, der nicht in APP/PS1 Tieren nachgewiesen wurde. Zusammenfassend liefert die vorliegende Arbeit wichtige Erkenntnisse bezüglich der Charakteristika eines Engramms und deckt einen neuen Mechanismus der hippocampalen Gedächtnisstörung bei der Alzheimer-Krankheit auf.

## ABSTRACT

Alzheimer's disease (AD) is characterized by synaptic dysfunction and progressive memory loss. The hippocampus is indispensable for memory processes and early affected by disease-associated pathology. It is still debated how in particular encoding and retrieval of memories is impaired in AD. Therefore, the current study investigated how individual neurons in the hippocampus encode a memory and whether this process is disturbed under AD-like conditions in a pre-clinical model. To achieve this goal a cutting-edge technology – two-photon *in vivo* imaging – was used to repetitively analyze the activity of neurons in the hippocampus throughout a hippocampus-dependent memory test. Initially, this study revealed two populations of hippocampal CA1 neurons that differ in their long-term activity: a subset of neurons was continuously active over several days, whereas another population showed variable activity. The latter provided the population that responded to memory encoding as well as retrieval and hence, formed the cellular memory trace, also known as engram. Interestingly, network activity and engram formation under AD-like conditions (APP/PS1 mice) was intact. However, a further analysis of neurons composing the “retrieval network” identified an additional neuronal ensemble in CA1 that superimposed the memory trace suggesting a causal relationship of memory trace superimposition and memory impairment. Indeed, mimicking superimposition by artificial activation of a non-related memory trace coding a different context caused reduced memory performance in healthy mice and thus, presents a potential mechanism for impaired memory retrieval in APP/PS1 mice. Furthermore, parvalbumin-expressing (PV<sup>+</sup>) interneurons in CA1 were indispensable for successful memory encoding and retrieval in healthy mice. Their functional impairment represented a potential explanation of the observed engram superimposition in APP/PS1 mice. Finally, a learning-related loss of synaptic connections was discovered on dendrites of CA1 pyramidal neurons in healthy mice suggesting a mechanism of synaptic selection important for encoding of new information. Learning-induced changes of synaptic connectivity were absent in APP/PS1 mice indicating that synaptic connectivity deficits might be causally related to memory trace superimposition and ultimately memory impairment under AD-like conditions. Summarized, the present study provides a refinement of the engram's characteristics and furthermore, identifies a novel mechanism of memory impairment on the cellular and synaptic level in a mouse model of AD.

# CONTENTS

1. INTRODUCTION .....	1
<b>1.1. Learning &amp; Memory.....</b>	<b>1</b>
1.1.1. Role of the hippocampus.....	1
1.1.2. Structure and function of CA1 .....	2
1.1.3. Neuronal basics of learning & memory .....	4
1.1.4. Functions of inhibitory interneurons.....	5
1.1.5. The engram hypothesis .....	6
1.1.6. Fos as a marker for neuronal activity .....	7
<b>1.2. Alzheimer's disease.....</b>	<b>9</b>
1.2.1. Brief history and mechanisms of AD .....	9
1.2.2. Genetic mutations linked with AD.....	11
1.2.3. Mouse models for studying AD.....	12
1.2.4. Treatment strategies .....	13
<b>1.3. Aim of the study.....</b>	<b>14</b>
2. METHODS .....	15
<b>2.1. Transgenic mice .....</b>	<b>15</b>
<b>2.2. Adeno-associated virus (AAV) injection .....</b>	<b>16</b>
<b>2.3. Cranial hippocampal window .....</b>	<b>16</b>
<b>2.4. Optical fiber implantation .....</b>	<b>18</b>
<b>2.5. Behavioral experiments.....</b>	<b>18</b>
2.5.1. Handling.....	18
2.5.2. Contextual fear conditioning.....	19
2.5.3. Open field test (OFT) .....	20
2.5.4. Behavior analysis .....	20
<b>2.6. Behavior manipulation .....</b>	<b>20</b>
2.6.1. Light stimulation via optical fibers .....	20
2.6.2. Tagging neuronal ensembles.....	21
2.6.3. DREADD activation.....	22
<b>2.7. Immunohistochemistry .....</b>	<b>22</b>
2.7.1. Tissue extraction and preparation.....	22
2.7.2. Immunohistochemical staining.....	22
<b>2.8. Image acquisition.....</b>	<b>23</b>
2.8.1. Animal preparation .....	23
2.8.2. Two-photon <i>in vivo</i> images .....	23
2.8.3. Confocal images .....	24
<b>2.9. Image processing and analysis.....</b>	<b>24</b>
2.9.1. Two-photon data processing .....	24
2.9.2. Confocal data processing.....	26
2.9.3. Statistics .....	27
3. RESULTS.....	28
<b>3.1. FosGFP is a reliable marker of endogenous Fos.....</b>	<b>28</b>
<b>3.2. Presence of amyloid-beta induces neuronal hypoactivity <i>in vivo</i>.....</b>	<b>29</b>
<b>3.3. Two major populations among fosGFP expressing neurons.....</b>	<b>30</b>
<b>3.4. Intact CA1 activity of APP/PS1 mice during learning &amp; memory.....</b>	<b>31</b>
<b>3.5. Reactivated neuronal ensembles occur independent of memory .....</b>	<b>33</b>
<b>3.6. Impurity of the memory trace impairs retrieval performance .....</b>	<b>35</b>
<b>3.7. PV<sup>+</sup> interneurons are crucial for CA1 activity modulation .....</b>	<b>39</b>
<b>3.8. Altered synaptic correlates of learning under AD-like conditions .....</b>	<b>41</b>

4. DISCUSSION .....	44
4.1. Functional and methodological aspects of fosGFP .....	44
4.2. Influence of amyloid- $\beta$ pathology on fosGFP expression .....	45
4.3. CA1 network dynamics .....	46
4.4. FosGFP expression changes during learning and memory .....	48
4.5. Characteristics of the reactivated neuronal ensemble .....	49
4.6. Independence of cellular reactivation and memory performance .....	50
4.7. Analysis of activity patterns .....	51
4.8. The importance of purity for the retrieval network .....	52
4.9. The characteristics and regulation of potential superimposition .....	53
4.10. False mismatch detection in Alzheimer's disease .....	53
4.11. Role of PV <sup>+</sup> interneurons during learning and memory .....	55
4.12. Monitoring structural plasticity of CA1 dendrites .....	56
4.13. Reduced spine density on CA1 pyramidal neuron dendrites .....	56
4.14. Role of spine loss in learning .....	57
5. CONCLUSIONS AND OPEN QUESTIONS .....	59
6. APPENDIX .....	60
6.1. Abbreviations .....	60
6.2. Supplementary data .....	62
6.2.1. Intra-group changes in fosGFP expression .....	62
6.2.2. Relative pattern frequencies .....	63
6.2.3. Cellular and structural data .....	63
6.2.4. Behavioral data .....	64
6.3. List of figures .....	65
6.4. Consumables .....	66
6.4.1. Surgery .....	66
6.4.2. Behavior .....	67
6.5. Reagents .....	67
6.5.1. Anaesthesia and medication .....	67
6.5.2. Adeno-associated viruses (AAVs) .....	67
6.5.3. Immunohistochemistry .....	68
6.6. Equipment .....	69
6.6.1. Microscopes .....	69
6.6.2. Surgery .....	70
6.6.3. Behavior .....	71
6.6.4. Optogenetics .....	71
6.6.5. Miscellaneous .....	72
6.6.6. Software .....	72
6.7. Contributions and remarks .....	73
7. REFERENCES .....	74
DANKSAGUNG .....	85

# 1. INTRODUCTION

Our mind, one of the most difficult things to understand, defines our personality and constitutes who we are. It sets us apart from other creatures, gives us independence, shape and an identity. Hence, suffering from loss of memories that represent a substantial part of our mind and shape our character is one of the most tremendous concerns a human being might face during dementia. And this is what turns Alzheimer's disease (AD) into such a tenuous matter. People are not just suffering from memory loss and the declining ability to orientate themselves in the outside world; they are changing their personality, losing a definition of themselves that took a lifetime to develop. Alzheimer's disease is a global issue with an estimated number of 46.8 million people worldwide, living with dementia (Prince 2015). A rising life expectancy contributes to the higher prevalence of chronic diseases like dementia. Consequently, the incidents of AD are expected to almost double every 20 years (Prince 2015). Hence, basic research, leading to a better understanding of brain function is indispensable to advance our understanding about the disease. This knowledge will ultimately lead to the development of effective treatment strategies against AD and dementia.

## 1.1. Learning & Memory

### 1.1.1. Role of the hippocampus

The question of where memory formation and storage happens, was discovered in 1957, when Scoville and Milner described their patient Henry Gustav Molaison (patient H.M.) that received a bilateral resection of the hippocampal formation and adjacent structures (Scoville and Milner 1957). This work and following research revealed the hippocampus to be responsible for the formation and recent retrieval of spatial as well as non-spatial forms of explicit (declarative) memory (Squire, Stark et al. 2004). Explicit memory comprises knowledge of places, facts and events. In contrast, implicit (non-declarative) memory, for perceptual and motor skills mostly involves the cerebellum, the striatum and the amygdala (Kandel, Dudai et al. 2014). The hippocampal formation is a part of the medial temporal lobe (MTL) and consists of the dentate gyrus (DG), the hippocampus, subiculum, presubiculum, parasubiculum and entorhinal cortex (EC) (Andersen 2007). It has a unique organization and is well conserved among mammals, which allows studies in rodents to be reliable predictors of

the human situation (Andersen 2007). The classical trisynaptic circuit starts at the EC, representing the major cortical input source to the hippocampus with its strongest connections projecting to the DG via the perforant path. The DG granule cells send mossy fibers to CA3, from where the Schaffer Collaterals extend to CA1, the main output region of the hippocampus. CA1 in turn projects back to the deeper layers of the EC, closing the circuit (Knierim 2015) (**Fig. 1.1**). The hippocampus is thought to be indispensable for memory formation, but has a temporally-graded role in storing information (Squire, Stark et al. 2004). Initial labile memories are converted into more stable forms during a process termed consolidation. This happens on a cellular as well as on a systems level, involving both, changes in the connectivity of single cells and brain regions, respectively. Here, cortical regions were found to gain in importance whereas the hippocampus became less relevant for the retrieval of remote memories (Frankland and Bontempi 2005). The structure and function of all hippocampal regions, their excitatory and inhibitory connections and comprising microcircuits were intensively studied in the past decades. Today the hippocampus is known to represent a spatiotemporal framework for the brain (Knierim 2015). It processes, represents and stores high-order information about time and space (Roux and Buzsaki 2015), and provides the indispensable distributor of conscious recollection of declarative memories.

### 1.1.2. Structure and function of CA1

CA1 represents the main output region of the hippocampus and has a unique position within the hippocampal circuitry receiving multimodal inputs that are compartmentalized between the different layers (Spruston 2008). CA3 relays processed information to CA1 basal and proximal apical dendrites via Schaffer collaterals (SCs) (Schaffer 1892). Direct cortical input on CA1 arrives on the distal apical dendrites in *stratum lacunosum moleculare* (S-LM) originating from layer II of the entorhinal cortex (EC) via the perforant path (PP) (Lopes da Silva, Witter et al. 1990) (**Fig. 1.1**). Derived by its multimodal inputs from EC (direct sensory information) and CA3 (mnemonic information), CA1 was ascribed the role of comparing current experiences with expectations, based on past experiences (*i.e.* memory), and assess its outcome (Lisman and Otmakhova 2001, Vinogradova 2001, Bittner, Grienberger et al. 2015). In case of a mismatch between current and past experience, CA1 was described to signal novelty (Knight 1996) characterized by an overall increase of firing and excitability within CA1 pyramidal neurons (Lisman and Otmakhova 2001, Larkin, Lykken et al. 2014).

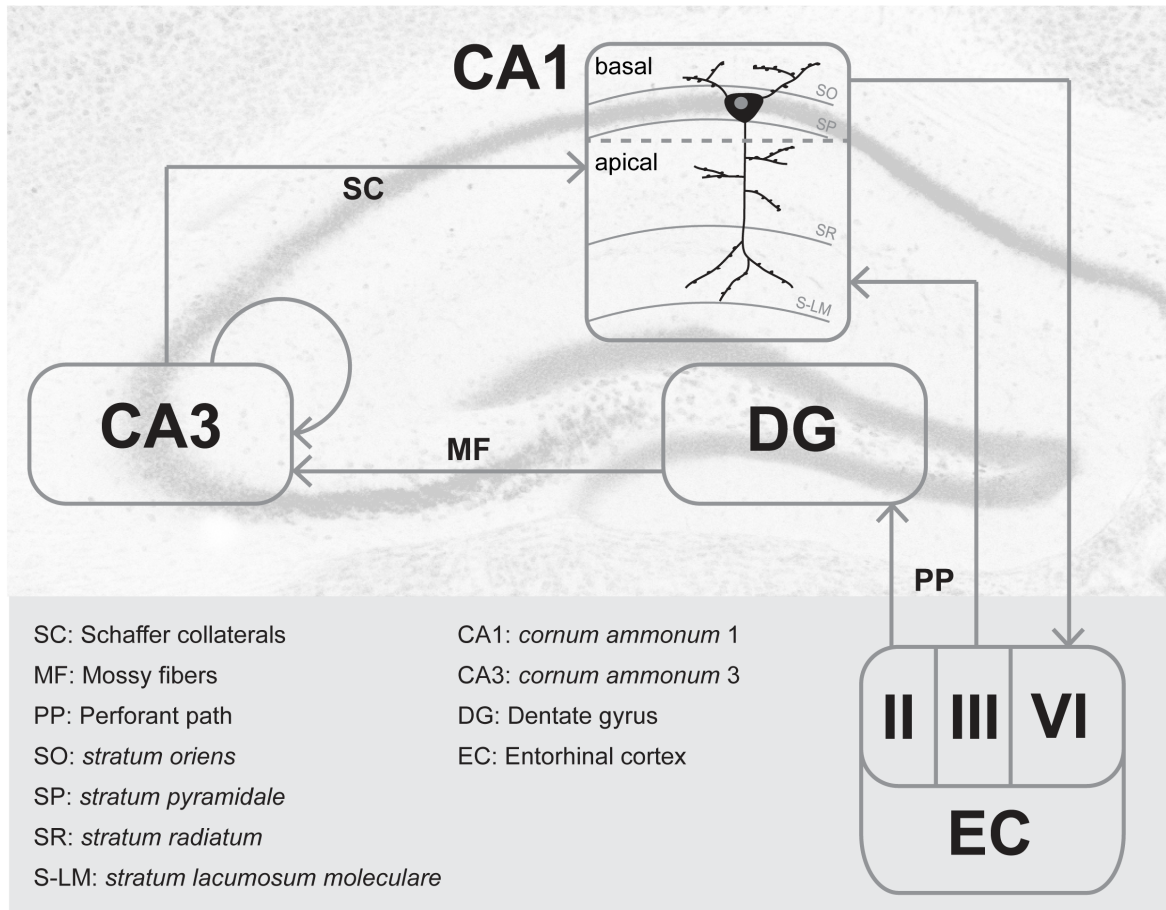


**Figure 1.1 CA1 within the hippocampal circuitry.** The simplified scheme displays the main hippocampal excitatory connections. Cortical input from EC layer II innervates DG via PP fibers. MFs connect DG with CA3 pyramidal neurons, which then either form an internal loop or project to CA1 pyramidal neurons via SCs, targeting basal and proximal apical dendrites, in SO and SR, respectively. CA1 finally relays the information to deeper layers of the EC (layer VI) and closes the loop. CA1 additionally receives direct input from EC layer III via PP fibers targeting the apical tuft in S-LM.

Furthermore, the importance of CA1 during learning and memory processes was extensively studied. Expanding the results of former lesion studies (Maren, Aharonov et al. 1997), precise optogenetic inactivation confirmed the necessity of CA1 for both, acquisition and retrieval of recent and remote memories, respectively (Goshen, Brodsky et al. 2011). Nevertheless, the brain was able to compensate for CA1 inactivation during retrieval if enough time was given (Goshen, Brodsky et al. 2011). Additionally, CA1 features the coding of spatial information. A subset of pyramidal neurons, so-called place cells, was shown to fire at specific spatial locations (O'Keefe 1971). The specificity of their firing was found to change over time, but increase in association with learning processes (Kentros, Hargreaves et al. 1998, Nakazawa, McHugh et al. 2004).

### 1.1.3. Neuronal basics of learning & memory

Learning is the acquisition, memory the retention of information or knowledge (Bear 2007). These abilities enable all kinds of creatures that exhibit a nervous system, to adapt to their environment. The fundamental principle that forms the basis for learning and the storage of information is plasticity (Kandel, Dudai et al. 2014). The idea that memory is the change in strength of synaptic connections – the cellular connectionist approach - was born by Ramon y Cajal in 1894 (Cajal 1894) and was later named synaptic plasticity (Konorski 1948). Learning can be examined in the brain at different levels that are mostly pre-defined by the applied techniques: from analysis on the macroscale that focuses on the involvement of different brain regions, across mesoscale analysis that deals with connections between different neurons, to the point of microscale examinations that analyze changes of single synapses (Ganguly and Poo 2013). Early research in invertebrates gave rise to the elementary building blocks of learning and memory, that were later revealed also in vertebrates, from rodents to the point of humans (Kandel, Dudai et al. 2014). One of those building blocks is the discovery of long-term potentiation (LTP), a process that enhances the efficacy of synaptic connections in the hippocampus due to stimulation of the perforant path to the DG (Bliss and Lomo 1973). A concept that was born by Donald O. Hebb in 1949 and that explained the link of two neurons as a consequence of their parallel firing (Hebb 1949). This “Hebbian” LTP was later also found in CA3 to CA1 synapses (Mayford, Siegelbaum et al. 2012), whereas in mossy fiber synapses a non-Hebbian form of LTP was demonstrated that just required presynaptic activity. LTP has a brain shaping function as it was shown to influence the size of dendritic spines (Matsuzaki, Honkura et al. 2004), small protrusions of the dendritic shaft that carry excitatory synapses (Rocheffort and Konnerth 2012). Polymerization of the spines’ internal actin cytoskeleton, that defines their shape, is closely linked to LTP (Honkura, Matsuzaki et al. 2008) and synaptic efficacy (Cingolani and Goda 2008). The counterpart of LTP and another building block of learning and memory is long-term depression (LTD), a process that decreases synaptic efficacy (Ito 2001). The combination of LTP and LTD provides an efficient way to specifically strengthen and weaken synaptic connections to tag memory relevant neuronal connections and hence, to store memories. The *in vivo* relevance of both mechanisms regarding memory processes was demonstrated by inhibiting and inducing learned behaviors, with LTD and LTP, respectively (Nabavi, Fox et al. 2014). Memories have to be divided in at least two different forms regarding their age: short-term memory is believed to rely on changes

in strength of existing synapses, whereas long-term memory storage is thought to involve structural changes and thus, the loss or gain of synaptic connections, termed structural plasticity (Bailey and Kandel 1993). Differences in the nature of a memory are predetermined by the kinetics of underlying molecular changes, whose structural influence dictates the information flow that finally triggers an behaviorally relevant output (Mayford, Siegelbaum et al. 2012).

#### 1.1.4. Functions of inhibitory interneurons

The activity of excitatory principal neurons is driven by excitatory input and is precisely modulated by inhibitory interneurons (Basu, Srinivas et al. 2013). At least two major types of inhibition can be distinguished: feed-forward and feed-back inhibition (Buzsaki 1984). The former describes external excitatory input on interneurons that in turn inhibit local principal cells that might additionally receive the external excitatory input. Feed-back inhibition describes the excitation of interneurons that in turn inhibit the source of excitation. These and related forms of inhibition are principles that do not correspond to specific interneuron types and are furthermore, not mutually exclusive (Roux and Buzsaki 2015). Interneurons can be distinguished by their specific target on the principal cell, ranging from somata (basket cells), over axon initial segments (chandelier or axo-axonic cells) to dendrites (Roux and Buzsaki 2015). In CA1 a subclass of dendrite-targeting interneurons was shown to be involved in the compartmentalization of inputs to CA1 during contextual fear conditioning (Lovett-Barron, Kaifosh et al. 2014). Both contextual information and aversive stimulus evoked inputs reach the hippocampus at the distal dendrites of CA1 pyramidal neurons. Somatostatin (SOM)-positive interneurons inhibit the simultaneously arriving aversive information during cFC and thus, allow the processing of contextual information by the hippocampus. Inhibition of SOM-positive interneurons during learning impaired memory retrieval, demonstrating the indispensability of this interneuron type. Structural plasticity of inhibitory interneurons plays a major role during learning and memory processes, as its impairment on SOM-positive interneurons was associated with memory deficits in a mouse model of Alzheimer's disease (Schmid, Mittag et al. 2016). Furthermore, increased feed-forward inhibitory connectivity at DG to CA3 synapses was shown to regulate memory precision (Ruediger, Vittori et al. 2011). Another class of interneurons, i.e. parvalbumin (PV)-expressing (PV<sup>+</sup>) soma-targeting neurons, was shown to be differentially modulated by learning, dependent on the type of the learning task (Donato, Rompani et al. 2013). The increase in feed-forward inhibition was revealed to

correlate with learning and hence, suggested to be a general mechanism of learning in hippocampal and cerebellar circuits (Caroni 2015).

### 1.1.5. The engram hypothesis

More than 100 years ago, the German scientist Richard Semon introduced his idea that experience leaves a footprint in the brain, a physical substrate of memory, called “the engram”, which later can be recalled from a dormant state to a state of manifested activity, a process called “ecphory” (Semon 1921). The idea was picked up and experimentally corroborated by Lashley. He focused his research on finding the location of the memory trace in specific brain areas (Josselyn, Köhler et al. 2015). Although most experimental approaches attempted to find memory traces in one particular region, it was self-evident that the trace manifests in various interconnected brain regions, dependent on the type of memory. The learning-dependent changes were analyzed in different dimensions, from micro- to macro-scale. The micro-scale readout described changes on the synaptic level, including structural and functional properties of synapses. These changes directly determine the strength of connections between neurons and thus, their participation in storing information on the macro-scale. It is assumed that learning involves in part the same neuronal population that participates in retrieving the memory (Schacter, Curran et al. 1999, Frankland and Bontempi 2005). However, there is an ongoing debate concerning the size of the reactivated neuronal ensemble (Josselyn, Köhler et al. 2015). Further research aimed at identifying the underlying molecular processes of memory formation and revealed that neurons are recruited to encode a memory based on their excitability immediately before training (Yiu, Mercaldo et al. 2014). In addition, it is important to mention that the idea of an engram indeed refers to a static memory trace. However, early ideas hypothesized and recent research revealed the dynamics of a memory trace (Nadel 2007). Retrieval can thus lead to an update of stored memories by a process named reconsolidation (Rodriguez-Ortiz and Bermudez-Rattoni 2007). Evolving technologies, e.g. the use of activity-dependent promoters, cre/loxP-expression systems, optogenetics and pharmacogenetics, together with accumulating knowledge allowed to label and to manipulate neuronal subsets, being part of a memory. Thus, it was shown for hippocampal CA1 and several other brain regions that artificially activating or inactivating neurons that participated in learning was sufficient for behaviorally retrieving or repressing a memory (Goshen, Brodsky et al. 2011, Garner, Rowland et al. 2012, Ramirez, Liu et al. 2013, Cowansage, Shuman et al. 2014, Kim, Kwon et al. 2014). Although the term “engram” was born 100 years ago, it

survived and was adapted to the current knowledge about experience-dependent changes in the nervous system on different scales. It comprises functionally interconnected groups of neurons, whose activity manage to implement a corresponding behavioral output (Holtmaat and Caroni 2016).

### 1.1.6. Fos as a marker for neuronal activity

Many different approaches exist to examine the activity of neurons that mainly differ in the number of captured neurons and temporal resolution. In addition to classical electrophysiological methods to record neuronal activity, the development of optical methods in combination with genetically encoded calcium indicators (GECIs) generated more and more interest, as it allowed the analysis of large neuronal populations with a high spatial and temporal resolution on the millisecond to second time-scale. In parallel, approaches like the expression of immediate early genes (IEGs) were refined that integrate neuronal activity over minutes and hours. After neuronal activity IEGs are the first fast and transiently transcribed genes. They connect incoming external signals to intracellular signaling cascades and are important regulators of gene expression (Sheng and Greenberg 1990). IEGs can be functionally categorized into two classes: IEGs that code for regulatory transcription factors (e.g. *c-fos*, *c-jun* and *zif268*) that effect the transcription of other genes, and effector IEGs (e.g. *Arc*, *Homer 1*) that directly influence cellular function (Lanahan and Worley 1998, Kubik, Miyashita et al. 2007). Due to their fast and activity-dependent expression they have been used as a marker for recent neuronal activity since 1988. Here, Sagar et al. first described an immunohistochemical approach for labeling Fos (FBJ osteosarcoma oncogene) protein and thereby enabling the post-mortem analysis of neuronal subsets that had been recently activated (Sagar, Sharp et al. 1988). Since then *c-fos* mRNA and Fos protein have been applied in many studies as approximation for neuronal activation (Curran 1991). Later, Guzowski et al. advanced the IEG research field with establishing a method called cellular compartment analysis of temporal activity by fluorescence *in situ* hybridization (catFISH) (Guzowski, McNaughton et al. 1999). Here, the time-dependent localization of *Arc* mRNA allowed for repeated observation of the same neuronal ensembles within the same subject responding to two separate events. This conventional post-mortem IEG analysis is a reliable indicator of recent activity. However, IEG analysis just allows the measurement of events separated by minutes to hours (Kubik, Miyashita et al. 2007). This characteristic excludes the analysis of long-term memory storage in the same neuronal ensembles. The usage of IEG promoters for

driving various expression systems that allow for experience-dependent tagging revolutionized the field and enabled the analysis and manipulation of neuronal populations participating in learning and memory. The development of IEG-reporter mouse models (Reijmers, Perkins et al. 2007, Eguchi and Yamaguchi 2009, Tayler, Lowry et al. 2011) and the parallel progress in *in vivo* imaging approaches that allowed for deep tissue penetration (Helmchen and Denk 2005, Svoboda and Yasuda 2006) opened further possibilities to monitor neuronal ensembles of recently active neurons, repetitively for periods of weeks or even months (Schoenenberger, Gerosa et al. 2009, Cruz, Koya et al. 2013, Tayler, Tanaka et al. 2013, Jouhanneau, Ferrarese et al. 2014). In 2004, the fosGFP mouse model utilized in the present study was developed. The mouse expresses the enhanced green fluorescent protein (eGFP) under the *c-fos* promoter and hence, allows for visualization of recent neuronal activity (Barth, Gerkin et al. 2004). The expressed transgene generates a fosGFP fusion protein preserving the biological function of Fos (Barth, Gerkin et al. 2004). It was shown to be involved in the induction of LTP at CA1-CA3 synapses and necessary for spatial and associative learning tasks (Fleischmann, Hvalby et al. 2003), as well as memory consolidation (Guzowski and McGaugh 1997). Endogenous *c-fos* expression is triggered by activity-mediated influx of  $\text{Ca}^{2+}$  through voltage-gated calcium channels (Morgan and Curran 1986) that subsequently activates the extracellular signal-regulated kinase (ERK)/mitogen-activated protein kinase (MAPK)-dependent phosphorylation of transcription factors, which in turn bind to the *c-fos* promoter (Cohen and Greenberg 2008) (**Fig. 1.2**). Hence, the resulting *c-fos* expression is a summation of  $\text{Ca}^{2+}$  events inside a neuron.

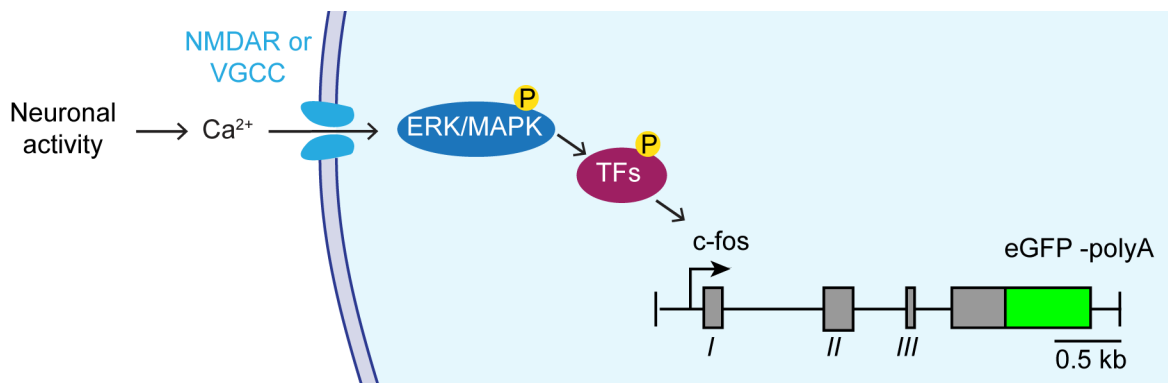


**Figure 1.2 Activation of the *c-fos* promoter in fosGFP mice.** Neuronal activity leads to the opening of N-methyl-D-aspartate (NMDA) receptors and voltage-gated calcium channels (VGCCs) that allow the influx of calcium ( $\text{Ca}^{2+}$ ) into the intracellular space (light blue). Increasing calcium levels trigger the phosphorylation of extracellular signal-regulated kinase (ERK)/mitogen-activated protein kinase (MAPK) that subsequently phosphorylates transcription factors (TFs) that then start expression of *c-fos* and a fused enhanced green fluorescent protein (eGFP). Modified according to Box2 in (Cruz, Koya et al. 2013).

It was hypothesized that only strong and consistent activity in a certain time frame elicits expression (Cruz, Koya et al. 2013). Indeed, electrophysiological characterization of fosGFP expressing neurons in layer 2/3 of the primary sensory cortex possessed a higher firing rate than fosGFP-negative neurons (Yassin, Benedetti et al. 2010).

## 1.2. Alzheimer's disease

### 1.2.1. Brief history and mechanisms of AD

In 1906, when the German physician Alois Alzheimer first described a “peculiar” disease with abnormal deposits in and around neurons and a profound shrinkage of the brain structure, he was a pioneer in bridging microscopic methods and clinical interest in patients to gain causal links between pathology and clinical symptoms (Hippius and Neundorfer 2003). Emil Kraepelin first named this disease after his colleague in 1910 (Hippius and Neundorfer 2003). It took almost another seventy years before Alzheimer's disease was recognized as the most common form of dementia by the neurologist Robert Katzman in 1976 (Katzman 1976) and even eight years more until the first hallmark of AD, amyloid- $\beta$  ( $A\beta$ ), was identified by George Glenner and Cai'ne Wong in 1984 (Glenner and Wong 1984). In 1986, just two years later the second hallmark, neurofibrillary tangles (NFTs), was described to largely consist of the microtubule-associated hyperphosphorylated protein tau (Grundke-Iqbal, Iqbal et al. 1986). Since then, research accelerated. Today, it is known that  $A\beta$  derives from a larger protein, consequentially named amyloid precursor protein (APP) and that multiple  $A\beta$  species can arise depending on the participating cleavage enzyme (Weidemann, Konig et al. 1989). The proteolytic cleavage of APP is occurring in two different ways: the non-amyloidogenic pathway is initiated by the  $\alpha$ -secretase and leads to several soluble protein fragments (Van Dam and De Deyn 2006). The amyloidogenic pathway describes the cleavage by  $\beta$ -site APP cleaving enzyme 1 (BACE-1), also named  $\beta$ -secretase that produces a soluble N-terminal fragment and an amyloidogenic C-terminal fragment (Vassar, Bennett et al. 1999). The latter is further processed by the  $\gamma$ -secretase complex, containing presenilin-1 (PSEN1), leading to an intracellular APP domain (LaFerla, Green et al. 2007) and soluble  $A\beta$ -monomers (Van Dam and De Deyn 2006) (**Fig. 1.3**). Here, several variants differing in their self-aggregating potential arise, namely  $A\beta_{42}$ ,  $A\beta_{40}$  and  $A\beta_{38}$ , whereas the former is more prone to aggregate *in vitro* and *in vivo* (Jarrett, Berger et al. 1993, Haass and Selkoe 2007) and represents the

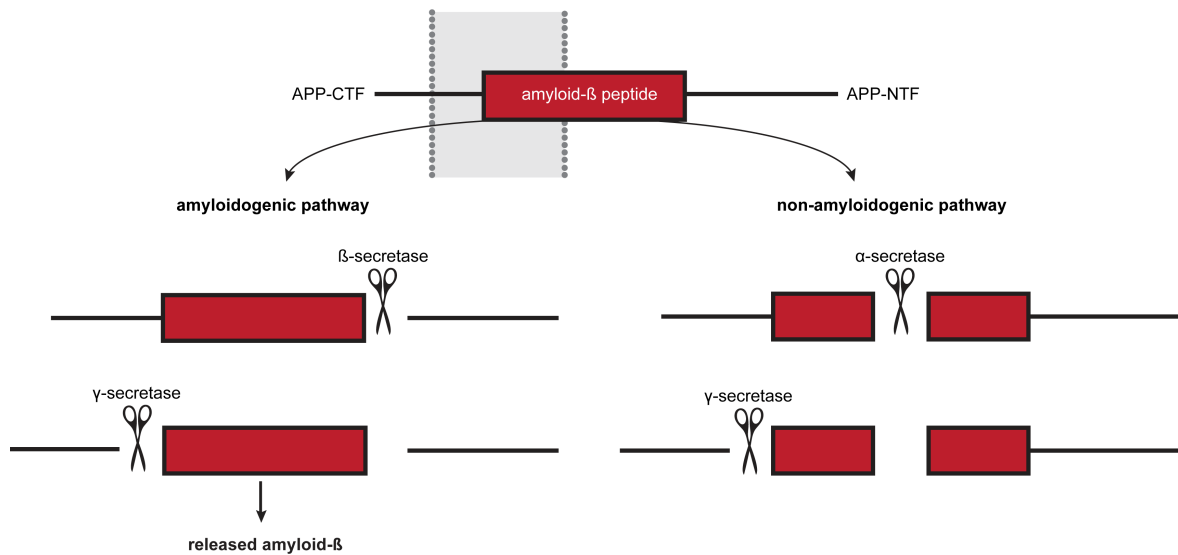


**Figure 1.3 Processing of APP.** The amyloid precursor protein (APP) is a membrane bound protein and can be processed via the non-amyloidogenic and the amyloidogenic pathway, resulting in soluble or insoluble species of APP fragments, respectively.  $\alpha$ -,  $\beta$ - and  $\gamma$ -secretases cleave APP at different target sites resulting in fragments with distinct aggregation properties. The toxic species that is related to AD is generated by  $\beta$ - and  $\gamma$ -secretase cleavage, resulting in amyloid- $\beta$ . APP-CTF, APP C-terminal fragment; APP-NFT, APP N-terminal fragment. Modified according to Figure 1 in (LaFerla, Green et al. 2007).

major variant that was found in the brains of AD patients (Iwatsubo, Odaka et al. 1994).  $A\beta$ -monomers alone do not define the pathology, as it is also found in the cerebrospinal fluid of non-diseased human individuals (Shull, Heintz et al. 1991, Seubert, Vigo-Pelfrey et al. 1992). In AD, the production of the highly amyloidogenic form of  $A\beta$ , *i.e.*  $A\beta_{42}$ , lead to its aggregation into oligomers that causes synaptic dysfunction (Haass and Selkoe 2007), and to the formation of long, insoluble fibrils that constitute the “spherical microscopic deposits”, known as  $A\beta$  plaques (Haass and Selkoe 2007). Oligomeric  $A\beta$  species isolated from post-mortem brain tissue of AD patients were found to correlate with memory loss (Gong, Chang et al. 2003). Their toxicity becomes manifested in causing calcium dyshomeostasis (LaFerla 2002), inhibiting the induction (Shankar, Li et al. 2008) and affecting the maintenance of hippocampal LTP (Walsh, Klyubin et al. 2002) and lowering the threshold for LTD (Shankar, Li et al. 2008). Furthermore,  $A\beta$ -oligomers were demonstrated to reduce N-methyl-D-aspartate (NMDA) receptor-evoked currents and therefore cause synaptic failure (Selkoe 2002, Snyder, Nong et al. 2005). This and further molecular and functional implications lead to synaptic dysfunction, shrinkage and loss (Koffie, Hashimoto et al. 2012). The increasing collapse of synapses results in neuronal network dysfunction that furthermore accounts for cognitive decline (Verret, Mann et al. 2012). In human AD patients, an  $A\beta$ -mediated reduction in neuronal activity was shown, as their cortical and hippocampal brain

regions appeared hypometabolic in a positron emission tomography (PET) (Johnson, Fox et al. 2012). However, clinical observations detected also a high incidence of epileptic seizures in AD patients (Palop and Mucke 2009), hinting rather at hyper- than hypoactivity. This was further demonstrated by observing individual hyperactive neurons in the direct vicinity ( $< 60 \mu\text{m}$ ) of A $\beta$  plaques in the cortex (Busche, Eichhoff et al. 2008) and hippocampus (Busche, Chen et al. 2012) of transgenic AD mice *in vivo*. The second hallmark of AD, intracellular NFTs, are consistently found in the brains of AD patients (Braak and Braak 1991). Aberrant phosphorylation of the microtubule-associated protein (MAP) tau lead to its aggregation into paired helical fragments, to then form NFTs (Buee, Bussiere et al. 2000). The aggregation prevents tau to follow its biological functions in guaranteeing axonal transport by stabilizing microtubules and hence contributes to synaptic dysfunction and neuronal death (Roy, Zhang et al. 2005). Synapse loss and concomitant neuroinflammation are events that precede the formation of NFTs and are mainly caused by a loss-of-function due tau hyperphosphorylation (Ballatore, Lee et al. 2007). There is an ongoing debate whether and how A $\beta$  and tau abnormalities are linked and which presents the origin of disease (Small and Duff 2008). However, both pathologies are found in the brains of AD patients postmortem and together led to profound neuronal loss that is causing inflammation, brain shrinkage and associated symptoms (Small and Duff 2008).

### 1.2.2. Genetic mutations linked with AD

Mutations in the genes coding for human APP (Goate, Chartier-Harlin et al. 1991), PSEN1 or presenilin 2 (PSEN2), an homologue of PSEN1, are linked to autosomal-dominant early-onset AD (EOAD) and cause an increase in A $\beta$  through favoring the amyloidogenic processing of APP (Palop and Mucke 2010). Mutations within the A $\beta$  domain of the APP coding gene even lead to enhanced oligomerization (Haass 2004). EOAD accounts for about 1% of AD cases (Hardy 1997, Van Cauwenberghe, Van Broeckhoven et al. 2016), whereas late-onset AD (LOAD) starting at an age of 65 years and older represents the most common form (Small and Duff 2008). Here, a variant of the apolipoprotein E (APOE) named APOE  $\epsilon 4$  is known to increase the risk of developing LOAD (Corder, Saunders et al. 1993). Both forms of AD are usually indistinguishable in their clinical and histopathological phenotype, with the biggest difference being the age of onset (Selkoe 2002). Genome-wide association studies (GWAS) and massive parallel resequencing (MPR) approaches identified around 20

additional loci in the human genome that increase the risk for developing AD (Van Cauwenberghe, Van Broeckhoven et al. 2016). The location of these genes gave rise to the involvement of lipid metabolism, inflammatory responses and endosomal vesicle trafficking and hence, shed light on the genetic complexity of the disease (Van Cauwenberghe, Van Broeckhoven et al. 2016). The multifactorial nature of AD impedes the development of effective disease-modifying treatments. However, genetic profiling is a powerful tool for prediction and prevention of this devastating disease (Van Cauwenberghe, Van Broeckhoven et al. 2016).

### 1.2.3. Mouse models for studying AD

Today it is known that the disease is a complex interplay of A $\beta$  and tau pathologies, that themselves interact with many other molecules and signaling cascades leading to a broad influence on the neuronal network (Mucke 2009). Most existing mouse models do not mimic the complete facets of the complex disease. However, important aspects have been successfully recapitulated and helped already to develop treatment strategies and support preclinical trials (LaFerla and Green 2012). For this purpose, several isomorphic disease models that concentrate on the involvement of selected pathologies on the development and progression of AD, have been developed. Before the first transgenic mouse was developed in 1991, AD was and still is mimicked by infusing A $\beta$  peptides of various length into the brain tissue of mice (Harkany, O'Mahony et al. 1998, Yamada, Chiba et al. 2005, Van Dam and De Deyn 2006). Transgenic mouse models of amyloidosis as PDAPP (Games, Adams et al. 1995), Tg2576 (Hsiao, Chapman et al. 1996) and APP23 (Sturchler-Pierrat, Abramowski et al. 1997) express APP carrying different identified mutations and utilizing diverse promoters. In 2004 Jankowsky et al. developed a transgenic mouse with humanized mouse APP carrying the Swedish mutation (K670N, M671L) (Mullan, Crawford et al. 1992) and a mutant PS1 that both led to an increase in A $\beta$ <sub>42</sub> levels, characteristic for the brains of AD patients (Jankowsky, Fadale et al. 2004). Later, transgenic mice that additionally exhibit tauopathies were developed. These exhibit increased amyloid deposits, formation of NFTs and an overt loss of neurons (Gotz, Schild et al. 2004). Today, several mouse models vary in their validity that is defined by the degree the animal resembles the human condition in aetiology, pathophysiology and symptomatology and legitimate their importance for pre-clinical drug trials (Van Dam and De Deyn 2006). However, most animal models focus on single aspects of the disease (Van Dam and De Deyn 2006). This requires careful attention to prevent

neglecting other pathological features. In fact, a simplification of complexity is rather helpful for basic research that aims at understanding the involvement of each identified pathological feature during onset and disease progression (Palop, Chin et al. 2006, Radde, Duma et al. 2008).

#### 1.2.4. Treatment strategies

The need to tackle Alzheimer's disease with disease-modifying treatments will become stronger with our aging society. Current treatment strategies target either the cholinergic or the glutamatergic metabolism, since both are largely compromised by the disease (Cummings 2004). Cholinesterase inhibitors enhance neurotransmission by inhibiting the neurotransmitter degrading enzyme acetylcholinesterase (AChE). NMDAR antagonists reduce cell death by preventing excessive glutamate release. However, these approaches just improve symptoms, in a transient and moderate fashion (Huang and Mucke 2012). The genetic identification of mutations in APP (Goate, Chartier-Harlin et al. 1991), PSEN1 and PSEN2 (Sherrington, Rogaev et al. 1995), led to an A $\beta$  centric view of estimating the origin of the disease. The amyloid hypothesis describes A $\beta$  as main driver of pathology, causing tau hyperphosphorylation and further disease associated phenotypes, like calcium dyshomeostasis (LaFerla 2002) and synaptic dysfunction. Hence, treatment strategies focused on either decreasing A $\beta$  production, reducing its aggregation or increasing A $\beta$  clearance. Promising strategies represent the inhibition and modulation of APP processing enzymes, i.e.  $\beta$ - and  $\gamma$ -secretase (De Strooper, Vassar et al. 2010) that aim at reducing the amyloidogenic processing of APP. However, prevailing challenges are the reduction of side effects by enhancing the specificity of inhibitors to APP processing secretases and overcoming the blood brain barrier (BBB) (Huang and Mucke 2012). Unfortunately, phase III trials with secretase blockers failed due to worsening of cognitive impairments (Schor 2011) or inefficiency (Huang and Mucke 2012). A $\beta$  clearing was targeted via active or passive immunization using A $\beta$ -peptides or anti-A $\beta$ 42 antibodies, respectively (Wisniewski and Konietzko 2008). Immunopathological side effects stopped the active immunization approach (Gilman, Koller et al. 2005), however, passive immunization approaches reached phase III and are still ongoing. Furthermore, drugs targeting the second hallmark of AD, i.e. neurofibrillary tangles (NFTs), were developed. As NFTs are composed of the microtubule-stabilizing protein tau, treatment approaches aim at reducing tau levels, its aggregation or phosphorylation. Additionally, microtubule-stabilizing

drugs have been a valuable tool to prevent axonal transport impairments and the concomitant neuronal loss (Trojanowski, Smith et al. 2005). Besides challenges regarding BBB penetration and drug specificity, an underestimated matter is the composition of the phase III treated group of humans. Most of the patients enrolled in these trials already exceeded the pre-symptomatic stage. Hence, their treatment will not be suited to assess the ameliorating properties of treatments aiming at preventing AD in the pre-symptomatic stage (Huang and Mucke 2012). The complexity of the disease with its tight enmeshment with the general health status of human individuals (Huang and Mucke 2012) suggests a combined therapy as potential solution (Huang and Mucke 2012). Although more than ten approaches failed in phase III, careful optimism can be spread, as a lot more potential drugs entered clinical trials.

### 1.3. Aim of the study

Basic research is indispensable to further shed light on mechanisms underlying Alzheimer's disease (AD) and hence, to provide targets for the development of efficient treatment strategies. The hippocampus is one of the first regions affected by the disease and indispensable for learning and memory processes that are considerably affected in AD. The current study has two main goals: First, finding cellular and synaptic correlates of learning and memory that manifest in the hippocampus. Second, identifying alterations induced by pathology in a preclinical model of Alzheimer's disease (APP/PS1 mice). On the cellular level, the CA1 neuronal population participating in learning and retrieval will be examined, to define the size and characteristics of the memory encoding neurons – the so-called engram. It is known that neuronal firing is strictly regulated by inhibitory neurons. Therefore, the importance of PV<sup>+</sup> interneurons for learning and memory will be assessed. Moreover, structural changes of excitatory neurons on the level of dendritic spines that potentially relate to memory will be investigated. To tackle these questions, the current study will utilize two-photon *in vivo* imaging to repetitively monitor the same neuronal populations and will furthermore apply neuronal cell type-specific manipulation methods in healthy and APP/PS1 mice, respectively. Based on the cellular and structural findings in healthy mice, this study aims at elucidating whether the memory impairment in APP/PS1 mice is due to altered memory formation or a deficiency in retrieval.

## 2. METHODS

### 2.1. Transgenic mice

B6.Cg-Tg(Fos/EGFP)1-3Brth/J mice (Barth, Gerkin et al. 2004) (Stock number: 014135, The Jackson Laboratory) carry a fusion transgene consisting of the murine FBJ (Finkel-Biskis-Jinkins) osteosarcoma oncogene (*Fos*) and enhanced green fluorescent protein (*eGFP*). The *eGFP* was fused to the c-terminus of the *Fos* gene, leaving the function of Fos intact. Throughout the text mice will be referred to as fosGFP mice. B6.Cg-Tg(APP<sup>swe</sup>,PSEN1<sup>dE9</sup>)85Dbo/Mmjax (APP/PS1) double transgenic mice (Jankowsky, Fadale et al. 2004) (MMRRC Stock No: 34832-JAX) express a chimeric human/mouse amyloid precursor protein (Mo/HuAPP695<sup>swe</sup>) under the mouse prion protein promoter and a mutant PS1 with a deletion of exon 9 (PS1-dE9). Both, the Swedish mutation in APP and the PS1 mutant led to increased A $\beta$ <sub>42</sub> levels. Mice were crossbred with fosGFP mice. Offspring carrying both transgenes will be referred to as APP/PS1 mice, whereas mice just carrying the fosGFP transgene will be named wild-type mice throughout the text. Furthermore, APP/PS1 mice will additionally be referred to as mouse model of Alzheimer's disease (AD), aware of the fact that it mimics not every aspect of the disease. Experiments were carried out at an age of 13-18 months. Slc17a6<sup>tm2(cre)Lowl</sup>/J (Vglut2-ires-cre) mice (Stock number: 016963, The Jacksons Laboratory) were on a 129S4 background and 6-8 months of age. C57BL/6J mice (Stock number: 000664, The Jacksons Laboratory) were four month of age. B6.129P2-*Pvalb*<sup>tm1(cre)Arbr</sup>/J mice (Stock number: 008069, The Jacksons Laboratory) express Cre recombinase in parvalbumin-expressing (PV<sup>+</sup>) interneurons, without disrupting endogenous PV expression (Hippenmeyer, Vrieseling et al. 2005). Mice were backcrossed to C57BL/6J background and referred to as PV-Cre mice throughout the text. Experiments were carried out at an age of 19-21 months. B6.Cg-Tg(Thy1-YFP)HJrs/J (YFP-H) mice (Stock number: 003782) were crossbred with APP/PS1 mice. Offspring carrying both transgenes will be referred to as APP/PS1 mice, whereas mice just carrying the YFP-H transgene will be named wild-type mice throughout the text. All animals were housed with a 12/12 light/dark cycle under specific pathogen-free (SPF) conditions in individually ventilated cages (IVCs), either alone or in groups of 2 to 5 mice, separated by gender. Temperature and relative humidity were kept constant (22°C, 40 % RH). Food and water was available ad libitum.

## 2.2. Adeno-associated virus (AAV) injection

Mice were anesthetized with an intraperitoneal (i.p.) injection of ketamine (0.13 mg/g bodyweight, Ketavet®) and xylazine (0.01 mg/g bodyweight, Rompun®). The head was wiped with 70% ethanol using sterile collection swabs (EUROTUBO®) before a small incision was made right above the midline ranging approximately from bregma to lambda. The periosteum was carefully pushed aside and coordinates of interest were marked. For optogenetic manipulation of CA1 neurons the virus was delivered to the hippocampus without damaging the pyramidal layer (AP: -1.9 mm, ML:  $\pm 1.5$  mm, DV: -1.0 mm (from brain surface)). For pharmacogenetic experiments the focus was set at achieving a broad, but exclusive infection of CA1 neurons (AP: -1.85 mm, ML:  $\pm 1.5$  mm, DV: -1.10 mm (from brain surface)). The holes were drilled and the dura mater was incised. Then the tip of the needle was slowly lowered to the depth of interest and the appropriate volume of AAV (AAV1-EF1a-DIO-eNpHR-eYFP-WPRE-hGH and AAV2-FLEX-tdTomato, 1  $\mu$ l/hemisphere; AAV2-hSyn-DIO-hM3D(Gq)-mCherry, 0.5  $\mu$ l/hemisphere; AAV2/1-Fos-tTA + AAV2/1-PTRE-tight-hM3D(Gq)-mCherry (1:2), 0.5  $\mu$ l/hemisphere) was injected with a speed of 100 nl/minute. After injection the needle was left in place for another 5 minutes to let the virus diffuse into the tissue. This procedure was repeated at the contralateral injection side. Finally, the wound was properly stitched and disinfected with povidon-iodine (Betaisodona®). During the next three days mice were monitored and received a post-surgery treatment with buprenorphine (Temgesic®). Mice were allowed to recover from surgery for at least two weeks.

## 2.3. Cranial hippocampal window

Mice were deeply anesthetized with an intraperitoneal (i.p.) injection of ketamine (0.13 mg/g bodyweight, Ketavet®) and xylazine (0.01 mg/g bodyweight, Rompun®). Additionally, an analgesic (0.05 mg/kg bodyweight, buprenorphine, Temgesic®), an antibiotic (0.25 mg/g bodyweight, cefotaxim) and an immunosuppressant drug (0.2  $\mu$ g/g bodyweight, Dexamethasone 21-phosphate disodium salt) were applied subcutaneously (s.c.) before surgery. Eyes were covered with eye ointment (Bepanthen®) to prevent drying. After confirming a deep anesthesia with testing the paw pinch withdrawal reflex, the mouse head was wiped with 70% ethanol using sterile collection swabs (EUROTUBO®), to clean and disinfect the spot of surgery. A triangular skin cut was made to expose the skull. The trimmed sites of the skin were rinsed with 0.9% NaCl and cleaned from excess hair before the

periosteum covering the exposed bone was carefully removed with a scalpel. To prepare the bone for the first layer of glue serving as a ground coat, Gel Etchant (OptiBond™ FL bottle kit) was spread across the bone for 15 seconds, before it was removed by thoroughly rinsing the bone with 0.9% NaCl. The bone was then dried by carefully applying compressed air. After complete drying of the bone (crucial step!), light-curing glue was subsequently applied in a two-step procedure (OptiBond™ FL bottle kit). First, the “Primer” was distributed and air-dried for five seconds. Second, the “Adhesive” was applied, air-thinned for five seconds and then dried by blue light (420-480 nm) using light-curing device. Next, a circle ( $\varnothing$  3mm) was marked on the right hemisphere above the hippocampal formation (center coordinates, AP: -1.90 mm, ML: +2.10 mm) using a biopsy punch (**Fig. 2.1a**). A dental drill was used to cut out this circular bone piece. The dura mater was removed using fine forceps, before the cortical tissue above the hippocampus was aspirated. This was achieved by using a blunt needle (gauge 21) connected via flexible thick-walled tubing to a vacuum pump. As soon as the axonal fibers of the external capsule were reached, which can be easily distinguished by eye from the above lying cortical tissue (**Fig. 2.1b**), the needle size was decreased to gauge 27 to allow a more precise control of the aspirated volume. The external capsule of the hippocampus was carefully peeled away, exposing the fibers of the underlying alveus that was kept intact (**Fig. 2.1b**). As soon as the depth of interest was reached the blood flow was stopped with an absorbable gelatin sponge (GELITA-SPON®). The exposed brain was rinsed with 0.9% NaCl before the sterilized hippocampal window consisting of a stainless-steel tube, closed on one

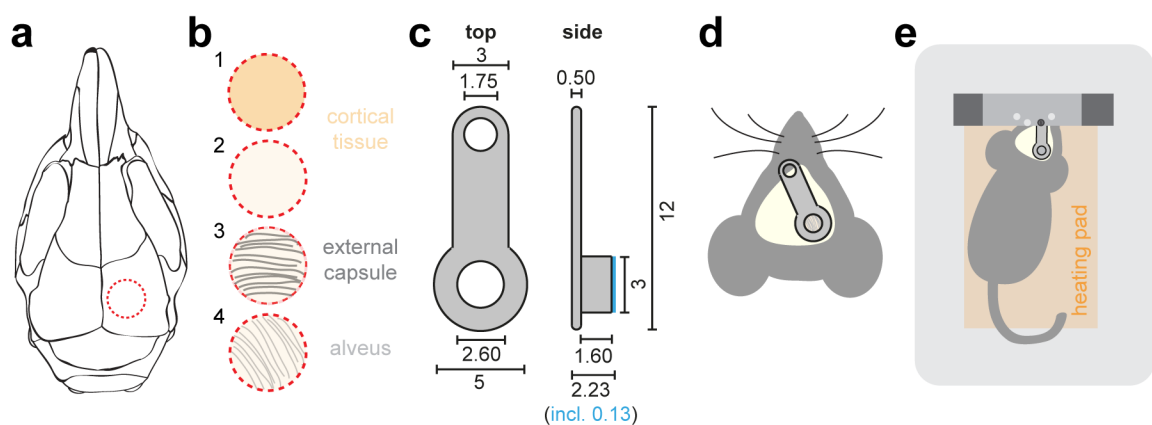


**Figure 2.1 Hippocampal window.** (a) Scheme showing the position of the hippocampal window ( $\varnothing$  3mm, red dashed circle) on top of the mouse’ skull. (b) Schematic representation of the exposed brain tissue during the aspiration procedure. Superficial (1) and deep (2) cortical layers as well as the fibers of the external capsule (3) and alveus (4) with their depth-dependent orientation can be distinguished by eye. (c) Top and side view of the fixation bar without and with attached stainless-steel cylinder, respectively. Blue, cover glass; numbers depict mm. (d) Scheme of an implanted hippocampal window. (e) Fixation of the mouse head during imaging in anesthesia. A heating pad maintains the body temperature.

side by a cover glass, and a fixation bar (**Fig. 2.1c**) was lowered into the cavity, orienting the fixation bar to the front of the mouse head (**Fig. 2.1d**). While gently pressing and holding the headpiece in place, all excessive liquid was removed from the bone until it was completely dry (crucial step!). Then the headpiece was fixed with liquid instant glue, thereby sealing the gap between bone and metal completely. Finally, a light-cured flowable composite (GRADIA® DIRECT Flo) was spread all across the exposed bone, surrounding the headpiece and fixing it to the skull. Blue light was applied for at least 30 seconds to cure the composite. Mice were released from the fixation frame (custom build) and kept separate and warm until complete recovery from anesthesia. Mice were under surveillance for at least three days, received post-surgery applications of analgesic and antibiotics, and were monitored thoroughly.

## 2.4. Optical fiber implantation

Mice were anesthetized with an i.p. injection of ketamine (0.13 mg/g bodyweight, Ketavet®) and xylazine (0.01 mg/g bodyweight, Rompun®). The head was wiped with 70% ethanol before a triangular skin cut was made to expose the skull. The periosteum was removed and the underlying bone was dried properly. The skull was roughened with a scalpel and covered with a liquid instant adhesive. Two holes were drilled at the sites of previous injections using a dental drill. After ensuring that the dura was opened by an incision (crucial!) the two-ferrule cannula was carefully lowered to a depth of 1 mm by using micromanipulators (LN Junior RE/LE, 3 axes). Cement (Cyano Veneer® Pulver and Cyano Fast) was applied until the cannulas were fixed to the skull. The exposed bone was additionally covered with cement to increase the stability of the composition. Mice were released from the fixation frame and kept separate and warm until complete recovery from anesthesia. Mice were under surveillance for at least three days, received post-surgery applications of analgesic and were monitored thoroughly.

## 2.5. Behavioral experiments

### 2.5.1. Handling

Mice were accustomed to the handling by the experimenter on two consecutive days before the actual experiment started. For this purpose, mice were grabbed at the most proximal part of

their tail and placed on the palm for ~15 seconds before they were placed back into their cage. This procedure was repeated four times with a spacing of ~2 minutes. Handling was carried out at the same time of day as the upcoming experiments. Transportation from the animal holding to the experimental room was also included in the handling procedure. For experiments involving optical stimulation, the light fiber attachment procedure including freely movement with attached light fiber was included within the handling procedure.

### 2.5.2. Contextual fear conditioning

For contextual fear conditioning, mice were allowed to explore the conditioning chamber (context A) for two minutes (pre-shock) before the first electric shock was applied (S#1, 0.75 mA, 2 seconds), followed by two additional shocks (S#2 and S#3), separated by 60 seconds. 60 seconds after the last shock, mice were returned to their home cage (**Fig. 2.2a**). 48 hours after the conditioning, mice were either placed back into context A or a novel context B for five minutes (test) (**Fig. 2.2b**). Mice were video recorded from above throughout the experiment using a camcorder or a webcam. Videos were analyzed post-hoc by an experimenter blind to the experimental conditions using the software EthoVision XT (see section 2.5.4). Context A was a rectangular chamber (21.5 cm x 20.0 cm x 40.0 cm) consisting of four transparent acrylic glass walls (**Fig. 2.2c**). The floor was composed of a metal grid, connected to a stand alone shocker/scrambler.

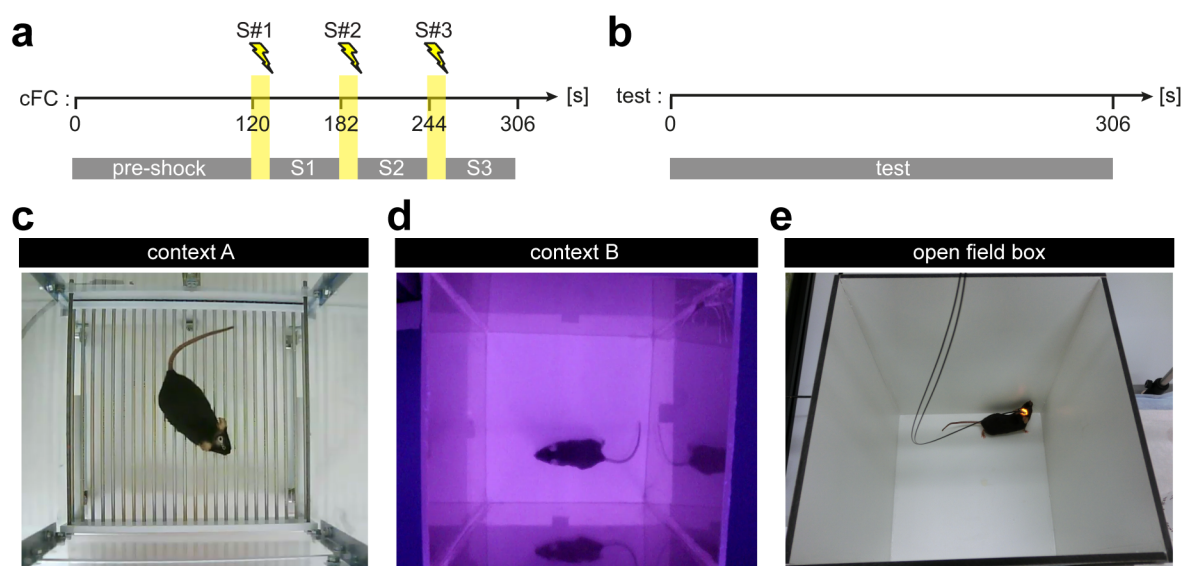


**Figure 2.2 Behavioral setups.** (a) Timeline for contextual fear conditioning (cFC): after 120 seconds exploration (pre-shock), three shocks were applied (S#1-S#3) with a duration of two seconds (yellow). Pre-shock interval: 120 seconds; inter-shock intervals S1, S2 and S3: 60 seconds. (b) Timeline for contextual fear memory test. (c-e) Pictures showing the fear conditioning chamber (context A, c), the novel context B (d) and the open field box (e) from above. Sizes of the boxes' floors are: 21.5 cm x 20 cm (c), 21 cm x 21 cm (d) and 25 cm x 25 cm (e). The height was 40 cm for all boxes.

Light conditions were kept constant. Before and after every single session, the chamber was wiped with 70% ethanol. Context B was placed in a different room than context A, consisted of four red transparent acrylic glass walls (21.0 cm x 21.0 cm x 40.0 cm) and a white soft plastic floor (**Fig. 2.2d**). The light conditions for context B were darker than for context A. Here, the chamber was wiped out with hygienic paper before and after every single session.

### 2.5.3. Open field test (OFT)

The rectangular open field box (25 cm x 25 cm x 40 cm) was made of white medium density fiberboard plates with an open top (**Fig. 2.2e**). Preceding the behavioral testing the box was wiped with 70% ethanol. Fiber-attached mice (see section 2.6.1) were placed in the middle of the box and were given ten minutes to explore the box during light stimulation. Subsequently, mice were placed back into their home cage. Mice were video monitored during exploration using a camcorder.

### 2.5.4. Behavior analysis

For every behavior analysis EthoVision XT was utilized for post-hoc video analysis and behavioral scoring. The travelled distance was scored automatically. Freezing, used as a readout for learned fear (Blanchard and Blanchard 1969), was defined as the complete absence of movement, except for breathing (De Oca, DeCola et al. 1998) and was scored manually and blind to the experimental conditions. The time freezing was depicted as percentage to the total time analyzed (see section 6.2.4).

## 2.6. Behavior manipulation

### 2.6.1. Light stimulation via optical fibers

Animals with implanted cannulas (**see Fig. 3.7b**) were attached to long flexible fibers via a magnetic mechanism. Both fibers are connected to the light sources via a rotary joint that allowed the attached animals to freely move within the behavioral setup. During the stimulation periods (light ON), mice received continuous light stimulation at 594 nm (~20 mW).

### 2.6.2. Tagging neuronal ensembles

Activity-dependent labeling of neurons in CA1 was achieved via injection of AAV2/1-cFos-tTA and AAV2/1-PTRE-tight-hM3D(Gq)-mCherry (Zhang, Ferretti et al. 2015). The *cfos* promoter ( $P_{cFOS}$ ) allows the activity-dependent expression of tetracycline-dependent transactivator (tTA). The presence of doxycycline (DOX), an antibiotic belonging to the class of tetracyclines, prevents the binding of tTA to the hM3D(Gq) promoter ( $P_{TRE-tight}$ ). Withdrawal of DOX starts the activity-dependent expression of hM3D(Gq) via binding of tTA to  $P_{TRE-tight}$  (**Fig. 2.3**). DOX was delivered with the drinking water in lightproof bottles at 2 mg/ml and 5% sucrose from the day of injection on (Zhu, Aller et al. 2007). For tagging, mice received usual tap water without DOX for two days before they were exposed to the novel context B for ten minutes. DOX treatment was continued immediately after context B exposure and continued for another four days before contextual fear conditioning started. To control for DOX efficiency in preventing the expression of hM3D(Gq), a group of mice received DOX, continuously (non-labeled).

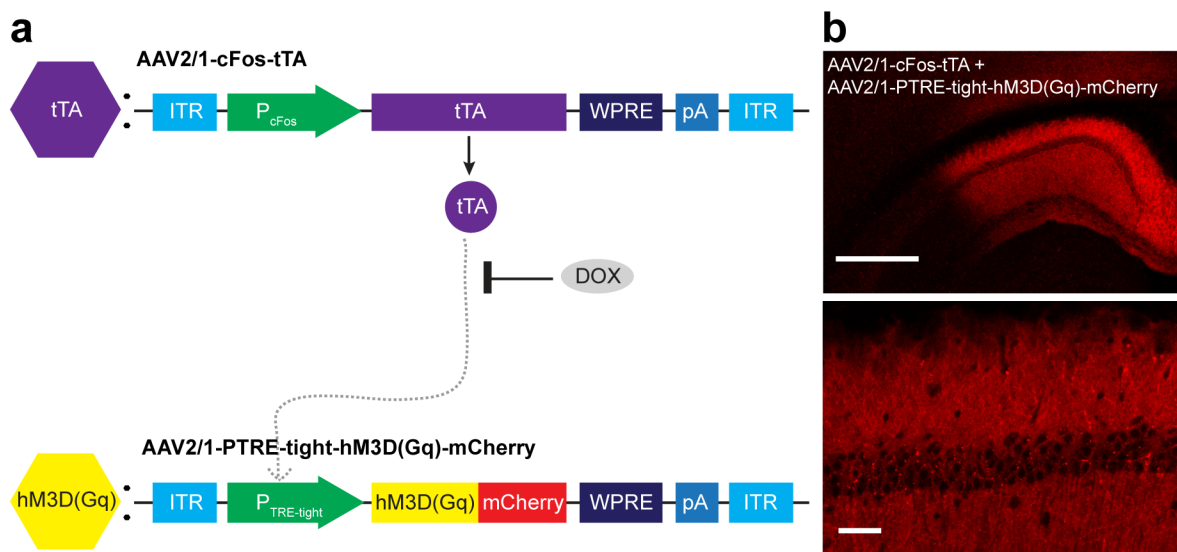


**Figure 2.3 TetTag-system for activity-dependent labelling within a specified time window.** (a) Scheme representing the genomes of AAV2/1-cFos-tTA (top) and AAV2/1-PTRE-tight-hM3D(Gq)-mCherry (bottom). The transcriptional transactivator (tTA) is expressed in an activity-dependent manner utilizing the *c-fos* promoter ( $P_{cFOS}$ ). In the absence of doxycycline (DOX) tTA binds to the promoter of hM3D(Gq) ( $P_{TRE-tight}$ ) and starts its expression. Otherwise tTA is bound by DOX and hM3D(Gq) expression is prevented. ITR, inverted terminal repeats; WPRE, woodchuck hepatitis virus posttranscriptional regulatory element; pA, polyadenylation site. (b) Overview (top) and enlarged (bottom) confocal images showing hM3D(Gq)-mCherry expression in absence of DOX in CA1. Scale bar: 500  $\mu$ m (top), 50  $\mu$ m (bottom). Modified according to Figure 3 in (Zhang, Ferretti et al. 2015).

### 2.6.3. DREADD activation

Activation of DREADD (designer receptor exclusively activated by designer drugs) was achieved via an i.p. injection of 3 µg/g bodyweight clozapine-N-oxide (CNO) 40 minutes before memory retrieval (4 mg/ml in 0.9 % NaCl, 1% DMSO). Control mice received an injection of a placebo (solvent without CNO). Solutions were prepared freshly at the day of experiment.

## 2.7. Immunohistochemistry

### 2.7.1. Tissue extraction and preparation

Mice were cardially perfused with ice-cold (~4 °C) PBS for about five minutes until the liver lost its dark red appearance. Brains were carefully removed from the skull without damaging the tissue and immediately stored in 4 % paraformaldehyde (PFA). After 24 hours PFA was replaced by PBS with 0.01 % of sodium azide (NaN<sub>3</sub>) for long-term storage at 4 °C, preventing bacterial growth. For further immunohistochemistry brains were sliced in PBS using a Vibratome.

### 2.7.2. Immunohistochemical staining

Free-floating 100 µm thick brain slices were incubated over night (RT, 300 rpm) in 0.8 % Triton<sup>TM</sup>-X100, (Sigma) 4 % normal goat serum (NGS) and 4 % bovine serum albumin (BSA), including the first antibody (see section 6.5.3) to obtain permeabilization of the tissue and specific antibody binding at the epitopes of interest. After washing with PBS (three times for five minutes) the second antibody (1:400, in 3 % BSA) was incubated for 1.5 hours (RT, 300 rpm). Brain slices were washed with 2% Triton<sup>TM</sup>-X100 for two minutes and three times with PBS for five minutes before either mounting slices on an object plate or continuing subsequent chemical staining (Nissl). Chemical stains were incubated (1:200, in 3 % BSA) for 20 minutes, again including subsequent washing with 2 % Triton<sup>TM</sup>-X100 and PBS.

## 2.8. Image acquisition

### 2.8.1. Animal preparation

For staining A $\beta$  plaques *in vivo* APP/PS1 mice received 2  $\mu$ g/g bodyweight methoxy-XO4 (MeXO4) (0.5  $\mu$ g/ $\mu$ l MeXO4, 10% DMSO, 45% 1,2-propanediol) (Burgold, Bittner et al. 2011) i.p. during the handling sessions. Wild-type mice received the same volume of a placebo (solvent without MeXO4). To avoid the induction of fosGFP expression by the data acquisition procedure itself, mice were anesthetized in their home cage with an i.p. injection of ketamine/xylazine, and were carried to the microscope and back under anesthesia. During anesthesia eyes were covered with ointment (Bepanthen®) to avoid the eyes from drying. A complete imaging session required around 30 minutes. Behavioral experiments, cFC and memory test, were conducted 1.5 hours before image acquisition started. During imaging under anesthesia mice were attached to a self-made frame that assured proper and reproducible fixation of the head below the microscope (**Fig. 2.1e**).

### 2.8.2. Two-photon *in vivo* images

FosGFP expression data were acquired with an upright Zeiss Axio Examiner LSM7MP setup (Carl Zeiss Microscopy, Jena) equipped with a Coherent Cameleon Ultra II two-photon laser (Coherent, Dieburg) and a 16x water immersion objective with a numerical aperture of 0.8 (Nikon, Tokio). Image acquisition was performed with the software ZEN2010 (Carl Zeiss Microscopy, Jena). The eGFP of the fosGFP fusion construct was excited at 920 nm. Fluorescence emission was separated by a dichroic mirror (LP555), to detect the green (BP 500-550) and red (BP575-610) emitted light with non-descanned detectors. A tile scan consisting of 3 x 3 separate z-stacks of 120  $\mu$ m depth with 3  $\mu$ m z-spacing, starting at the surface of the *stratum pyramidale* was acquired with a x,y-resolution of 0.496  $\mu$ m/pix. Tile scans were set to a depth of 120  $\mu$ m to compensate for the curvature of dorsal CA1. For image processing and analysis, one to three regions of interest (ROIs) with a depth of 90  $\mu$ m were cut out (see section 2.9.1.). In addition fluorescence of MeXO4-stained A $\beta$  plaque was acquired for APP/PS1 mice once per imaging week. Therefore, a 3 x 3 tile scan with a z-spacing of 5  $\mu$ m was performed by exciting at 780 nm and detecting blue light emission (BP420-480). Repetitive scanning of the same positions over time was achieved by orienting on the basis of the vascular pattern under reflected light illumination using a GFP filter set and a metal halide

lamp HXP100 (Carl Zeiss Microscopy, Jena). Baseline (BL) and cFC-test period (A-A/B) data were acquired for every animal, with a temporal distance of two to three weeks. Structural plasticity data of YFP-H mice were acquired at a TrimScopeII setup (La Vision Biotech, Bielefeld) equipped with a Coherent Cameleon Ultra II two-photon laser (Coherent, Dieburg) and a 16x water immersion objective with a numerical aperture of 0.8 (Nikon, Tokio). Image acquisition was performed with InspectorPro (La Vision Biotech, Bielefeld). YFP-H was excited at 920 nm. Fluorescence emission was separated by a dichroic mirror (LP525), to detect the yellow (BP 555/55) and blue (BP460/80) emitted light with non-descanned detectors. Stacks of 70  $\mu\text{m}$  depth with 1  $\mu\text{m}$  z-spacing, spanning *stratum radiatum* were acquired with a x,y-resolution of 0.087  $\mu\text{m}/\text{pixel}$ . Out of every stack two to six dendrites were analyzed as previously described (Gu, Kleiber et al. 2014).

### 2.8.3. Confocal images

Confocal images of fixed and immunohistochemically stained brain slices were acquired using an inverted LSM700 microscope (Carl Zeiss Microscopy, Jena) equipped with a 20x air objective. Alexa Fluor® 488 (Life technologies, Carlsbad) and fosGFP were excited at 488 nm and detected in the green channel (BP 490-555). Alexa Fluor® 647 (Life technologies, Carlsbad) was excited at 639 nm and detected in the red channel (LP 640). MeXO4 was excited at 405 nm and detected in the blue channel (SP 490). The pinhole was set to an airy unit of one. Images with a x,y-resolution of 1.250  $\mu\text{m}/\text{pixel}$  (FosGFP, **see Fig. 3.1e**) and 0.625  $\mu\text{m}/\text{pixel}$  (Fos stain, **see Fig. 3.1c, Fig. 3.6.2c,d and Fig.3.6.3c-e**) were acquired.

## 2.9. Image processing and analysis

### 2.9.1. Two-photon data processing

Image processing was conducted using the open source software Fiji. For the analysis of fosGFP data first, the signal-to-noise ratio of the 8-bit raw data stacks (ROI: 500  $\mu\text{m}$  x 500  $\mu\text{m}$  x 90  $\mu\text{m}$ ) was improved by eliminating most of the auto-fluorescence, which was simultaneously present in the green and the red channel. For this purpose, the red channel was subtracted from the green channel. The 30 x 3  $\mu\text{m}$  stack spanning CA1 was maximum intensity projected (MIP). MIPs of every imaging time-point were aligned in x,y-direction

using the plugin TurboReg (Thevenaz, Ruttimann et al. 1998). For measuring the fluorescence intensity of fosGFP expressing neurons, circular masks ( $\varnothing$  7.45  $\mu\text{m}$ ) with assigned numbers were placed above every nucleus to identify individual neurons throughout the experiment. Mean gray values were determined and displayed in arbitrary units (AU). To determine background fluorescence (BG), ten circular masks were placed in regions without fosGFP expressing nuclei to measure their mean background intensity ( $\text{BG}_1, \text{BG}_2, \dots, \text{BG}_{10}$ ) (**Fig. 2.4a**). A threshold was applied to define a neuron as fosGFP-positive (fosGFP<sup>+</sup>) or -negative (fosGFP<sup>-</sup>):  $\text{TH} = \text{mean}(\text{BG}_{1-10}) + 6 * \text{standard deviation}(\text{BG}_{1-10})$ . Neurons with intensity values above or below the threshold were defined as fosGFP<sup>+</sup> (cyan) or fosGFP<sup>-</sup> (black) respectively. Applying the TH resulted in binary images (**Fig. 2.4b,c**). Density and fluorescence intensity measurements for intra- and intergroup comparisons concerning A $\beta$  plaque-dependent fosGFP expression were carried out exclusively in the MIP of the first imaging time-point (d1), considering exclusively fosGFP<sup>+</sup> neurons (**see Figure 3.2**). Fluorescence intensity values of every mouse were normalized (stretched to a range of 0-256) to enhance the contrast. Densities of fosGFP expressing neurons are displayed in neurons per 1000  $\mu\text{m}^2$ . FosGFP expression changes within one day were defined as follows: neurons that gain, lose or continue fosGFP expression above TH were assigned to categories of ON (green), OFF (magenta) and CON (blue) neurons, respectively (**see Fig. 2.4d**). The percentage of ON, OFF and CON neurons per category referring to the sum of all categories (ON+OFF+CON) was calculated and displayed over time. Measuring the average time a neuron needs to turn ON and OFF, respectively, confirmed the one-day imaging interval to be sufficient to resolve fosGFP expression changes (**Fig. 2.4e**). FosGFP expression pattern analyses (**see Fig. 3.5, Fig. 3.6.1 and Fig. 6.2**) were calculated by considering d2 to d5, but neglecting d1. To analyze A $\beta$  plaque deposition, MeXO4-fluorescence containing z-stacks were spatially aligned with corresponding fosGFP-fluorescence containing z-stacks. Subsequently, MIPs were prepared. Circular masks with a diameter of 100  $\mu\text{m}$  were placed around the center of each MeXO4-positive A $\beta$  plaque to define the different proximity regions: (< 50  $\mu\text{m}$ ), for neurons residing proximal or (> 50  $\mu\text{m}$ ), for neurons residing distant to MeXO4-positive A $\beta$  plaques. As a control, the same circular masks were randomly applied to data of wild-type mice and referred to as randomly placed virtual A $\beta$  plaques. Analyzes in Fig. 3.2 to Fig.3.6.1 belong to the same data set. A detailed description of data set composition is mentioned elsewhere (see section 6.2.3.). For the analysis of YFP-H data, spines on 2 to 6 dendrites residing in *stratum*

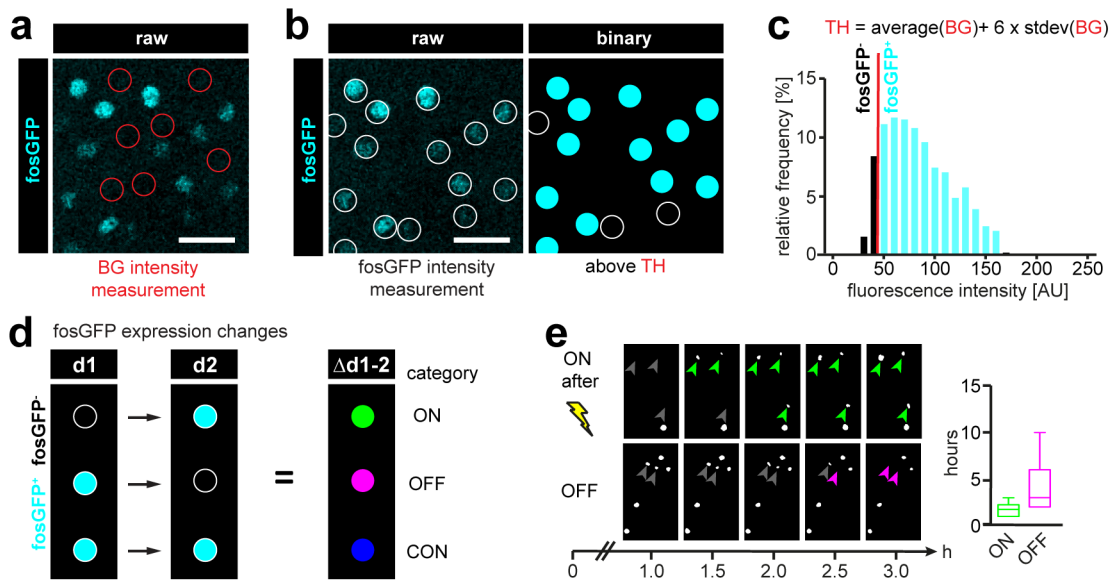


**Figure 2.4 Definition of fosGFP expressing neurons.** (a) Measurement of background fluorescence (BG). Representative fosGFP raw data image with manually placed circular masks (red,  $\varnothing$  7.45  $\mu\text{m}$ ) to measure background fluorescence. (b, c) Method to convert 8-bit raw data into binary images. Measurement of fosGFP intensity (b, left). Representative fosGFP raw data (left) and corresponding binary image (right). Circular masks (white) were manually placed above putatively fosGFP expressing nuclei. Nuclei with fosGFP fluorescence intensity above and below threshold (TH) were defined as fosGFP<sup>+</sup> and fosGFP<sup>-</sup>, respectively (c). (d) Scheme visualizing the definition of fosGFP expression changes of individual nuclei within one day ( $\Delta$ d1-2). Expression changes have been divided into three categories: Nuclei that become fosGFP<sup>+</sup> (ON, green), become fosGFP<sup>-</sup> (OFF, red) and nuclei that keep their expression from one to the other day (CON, blue). (e) Representative images after threshold application showing the delay of induced fosGFP expression (left, upper panel) and the degradation of the signal (left, lower panel). Average time a neuron needed to turn ON and OFF (right); data from n=52 fosGFP<sup>+</sup> neurons. Scale bar: 40  $\mu\text{m}$ .

*radiatum* of CA1 with an average length of  $34.9 \pm 3.3 \mu\text{m}$  (wild-type, mean  $\pm$  standard deviation) and  $34.2 \pm 5.8 \mu\text{m}$  (APP/PS1, mean  $\pm$  standard deviation) were counted as shown previously (Gu, Kleiber et al. 2014). Events of emerging (gained) or disappearing (lost) spines between two imaging time-points were counted and referred to the dendritic length, resulting in densities of lost and gained spines, respectively. The density of transient spines is calculated by the sum of lost and gained spine density. Spines that remained stable between two imaging time-points were referred to as persistent spines, which is depicted as density of persistent spines.

### 2.9.2. Confocal data processing

For measuring fosGFP and endogenous Fos expression in confocal images, circular masks ( $\varnothing$  6.88  $\mu\text{m}$ ) with assigned numbers were placed above every nucleus to identify individual Fos and/or fosGFP expressing neurons. Mean gray values were determined and displayed in arbitrary units (AU). To determine background fluorescence (BG), ten circular masks were

placed in CA1 surrounding the fosGFP and/or Fos-expressing nuclei to measure their mean background intensity (BG<sub>1</sub>, BG<sub>2</sub>, ..., BG<sub>10</sub>). A threshold was applied to define a neuron as fosGFP-positive (FosGFP<sup>+</sup>) and/or Fos-positive (Fos<sup>+</sup>): TH = mean (BG<sub>1-10</sub>) + 6 \* standard deviation (BG<sub>1-10</sub>). The number of fosGFP<sup>+</sup> and Fos<sup>+</sup> nuclei was counted in single planes of multiple slices per mouse (see section 6.2.3.) and displayed as nuclei per 1000 μm<sup>2</sup>.

### 2.9.3. Statistics

Statistical analysis and preparation of graphs was performed with GraphPad Prism7 (GraphPad Software Inc., La Jolla, USA). Subjects were assigned to experimental groups before data acquisition. Assignment was determined by genotype and by aiming at a balanced proportion of sexes in each group. For data collection, blinding was not possible. Data analysis was performed blind to the conditions of the experiment via encrypting file names by a third person. Mice were excluded if acquired data sets were incomplete. All data were tested for normality with the D'Agostino and Pearson normality test (if n>6) or Shapiro-Wilk normality test (if n<6). Normally distributed data are displayed with mean ± standard error of the mean (SEM), showing single values in light grey. Pattern frequencies and fosGFP expression changes are presented by continuous and dashed lines, reporting the mean ± SEM, respectively. Non-normally distributed data are displayed in box plots that report the median, 25%- and 75%-quartile, with whiskers depicting minimum and maximum values of the data. All statistical tests applied in this study were two-sided and were mentioned in the corresponding figure legend. Figures were prepared with Illustrator CS5 Version 15.0.1 and Photoshop CS5 Version 12.1 (Adobe, San José, USA).

### 3. RESULTS

#### 3.1. FosGFP is a reliable marker of endogenous Fos

The expression of immediate early genes (IEGs) is an established marker for neuronal activity and was frequently utilized to visualize memory traces (Horn 2004, Reijmers, Perkins et al. 2007, Rudinskiy, Hawkes et al. 2012, Denny, Kheirbek et al. 2014). We crossbred fosGFP and APP/PS1 mice to monitor fosGFP under healthy (wild-type) and AD-like (APP/PS1) conditions (**Fig. 3.1a**). An immunohistochemical staining for GAD67 revealed Fos to be preferentially expressed in excitatory rather than in inhibitory neurons in the CA1 region of

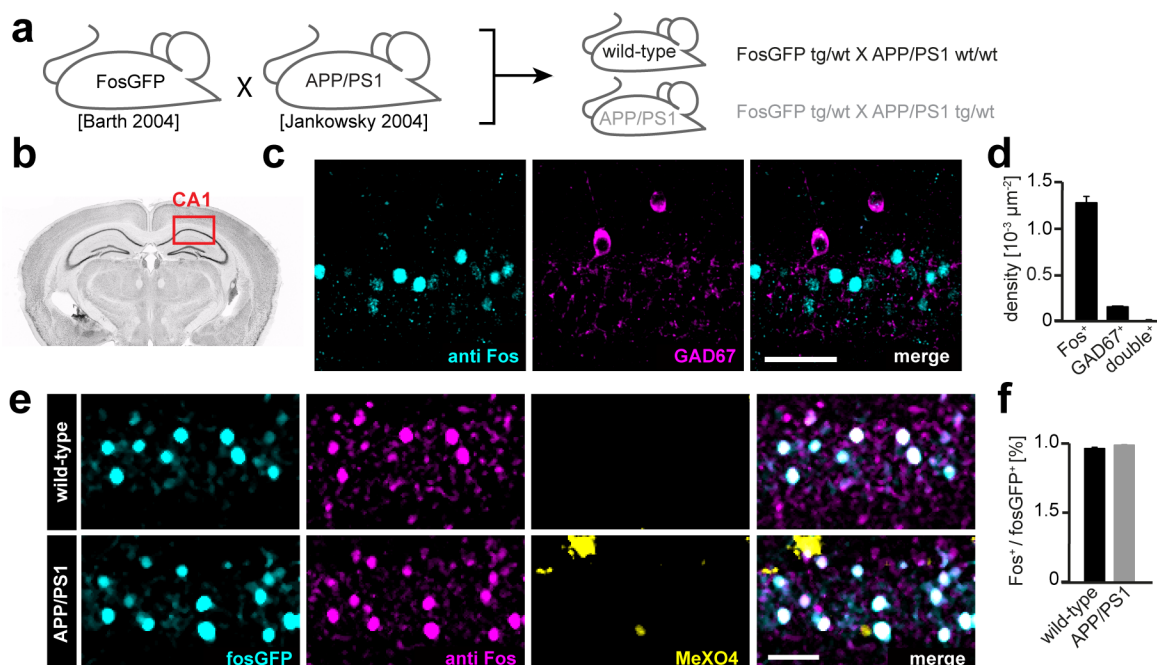


**Figure 3.1 Immunohistochemical validation of fosGFP.** (a) FosGFP and APP/PS1 mice have been crossbred to monitor neuronal activity under healthy and AD-like conditions. (b) Scheme of a coronal brain section and the analyzed part of the CA1 region (red). (c) Representative confocal images of endogenous Fos expression (anti-Fos) and GABAergic interneurons (GAD67) in CA1. (d) Density of Fos<sup>+</sup> nuclei, GAD67-positive (GAD67<sup>+</sup>) neurons and double positive fractions in immunohistochemically stained slices. Data from n=3 wild-type mice. (e) Representative confocal images of endogenous Fos and fosGFP expression in CA1 of wild-type and APP/PS1 mice. A $\beta$  plaques were stained by an i.p. injection of methoxy-XO4 (MeXO4). (f) Fraction of fosGFP<sup>+</sup> nuclei that were simultaneously positive for endogenous Fos protein. Data from n=3 wild-type and n=3 APP/PS1 mice. Scale bars: 50  $\mu$ m (c); 40  $\mu$ m (e).

the hippocampus (**Fig. 3.1b-d**). Additionally, fosGFP revealed to be a reliable representative of endogenous Fos expression levels as more than 95 % fosGFP-positive (fosGFP<sup>+</sup>) neurons were also positive for the endogenous Fos protein in wild-type and APP/PS1 mice (**Fig. 3.1e,f**). In summary, fosGFP expression proved to be a reliable marker for the study of

CA1 neuronal activity under healthy and AD-like conditions. To investigate whether CA1 neuronal activity dynamics were different in wild-type and APP/PS1 mice, fosGFP expression over time was monitored.

### 3.2. Presence of amyloid-beta induces neuronal hypoactivity *in vivo*

To monitor the expression of the fusion construct fosGFP *in vivo*, a chronic hippocampal window was established in our lab (Gu, Kleiber et al. 2014) (see section 2.3) that allows for repetitive scanning of the dorsal hippocampus via two-photon microscopy (**Fig. 3.2a-c**). A $\beta$

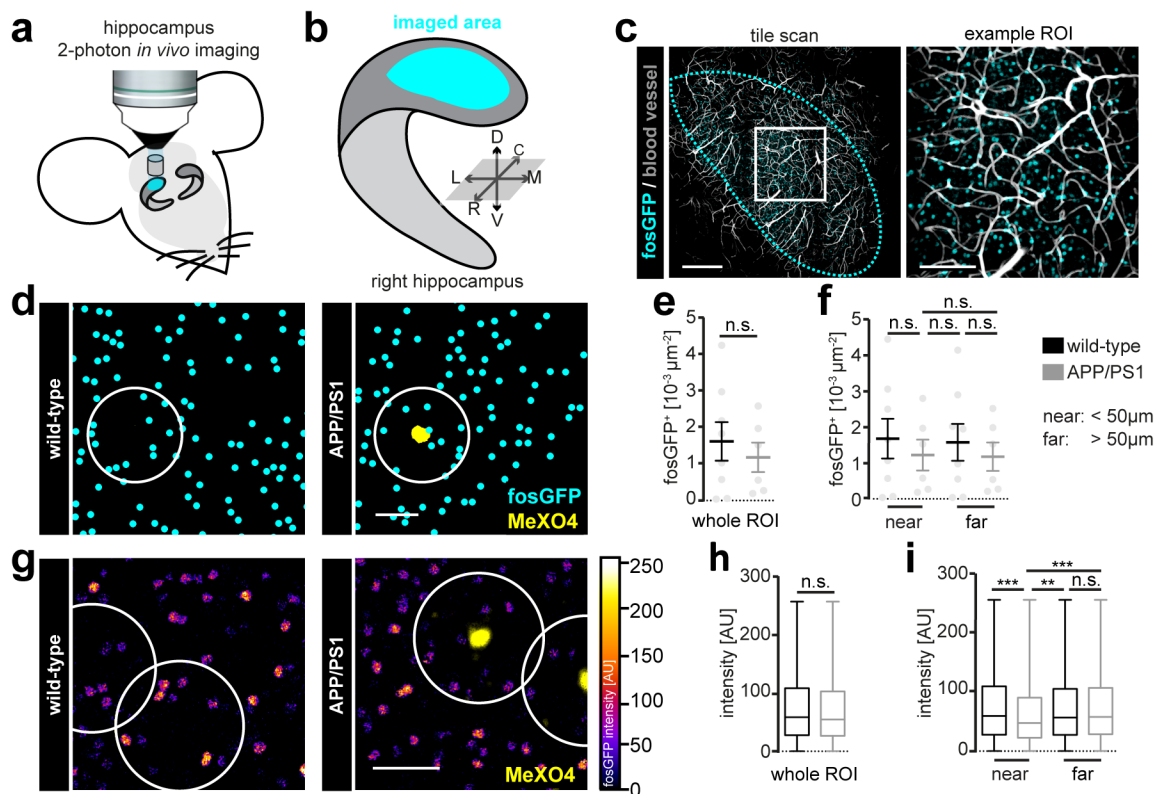


**Figure 3.2 Reduced fosGFP expression in A $\beta$  plaque vicinity.** (a, b) Hippocampus two-photon *in vivo* imaging approach. A stainless-steel cylinder with a glass bottom was implanted above the hippocampus, unilaterally (a) to allow repetitive imaging of dorsal CA1 (b). (c) Tile scan (left) and example ROI (right) of fosGFP expression (cyan) in dorsal CA1. The dashed cyan-colored line corresponds to the imaged area in (b). The white rectangle surrounds the enlarged example ROI (right). (d-f) Density of fosGFP<sup>+</sup> nuclei in dependence of A $\beta$  plaque vicinity. Binary images of fosGFP<sup>+</sup> nuclei in CA1 of wild-type (d, left) and APP/PS1 mice (d, right). Density of fosGFP<sup>+</sup> nuclei in the whole ROI (e), and near (<50 μm) and far (>50 μm) from MeXO4-positive A $\beta$  plaques, or randomly placed virtual plaques (f). (e)  $p=0.5476$ , unpaired t-test. (f)  $p=0.9827$  (wild-type near vs. APP/PS1 near),  $p=0.9827$  (wild-type far vs. APP/PS1 far),  $p=9863$  (wild-type far vs. APP/PS1 near),  $p=9827$  (APP/PS1 near vs. far), one-way ANOVA with Holm-Sidak's correction for multiple comparisons. (g-i) FosGFP intensity in dependence of A $\beta$  plaque vicinity. Images of fosGFP expressing nuclei in wild-type (g, left) and APP/PS1 mice (g, right). Fluorescence intensity distribution in the whole ROI (h), and near and far from MeXO4-positive A $\beta$  plaques, or randomly placed virtual plaques (i). (h)  $p=0.0979$  Mann-Whitney test; (i) \*\*\* $p=0.0003$  (wild-type near vs. APP/PS1 near),  $p>0.9999$  (wild-type far vs. APP/PS1 far), \*\* $p=0.0035$  (wild-type far vs. APP/PS1 near), \*\*\* $p=0.0004$  (APP/PS1 near vs. far), Kruskal-Wallis test with Dunn's correction for multiple comparisons. White circles (radius: 50 μm); (d, g) depict the area near to a MeXO4-positive A $\beta$  plaque or a virtual plaque (wild-type), respectively. Data from  $n=8$  wild-type mice (2874 neurons) and  $n=6$  APP/PS1 mice (2092 neurons). Scale bars: 250 (c, left), 100 μm (c, right); 50 μm (d, g).

plaques have been shown to influence neuronal firing in the cortex and hippocampus *in vitro* and *in vivo* (Palop, Chin et al. 2007, Busche, Chen et al. 2012). *Arc* expression, another IEG, was reduced in the vicinity of A $\beta$  plaques and its experience-induced expression regulation was altered in the visual cortex *in vivo* (Rudinskiy, Hawkes et al. 2012). In our mouse model, the density of fosGFP expressing neurons was independent of A $\beta$  plaque presence (**Fig. 3.2d-f**). Moreover, the fluorescence intensity distribution of fosGFP expression measured independent of A $\beta$  plaque presence was similar in APP/PS1 compared to wild-type mice (**Fig. 3.2g,h**). However, analyzing fosGFP expressing neurons according to their relative distance to MeXO4-positive A $\beta$  plaques revealed a significantly decreased expression of fosGFP in the direct proximity (<50  $\mu$ m, near), but not distant (> 50 $\mu$ m, far) to A $\beta$  plaques (**Fig. 3.2g,i**).

### 3.3. Two major populations among fosGFP expressing neurons

To analyze learning-induced expression changes of fosGFP, the baseline dynamics were monitored first. Therefore, fosGFP fluorescence in the pyramidal cell layer of CA1 was scanned daily for a period of five days (**Fig. 3.3a**). To visualize expression changes, the acquired images were transformed into binary images (see section 2.9.1) and color-coded to distinguish between neurons that switch on (ON, green), switch off (OFF, magenta) or continue their fosGFP expression (CON, blue) from one to the other day (**Fig. 3.3b and Fig. 2.4d**). Comparing the relative fractions of each category revealed the CON fraction to be the major subset of neurons comprising ~60%. In contrast, ON and OFF neurons represent just ~20% each. All categories were of similar size comparing wild-type and APP/PS1 mice (**Fig. 3.3c**). Furthermore, their sizes were consistently over time within both genotypes (**Fig. 3.3d,e**). The population of CON neurons contained a major fraction of neurons expressing fosGFP for the whole imaging period of five days. This was confirmed by subdividing neurons according to their expression duration: Neurons with constant five-day fosGFP expression represented the major fraction (**Fig. 3.3f,g**). Even three weeks later, 60% of this population exhibited five-day long fosGFP expression underscoring their long-term continuous activity (**Fig. 3.3h**). The second most frequent fraction consisted of neurons expressing fosGFP just once in five days, representing a variably active neuronal population of the CA1 network. The remaining population consisted of neurons with fosGFP expression durations of two, three and four days, with lower frequencies compared to afore mentioned populations. Similar frequencies were found in wild-type and APP/PS1 mice (**Fig. 3.3g**). In

summary, the analysis of fosGFP expression kinetics during baseline within the same CA1 pyramidal neurons revealed two major populations: a continuously active (CON) and a variably active one (ON, OFF).

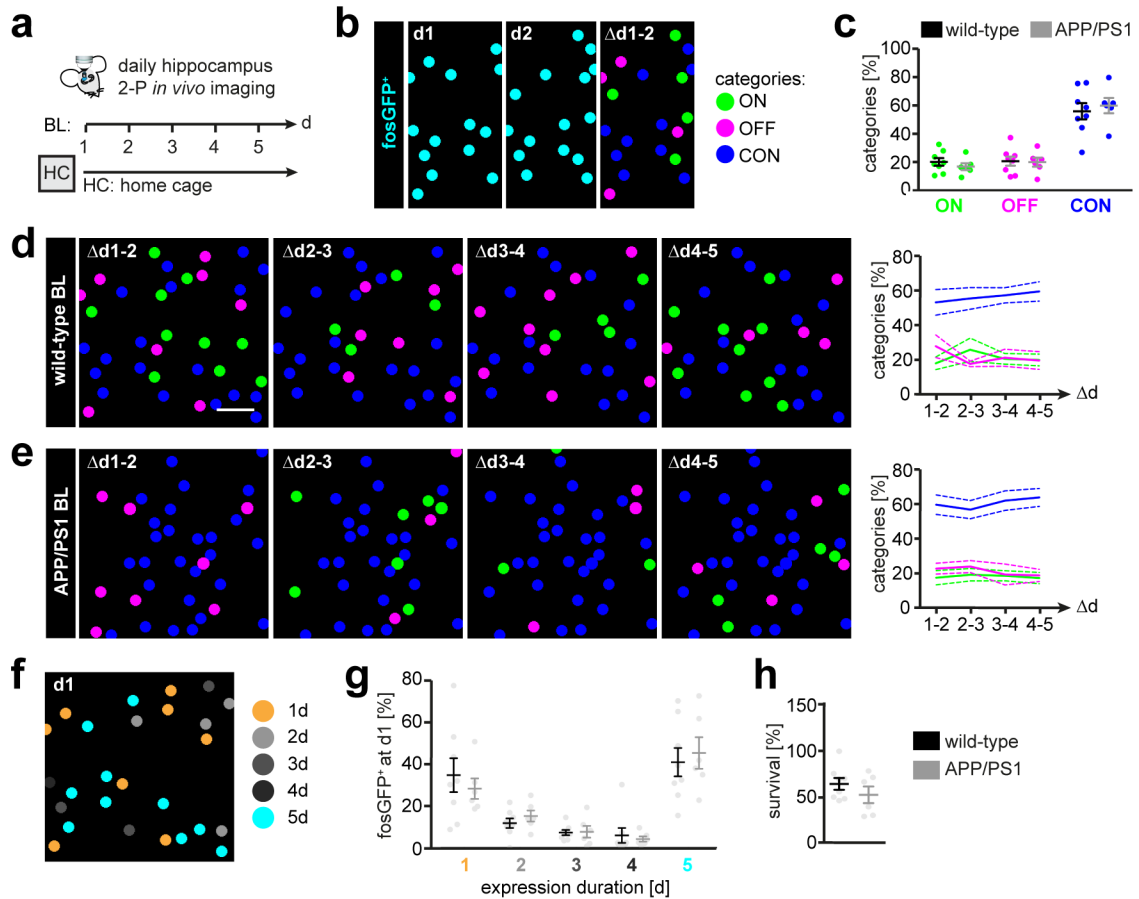


**Figure 3.3 FosGFP baseline dynamics revealed two distinct neuronal populations.** (a) Experimental paradigm to monitor daily fosGFP expression under baseline (BL) conditions, with mice residing in their home cage (HC). (b) FosGFP expression changes are visualized in green (ON, switch on), magenta (OFF, switch off) and blue (CON, continue expression). Categories define expression changes between two days, e.g.:  $\Delta d1-2$ , expression changes between d1 and d2. (c) Average fraction of each category within one week in wild-type and APP/PS1 mice. Inter-group comparisons: ON,  $p=0.8685$ ; OFF,  $p=0.9040$ ; CON,  $p=0.8685$ ; two-way ANOVA with Holm-Sidak's correction for multiple comparisons. (d, e) Representative example images (left) and corresponding graphs (right) depicting fosGFP expression changes within five days in wild-type (d) and APP/PS1 mice (e). (f) Example image showing fosGFP<sup>+</sup> nuclei and their fate regarding the expression duration (color-coded). (g) Fraction of neurons with different expression durations, from one to five days. Inter-group comparisons: 1,  $p=0.8966$ ; 2,  $p=0.9534$ ; 3,  $p=0.9630$ ; 4,  $p=0.9630$ ; 5,  $p=0.9534$ ; two-way ANOVA with Holm-Sidak's correction for multiple comparisons. (h) Three week survival of neurons with a expression duration of five days (d1 to d5) in wild-type and APP/PS1 mice, respectively;  $p=0.214$ , unpaired t-test. Data from  $n=8$  wild-type (4134 neurons) and  $n=6$  APP/PS1 mice (2993 neurons). Scale bar: 50  $\mu\text{m}$ .

### 3.4. Intact CA1 activity of APP/PS1 mice during learning & memory

It was hypothesized that impaired learning and memory on the behavior level is reflected by altered CA1 network activity in APP/PS1 mice. Therefore learning-induced expression changes of fosGFP in CA1 pyramidal neurons were examined (Fig. 3.4a). APP/PS1 mice

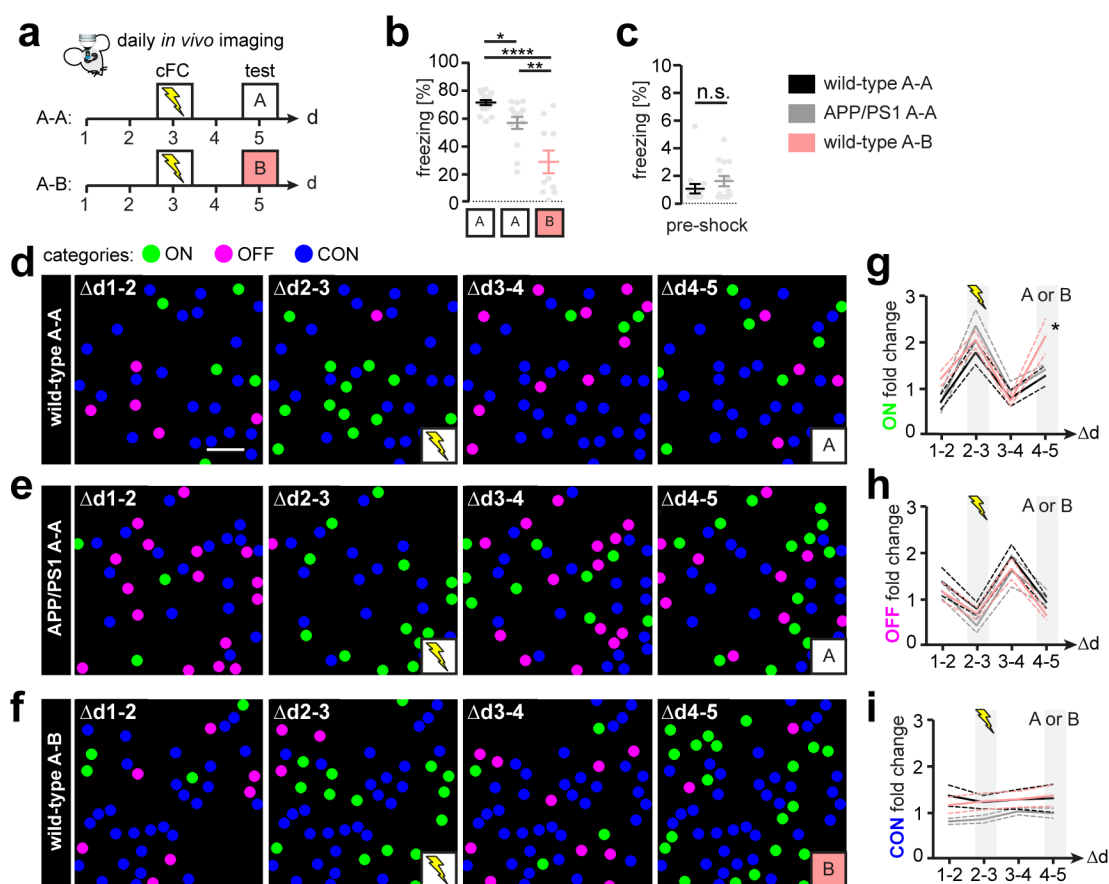


**Figure 3.4 CA1 network activity revealed to be intact in APP/PS1 mice.** (a) Experimental timeline to access fosGFP expression during learning and memory. Images were acquired every day for a period of five days. On day three, mice underwent contextual fear conditioning (cFC). On day five mice were either tested (test) in the conditioned context A (white-colored box) or in a novel context B (salmon-colored box). (b) Memory test performance measured by freezing behavior of wild-type and APP/PS1 mice in the conditioned context A, two days after conditioning. Freezing of wild-type mice conditioned in context A, but exposed to a novel context B two days after conditioning as a control for freezing specificity. Data from  $n=16$  wild-type A-A,  $n=14$  APP/PS1 A-A and  $n=10$  wild-type A-B mice;  $*p=0.0322$  (wild-type A-A vs. APP/PS1 A-A),  $**p=0.0014$  (APP/PS1 A-A vs. wild-type A-B),  $****p<0.0001$  (wild-type A-A vs. wild-type A-B); one-way ANOVA with Holm-Sidak's correction for multiple comparisons. (c) Freezing behavior during context A exposure, before the first shock was delivered (pre-shock). (d-f) Representative images of fosGFP expression changes in wild-type (d) and APP/PS1 mice (e) conditioned and tested in context A (A-A) and of wild-type mice conditioned in context A, but tested in context B (A-B) (f). (g-i) Inter-group comparisons of fold changes of ON (g), OFF (h) and CON (i) fractions during the cFC-test period. Average values from  $n=8$  wild-type A-A mice (4775 neurons),  $n=6$  APP/PS1 A-A mice (3776 neurons) and  $n=6$  wild-type A-B mice (5099 neurons);  $*p=0.0264$  ( $\Delta d4-5$ , wild-type A-A vs. wild-type A-B), all other comparisons resulted in  $p$ -values  $> 0.05$ , two-way ANOVA with Holm-Sidak's correction for multiple comparisons. Scale bar: 25  $\mu\text{m}$ .

have a long-term memory retrieval deficit (Kilgore, Miller et al. 2010, Roy, Arons et al. 2016). The contextual memory retrieval deficit was successfully confirmed in this work by exposing mice to the conditioned context A two days after conditioning. This revealed a significantly decreased freezing rate of APP/PS1 mice, compared to wild-type mice. A control group was conditioned in context A, but exposed to a novel context B, showing that the freezing behavior was specific to the conditioned context (Fig. 3.4b). General differences in freezing behavior

between genotypes can be excluded by comparing the baseline freezing rates during exploration of context A (pre-shock) (**Fig. 3.4c**). To identify whether the decreased memory test performance of APP/PS1 mice was due to impaired memory acquisition and/or retrieval on the cellular level, contextual fear conditioning (cFC) was combined with two-photon *in vivo* imaging, adapted to the previously applied experimental timeline (**see Fig. 3.3a**). To obtain stimulus-evoked fosGFP expression, behavioral experiments were carried out 1.5 hours before the imaging started to compensate for the delay of GFP expression (**Fig. 2.4e**). Indeed contextual fear conditioning evoked a strong increase of ON neurons causing an overall rise of fosGFP-positive (fosGFP<sup>+</sup>) nuclei (**Fig. 3.4d-g**). This effect was similar in wild-type and APP/PS1 mice, indicating intact memory acquisition on the level of neuronal activity. The following day was characterized by an increased OFF fraction, reducing the total number of fosGFP<sup>+</sup> nuclei back to baseline values (**Fig. 3.4d-f,h**). Contextual memory retrieval induced just a slight gain of ON neurons in wild-type mice that successfully retrieved the memory. The exposure of wild-type mice to a novel context B, two days after conditioning in context A induced a gain of ON neurons, similar to the gain after fear conditioning in context A (**Fig. 3.4g**). The fraction of CON neurons did not change after experience (**Fig. 3.4i**). Interestingly, exposing APP/PS1 mice to the conditioned context A, two days after conditioning led to a rise of the ON fraction, similar to wild-type mice exposed to the conditioning context, indicating intact memory retrieval on the level of integrated neuronal activity (**Fig. 3.4g**). Summarized, the CA1 network of APP/PS1 mice exhibited fosGFP expression dynamics during learning and memory similar to wild-type mice. To analyze the existence of any hidden difference between CA1 neuronal activity of wild-type and APP/PS1 mice, the activity of every individual neuron was examined.

### 3.5. Reactivated neuronal ensembles occur independent of memory

It is known that neurons involved in memory encoding are in part reactivated during memory retrieval. As the data above showed (**see Fig. 3.4g**), exposure of wild-type mice to the conditioned context A two days after learning induced an increase of ON neurons, although smaller compared to the gain after cFC (**see also Fig. 6.1**). To clarify whether those neurons were active during both events, encoding and retrieval, the fraction of reactivated neurons (standard reactivation) was calculated (**Fig. 3.5a-c**). This resulted in a population of

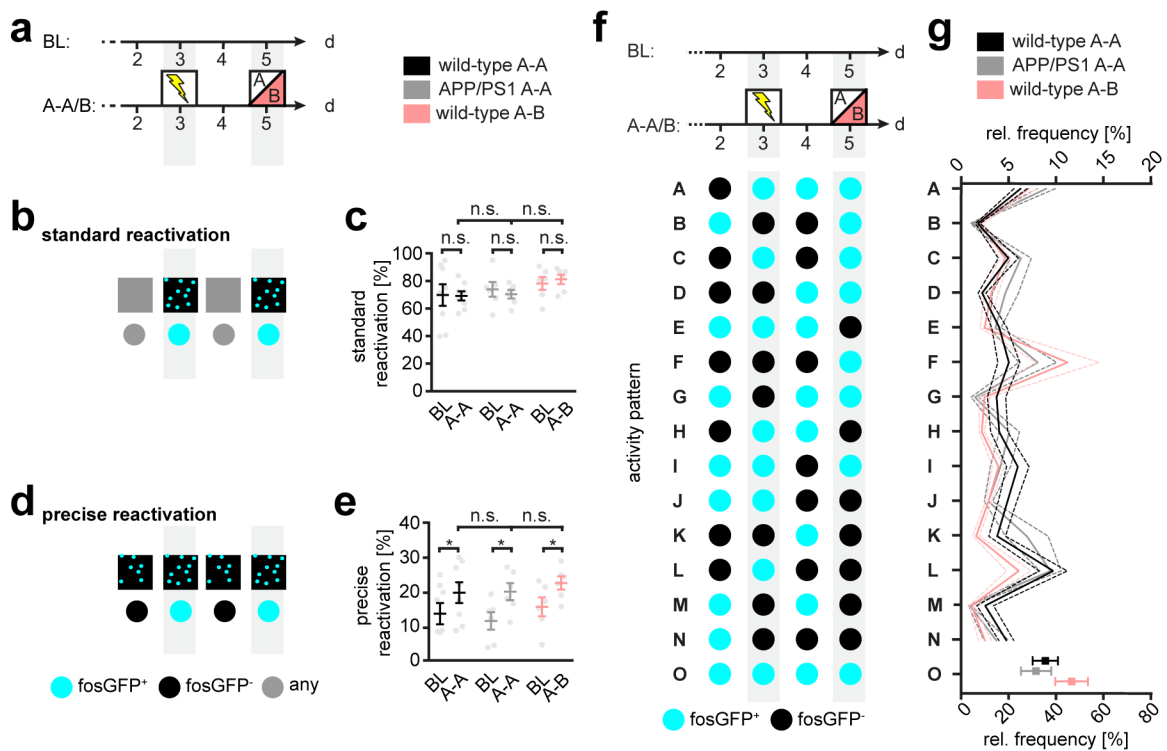


**Figure 3.5 Reactivated ensemble emerged independent of memory retrieval.** (a-e) Reactivation analysis. Experimental timeline (a) and definitions of standard (b) and precise reactivation (d) are visualized. Corresponding box plots showing reactivated fractions in all experimental groups for the standard (c) and precise (e) definition of reactivation. Average values from  $n=8$  wild-type A-A mice (4775 neurons),  $n=6$  APP/PS1 A-A mice (3776 neurons) and  $n=6$  wild-type A-B mice (5099 neurons);  $p$ -values for intra-group comparisons  $> 0.05$  (n.s.),  $*p=0.0341$  (wild-type A-A),  $*p=0.0127$  (APP/PS1 A-A),  $*p=0.0368$  (wild-type A-B), two-way ANOVA with correction for multiple comparisons using the two-stage linear step-up procedure of Benjamini, Krieger and Yekutieli. (f) Scheme for activity pattern analysis. During the BL, A-A and A-B periods four imaging days surrounding day three and five, respectively, were considered for analysis. Taking four different time-points and two possible activity states, *i.e.* fosGFP<sup>+</sup> and fosGFP<sup>-</sup>, individual neurons can show  $2^4-1$  different activity patterns (randomly named from A to O), excluding the neurons without activity. (g) Relative frequency of every activity pattern in wild-type and APP/PS1 mice during the cFC-test period A-A, and in wild-type mice during A-B.

70%, but surprisingly, for all experimental groups. Furthermore, standard reactivation during the cFC-test period (A-A/B) equals randomly reactivated fractions, as revealed by baseline (BL) data (Fig. 3.5c). As the standard two time-point approach was biased by the subset of neurons being continuously active during the experimental timeline, reactivation was defined more precisely. For this, just neurons fosGFP<sup>+</sup> during cFC and test, and fosGFP<sup>-</sup> elsewhere, were considered (Fig. 3.5a,d,e). This led to a reactivated fraction of around 20%, but again, the same for all experimental groups (inter-group comparison). However, this subset of neurons was increased compared to BL (intra-group comparison) and led to a specifically reactivated fraction of about 10%, subtracting randomly reactivated neurons (Fig. 3.5e). To consider other patterns of activity that may give rise to a neuronal correlate of the contextual memory and may explain memory impairment in APP/PS1 mice, the relative frequencies of

every possible activity pattern was calculated. Giving the possibility of two different states, namely  $\text{fosGFP}^+$  and  $\text{fosGFP}^-$ , and a consideration of four time-points, led to a total number of 15 different sequences of  $\text{fosGFP}^+$  and  $\text{fosGFP}^-$  states, *i.e.* possible activity pattern (**Fig. 3.5f**). By comparing the relative frequencies of all patterns during the cFC-test period (A-A/B) between the experimental groups confirmed the equal rise of the precisely reactivated neuronal subset (pattern C) (**Fig. 3.5f,g**). Interestingly, the comparison also uncovered a pattern that is clearly more prevalent in APP/PS1 mice, compared to wild-type mice (pattern F) (**Fig. 3.5g**). This pattern F was also found elevated in wild-type mice tested in the novel context B. The relevance of this activity pattern, comprising neurons that are activated exclusively after memory retrieval, needs to be examined. Therefore, the aim was to further dissect the CA1 network activity during retrieval.

### 3.6. Impurity of the memory trace impairs retrieval performance

In the previous section it was shown that reactivation of a potential memory trace during memory test was intact in APP/PS1 mice. The following analysis addresses whether additional neuronal ensembles (e.g. pattern F) may present a causal link to the behavioral deficit on the cellular level. Therefore, the composition of the retrieval network (RN) was dissected, *i.e.* the entity of neurons  $\text{fosGFP}^+$  during retrieval. Each neuron of the RN can have one of eight possible activity history patterns (**Fig. 3.6.1a**), consisting of the previously described activity patterns including just those being  $\text{fosGFP}^+$  on day five (**see Fig. 3.5f**). To identify learning and memory related patterns, the change in frequency of every activity history pattern, from the baseline (BL) to the cFC-test period (A-A/B), was calculated (**Fig. 3.6.1b**). Clearly, two of the eight possible activity history pattern stood out: REAH pattern (neurons with reactivation history, green) that is elevated in all experimental groups (**Fig. 3.6.1a-c**) and RONLY pattern (neurons only active during retrieval, red), that is elevated in APP/PS1 mice exposed to the conditioned context A and in wild-type mice exposed to a novel context B (**Fig. 3.6.1a,b,d**). To visualize the overall RN change between experimental groups, a network similarity map was designed. Here, activity history pattern were sorted according to their relative frequency change from the BL to the cFC-test period in descending order. Each corresponding pattern was connected by a line. A high number of intersections indicate a high dissimilarity, whereas a low number of intersections indicate a high similarity of the neuronal

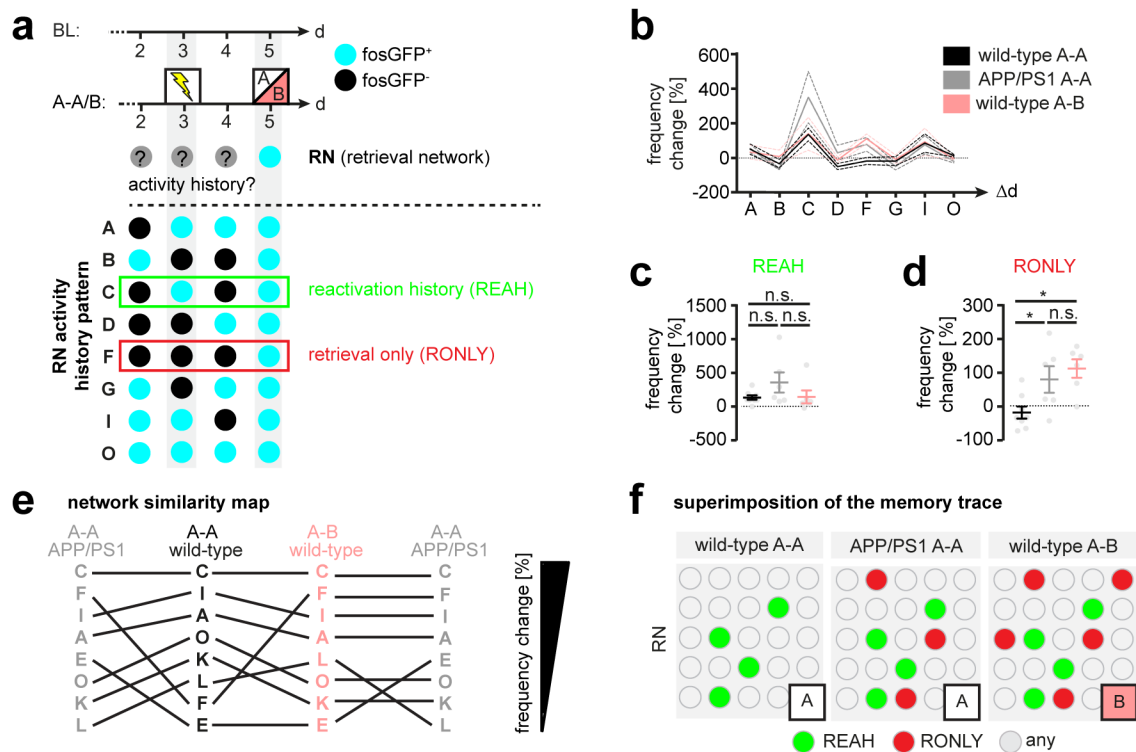


**Figure 3.6.1 Superimposition as determinant of retrieval performance.** (a) Scheme presenting the activity history analysis of neurons composing the retrieval network (RN). Every possible activity history is presented by a subset of previously introduced pattern (Fig. 3.5f). (b) Change of frequency of every RN activity history pattern from BL to A-A/B in percent. (c) Frequency change for neurons showing a reactivation history (REAH) from BL to A-A/B in percent. (d) Frequency change from BL to A-A/B in percent, for neurons being fosGFP<sup>+</sup> exclusively on day 5 (RONLY). (e) Network similarity map. RN activity history patterns of every experimental group are ordered by their frequency change, from top to bottom in a descending order. Lines connect corresponding patterns. The fewer intersections occur the more similar are the compared RNs. Data from n=8 wild-type A-A, n=6 APP/PS1 A-A and n=6 wild-type A-B mice; (c) p=0.2926 (wild-type A-A vs. APP/PS1 A-A), p=0.9441 (wild-type A-A vs. wild-type A-B), p=0.2926 (APP/PS1 A-A vs. wild-type A-B); (d) \*p=0.0426 (wild-type A-A vs. APP/PS1 A-A), \*p=0.0109 (wild-type A-A vs. wild-type A-B), p=0.4450 (APP/PS1 A-A vs. wild-type A-B); one-way ANOVA with Holm-Sidak's correction for multiple comparisons. (f) Model visualizing the superimposition of the memory trace.

network state (**Fig. 3.6.1e**). The network similarity map revealed a clear RN similarity between APP/PS1 mice exposed to the conditioned context A and wild-type mice exposed to a novel context B, especially for patterns with the highest frequency change. Summarized, the data revealed an intact potential engram in the RN, represented by REAH neurons (green), in all experimental groups. Additional activity consisting of RONLY neurons (red) was present in groups showing reduced recall performance. This suggests impaired retrieval performance through superimposition of the memory trace by impurity of the RN (**Fig. 3.6.1f**). To test this hypothesis, superimposition was induced artificially. Therefore, Vglut2-ires-cre mice were injected bilaterally with an AAV containing the genetic information for an activating DREADD (designer receptor exclusively activated by designer drug, hM3D(Gq)), flanked by

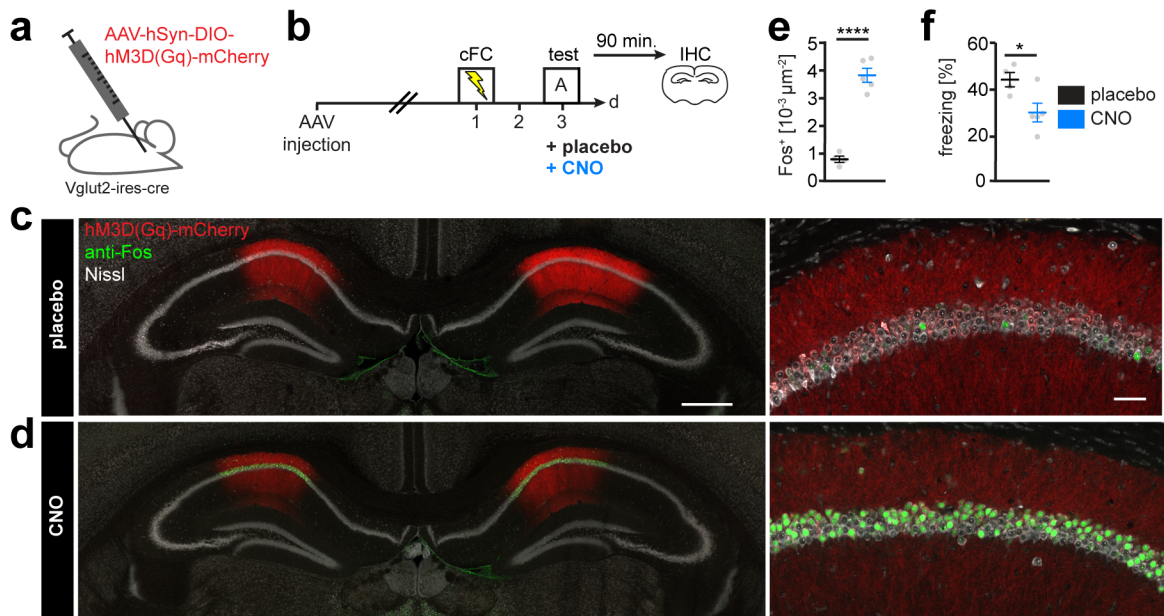


**Figure 3.6.2 Artificial superimposition in CA1 impaired retrieval performance.** (a, b) Schematic showing hM3D(Gq)-mediated activation of CA1 neurons during memory retrieval to artificially superimpose the memory trace. An AAV carrying an activating DREADD (designer receptor exclusively activated by designer drugs) flanked by loxP sites was injected into CA1 of Vglut2-ires-cre mice, bilaterally. (b) Experimental timeline for assessing memory retrieval performance during artificial memory trace superimposition. Two weeks after injections, mice underwent cFC and memory test. Here, mice received CNO or placebo, 40 minutes prior to test. 90 minutes after memory test, mice were sacrificed for postmortem immunohistochemical analysis of brain tissue (IHC). (c, d) Overview (left) and zoom (right) of exemplary confocal images of coronal brain sections showing CA1 targeted expression of hM3D(Gq)-mCherry and Fos in (c) placebo- and (d) CNO-treated mice. (e) Density of Fos expressing neurons in placebo- and CNO-treated mice; \*\*\*\*p<0.0001, unpaired t-test. (f) Freezing behavior of placebo- and CNO-treated mice; \*p=0.0316, unpaired t-test. Data from n=5 CNO-treated and n=4 saline-treated mice. Scale bars: (c) 500  $\mu\text{m}$  (left), 50  $\mu\text{m}$  (right).

loxP sites to target its expression to excitatory glutamatergic neurons in hippocampal CA1 (Fig. 3.6.2a). After a recovery period mice underwent contextual fear conditioning (cFC).

Memory was retrieved two days later, but with a previous activation of hM3D(Gq)-positive cells via an injection of clozapine-N-oxide (CNO) or placebo (just solvent) 40 minutes before memory test, respectively (Fig. 3.6.2b). CNO successfully increased neuronal activity in CA1 as revealed by an elevated number of Fos<sup>+</sup> nuclei, compared to placebo-injected control mice (Fig. 3.6.2c-e). Mice with increased neuronal activity in CA1 showed significantly reduced freezing behavior during memory test than placebo-injected control mice (Fig. 3.6.2f). This result supports the hypothesis established above: increased non memory-specific neuronal activity in CA1 during memory retrieval, superimposes the memory trace and hence, leads to reduced retrieval performance. To test whether activation of false context information alone is sufficient to impair memory, we utilized an activity-dependent and doxycycline (DOX)-controllable AAV expression system (TetTag-System) (Fig. 2.3)

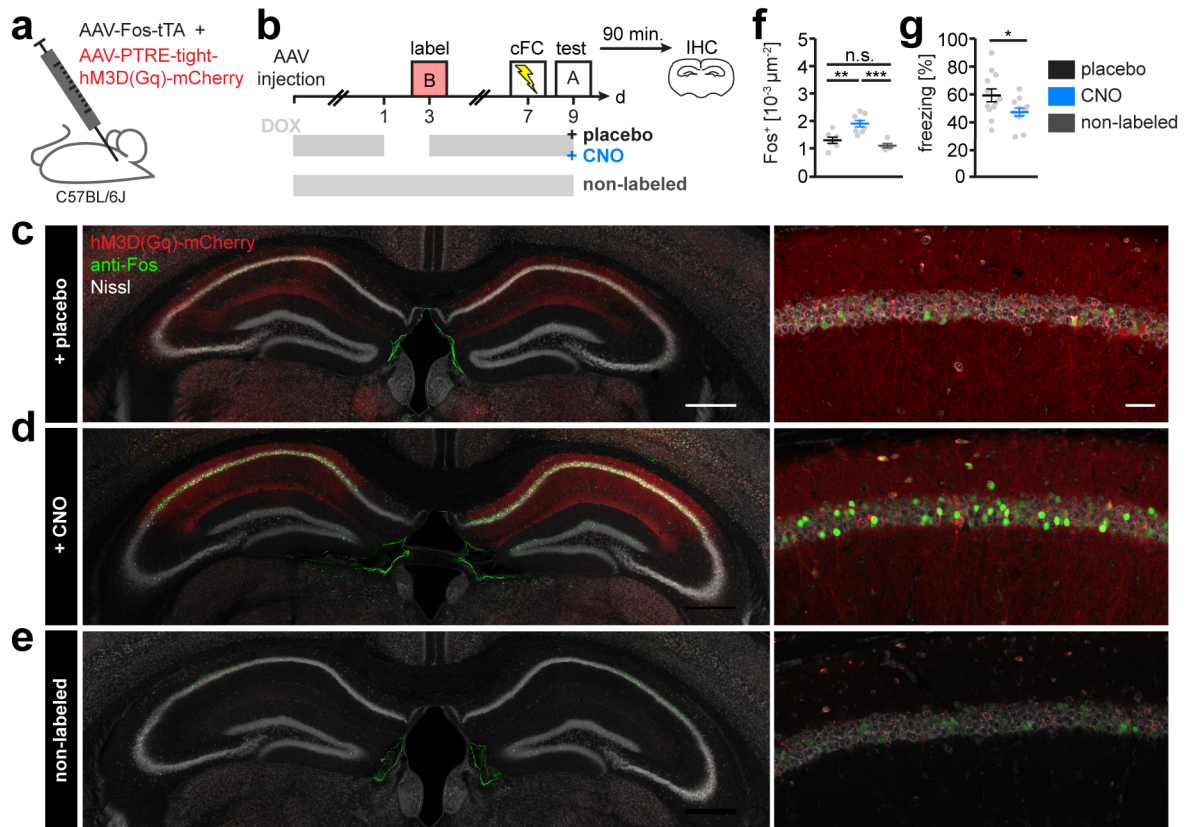


**Figure 3.6.3 Superimposition by false context information in CA1 impaired retrieval performance.** (a, b) Schematic showing the labeling and activation of CA1 neurons coding for false context information during memory retrieval to artificially superimpose the memory trace. A combination of two AAVs (TetTag-system) providing activity-dependent and doxycycline (DOX)-controlled expression of the activating DREADD hM3D(Gq) was injected into CA1, bilaterally. (b) Experimental timeline for tagging and activating neurons coding for a novel context B during memory retrieval of the conditioned context A. Mice were kept on DOX from the day of injections on (grey horizontal bar). For labeling neurons coding for a false context, mice were exposed to context B after two days without DOX. Control mice were kept on DOX during context B exposure (non-labeled). On d7 and d9, mice underwent cFC and memory test, respectively. Here, mice received CNO or placebo, 40 minutes prior to test. 90 minutes after memory test, mice were sacrificed for postmortem immunohistochemical analysis of brain tissue (IHC). (c-e) Overview (left) and zoom (right) of exemplary confocal images of coronal brain sections showing CA1 targeted expression of hM3D(Gq)-mCherry and Fos in placebo- (c) and CNO-treated (d) and non-labeled mice (e). (f) Density of Fos expressing neurons in placebo-treated, CNO-treated, and non-labeled mice. Data from  $n=7$  placebo-treated,  $n=8$  CNO-treated and  $n=5$  non-labeled mice;  $**p=0.0018$  (placebo- vs. CNO-treated),  $***p=0.0005$  (CNO-treated vs. non-labeled),  $p=0.2643$  (placebo-treated vs. non-labeled); ordinary one-way ANOVA with Holm-Sidak's correction for multiple comparisons. (g) Freezing behavior of CNO- and placebo-treated mice. Data from  $n=10$  placebo- and  $n=10$  CNO-treated mice;  $*p=0.0379$ , unpaired t-test. Scale bars: (c) 500  $\mu\text{m}$  (left), 50  $\mu\text{m}$  (right).

(Zhang, Ferretti et al. 2015). The first AAV provides the activity-dependent expression of a tetracyclin transactivator ( $\text{tTA}$ ). In absence of doxycycline (DOX),  $\text{tTA}$  binds to a promoter region present on the second virus genome ( $P_{\text{TRE-tight}}$ ), driving hM3D(Gq)-mCherry expression. The presence of DOX prevents  $\text{tTA}$  to bind on  $P_{\text{TRE-tight}}$  and thus, allows a temporally restricted expression of hM3D(Gq). Both AAVs were injected into CA1, bilaterally and DOX was given from that time on (Fig. 3.6.3a,b). For labeling neurons that encode

contextual information of a novel environment (context B), mice were deprived of DOX for two days and exposed to context B for ten minutes. To control for efficient expression prevention, a group of mice received DOX continuously (non-labeled). After four days mice were fear conditioned in context A. Memory was retrieved two days after cFC with a previous injection of CNO or placebo, respectively. CNO successfully induced the activation of the tagged neurons, as shown by an elevated number of Fos<sup>+</sup> nuclei compared to placebo-treated and non-labeled control mice (**Fig. 3.6.3c-f**). As expected, the change of activated neurons appeared much smaller, compared to the previous approach (**Fig. 3.6.2e**). Nevertheless, activation of tagged neurons during memory retrieval reduced memory recall performance, compared to placebo-treated control mice (**Fig. 3.6.3g**). Hence, activation of false context information in CA1 alone is sufficient to impair memory retrieval in the conditioned context. In the context of AD, an imbalance of excitation and inhibition was hypothesized to represent a possible cause of pathologies and thus, the cause of impaired memory (Palop, Chin et al. 2006). Whether a malfunction of inhibitory activity relates to our observed superimposition of the memory trace in APP/PS1 mice will be further analyzed.

### 3.7. PV<sup>+</sup> interneurons are crucial for CA1 activity modulation

Inhibitory interneurons are crucial for the complex interplay of neuronal circuits and have been shown to fulfill indispensable roles during learning and memory processes (Donato, Rompani et al. 2013). Especially in Alzheimer's disease, the fine balance of excitatory and inhibitory processes was shown to be disturbed (Palop, Chin et al. 2006). Therefore, it was hypothesized that the superimposition of the memory trace in APP/PS1 mice might originate indirectly from hypoactivity of inhibitory interneurons. To test this hypothesis and reveal the role of interneurons in contextual learning and memory processes within the hippocampus, interneuronal activity was suppressed artificially during learning and memory, respectively. APP/PS1 mice were crossbred to PV-Cre (parvalbumin-cre) mice to obtain PV-Cre transgenic mice with (APP/PS1) and without (wild-type) the APP/PS1 transgene. To manipulate interneurons' activity, the silencing opsin halorhodopsin (eNpHR) was delivered to parvalbumin-expressing (PV<sup>+</sup>) interneurons in a cre-dependent manner using AAV injections targeted to CA1 of wild-type and APP/PS1 mice, bilaterally (**Fig. 3.7a**). Two-ferrule cannulas were implanted above CA1 without damaging the pyramidal cell layer to repetitively

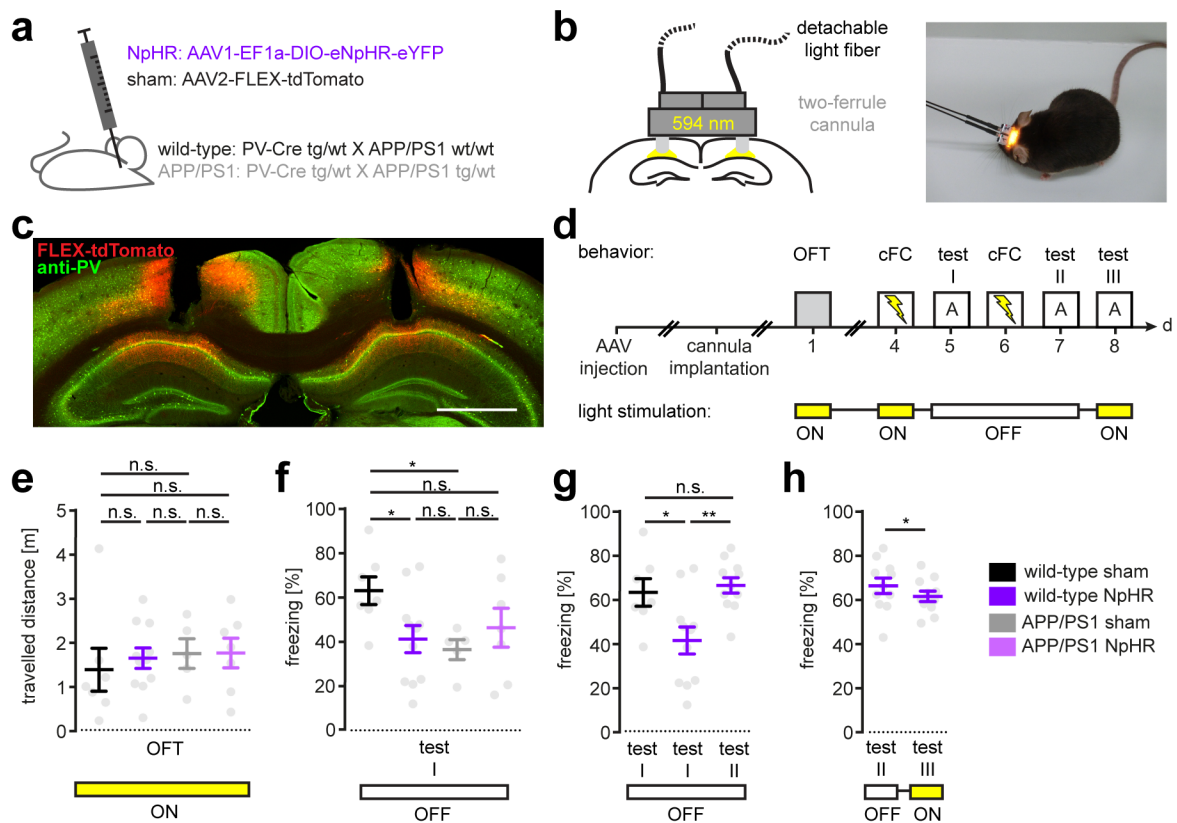


**Figure 3.7 PV<sup>+</sup> interneurons were crucial for memory encoding and retrieval.** (a-d) Experimental approach to selectively inhibit PV-expressing (PV<sup>+</sup>) interneurons in CA1 during learning and memory. (a) Expression of an inhibiting opsin (NpHR) flanked by loxP sites was targeted to PV<sup>+</sup> interneurons CA1 interneurons via bilateral AAV injection into wild-type and APP/PS1 mice. Control mice of both genotypes received a red fluorophore, flanked by loxP sites (sham). (b) Scheme (left) and exemplary picture (right) of an implanted two-ferrule cannula that can be reversibly coupled to a light source. (c) Exemplary confocal image of a coronal section showing tdTomato expression targeted to PV<sup>+</sup> interneurons and the site of implantation. (d) Experimental timeline to manipulate interneuron activity during learning and memory. OFT, open field test; ON (yellow bar), light stimulation; OFF (white bar), no light stimulation. (e) Travelled distances of all experimental groups in an OFT during light stimulation. (f) Freezing behavior of wild-type and APP/PS1 mice, NpHR- and sham- injected, during memory test I (f); \* $p=0.0254$  (wild-type sham vs. wild-type NpHR), \* $p=0.0248$  (wild-type sham vs. APP/PS1 sham), all other comparisons resulted in  $p$ -values  $> 0.05$  (n.s.); one-way ANOVA. (g) Freezing behavior of wild-type NpHR-injected mice during test I and III, and sham-injected mice during test I in absence of light stimulation (OFF); \* $p=0.0113$ , \*\* $p=0.0015$ ,  $p=0.6948$ ; one-way ANOVA. (h) Memory retrieval performance of wild-type NpHR-injected mice with (test III, ON) and without (test II, OFF) PV<sup>+</sup> interneuron inhibition; \* $p=0.0403$ , paired t-test. Data from  $n=7$  wild-type sham,  $n=11$  wild-type NpHR,  $n=5$  APP/PS1 sham and  $n=7$  APP/PS1 NpHR mice. Scale bar: 1 mm (c).

stimulate eNpHR-containing PV<sup>+</sup> interneurons (Fig. 3.7b). Control animals underwent the same procedures, with the eNpHR being substituted by a red fluorophore (tdTomato) without any biological effect (sham) (Fig. 3.7a,c). The experimental timeline was chosen to manipulate the activity of PV<sup>+</sup> interneurons during different stages of the behavioral paradigm to elaborate their necessity during learning and memory (Fig. 3.7d). An open field test (OFT) during light stimulation revealed equal exploratory behavior between genotypes, excluding a bias due to motor differences or fiber-attached behavior (Fig. 3.7e). Inhibiting

PV<sup>+</sup> interneurons during memory acquisition resulted in reduced memory retrieval performance in wild-type mice compared to sham mice (**Fig. 3.7f**). Inhibition of PV<sup>+</sup> interneurons during learning in APP/PS1 mice increased their memory retrieval performance, similar to the performance of wild-type sham mice. But an intra-group comparison did not reach significance (**Fig. 3.7f**). Interestingly, the performance of wild-type NpHR mice dropped to the level of APP/PS1 sham mice. Re-conditioning of wild-type mice that previously received inhibition of PV<sup>+</sup> interneurons during learning revealed a reversible effect (**Fig. 3.7g**). Inhibition of PV<sup>+</sup> interneurons during memory retrieval also reduced memory test performance of wild-type mice (**Fig. 3.7h**). This was shown by exposing the same group of wild-type mice again to the conditioned context, with (test III) and without (test II) inhibition of PV<sup>+</sup> interneurons during the test. In APP/PS1 mice, PV<sup>+</sup> interneuron inhibition during retrieval did not influence performance (data not shown). Summarized, the data revealed a crucial role of PV<sup>+</sup> interneurons during learning and memory processes and suggest a causal effect of hypoactive PV<sup>+</sup> interneurons for the memory retrieval impairment of APP/PS1 mice.

### 3.8. Altered synaptic correlates of learning under AD-like conditions

Dendritic spines represent the postsynapse of excitatory neurons and have been shown to exhibit structural plasticity. As a correlate of synapses, spines change their morphology and appearance upon experience in the cortex (Hubener and Bonhoeffer 2010). Structural plasticity of dendritic spines in *stratum radiatum* of the hippocampal area CA1 was recently demonstrated *in vivo* (Gu, Kleiber et al. 2014, Attardo, Fitzgerald et al. 2015). However, conflicting data exist regarding the turnover of dendritic spines in the hippocampus. In the present study, YFP-H transgenic mice were crossbred to APP/PS1 mice resulting in YFP expressing mice, with (APP/PS1) and without disease background (wild-type) (**Fig. 3.8.1a**). The experimental timeline was designed to measure spine density and turnover during baseline (BL) as well as throughout learning and memory (LM) (**Fig. 3.8.1b**). As shown before (see **Fig. 3.4b**) APP/PS1 mice freeze less during exposure to context A two days after (**Fig. 3.8.1c**), but not before conditioning (**Fig. 3.8.1d**). Image stacks spanning the *stratum radiatum* (SR) of CA1 were acquired repetitively from the same region of interest (**Fig. 3.8.1e,f**). Spine density was constant over time in wild-type and APP/PS1 mice, but significantly reduced in APP/PS1 mice (**Fig. 3.8.1g,h**). Interestingly, the decreased spine

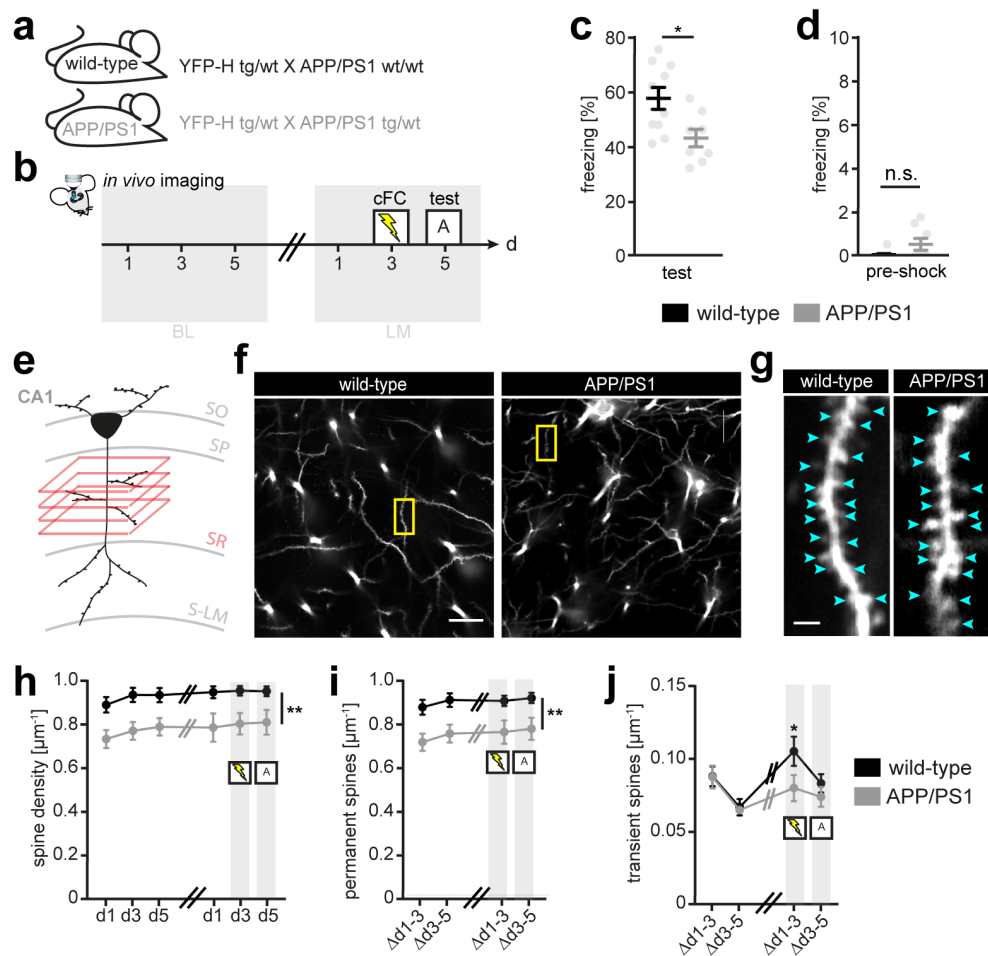


**Figure 3.8.1 Altered structural plasticity in CA1 of APP/PS1 mice.** (a) YFP-H and APP/PS1 transgenic mice were crossbred to obtain YFP-H transgenic mice with (APP/PS1) or without the APP/PS1 transgene (wild-type). (b) Experimental timeline to monitor the fate of dendritic spines during baseline (BL) and learning and memory (LM). (c, d) Freezing behavior of wild-type and APP/PS1 mice before conditioning (d, pre-shock) and during memory test, two days after conditioning (c). Data from  $n=10$  wild-type and  $n=8$  APP/PS1 mice;  $*p=0.0152$  (c),  $p=0.0704$  (d); unpaired t-test. (e) Scheme showing a pyramidal neuron of the hippocampal area CA1. Spine data of CA1 pyramidal neurons were acquired in the *stratum radiatum* (SR). SO, *stratum oris*; SP, *stratum pyramidale*; S-LM, *stratum lacunosum moleculare*. (f, g) Overview images (f) and corresponding excerpts of enlarged dendrites (g) of YFP-H expressing neurons in wild-type and APP/PS1 mice, respectively. (h) Density of dendritic spines throughout the experimental timeline;  $**p=0.0048$  (d1, BL),  $**p=0.0032$  (d3, BL),  $**p=0.0086$  (d5, BL),  $**p=0.0036$  (d1, LM),  $**p=0.0066$  (d3, LM),  $*p=0.0103$  (d5, LM); inter-group comparisons conducted with two-way ANOVA. (i) Densities of permanent spines during BL and LM;  $**p=0.0035$  ( $\Delta d1-3$ , BL),  $**p=0.0049$  ( $\Delta d3-5$ , BL),  $**p=0.0083$  ( $\Delta d1-3$ , LM),  $**p=0.0092$  ( $\Delta d3-5$ , LM), inter-group comparisons conducted with two-way ANOVA. (j) Densities of transient spines during BL and LM;  $p=0.9683$  ( $\Delta d1-3$ , BL),  $p=0.8658$  ( $\Delta d3-5$ , BL),  $*p=0.0366$  ( $\Delta d1-3$ , LM),  $p=0.4334$  ( $\Delta d3-5$ , LM).  $\Delta d1-3$ , interval between day one and day three;  $\Delta d3-5$ , interval between day three and day five. Data from  $n=8$  wild-type and  $n=4$  APP/PS1 mice. Scale bars:  $20 \mu\text{m}$  (f),  $2 \mu\text{m}$  (g).

density mainly originates from a reduction in permanent spines, with a lifetime of two or more days (**Fig. 3.8.1i**). In contrast, transient spines with a lifetime of less than two days are comparable between genotypes during BL (**Fig. 3.8.1i**). However, after cFC the density of transient spines significantly increased in wild-type mice, a change that was absent in APP/PS1 mice (**Fig. 3.8.1i**). In contrast, the density of permanent spines remained constant during

cFC and test (**Fig. 3.8.1h**). Analyzing learning-induced density changes of transient spines revealed that the increase of transient spines was related to significantly more lost spines. The density of gained spines remained constant (**Fig. 3.8.2a-c**). Memory retrieval did not induce any profound changes in spine density (**Fig. 3.8.2d-f**). Summarized, learning induced an increased density of lost spines on the apical dendrites of CA1 pyramidal neurons, whereas memory retrieval did not influence the structural plasticity of spines in *stratum radiatum*.

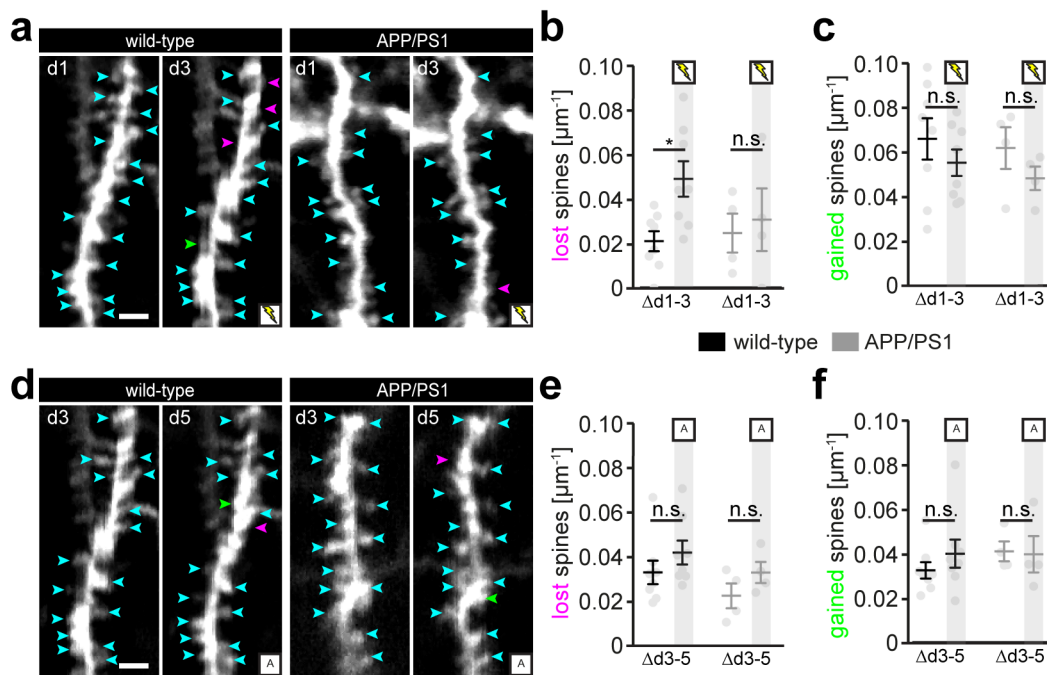


**Figure 3.8.2 Learning-induced spine loss was absent in APP/PS1 mice.** (a) Representative two-photon images of dendrites in SR of wild-type and APP/PS1 mice before (d1) and after cFC (d3). (b,c) Densities of lost (b) and gained (c) spines in wild-type and APP/PS1 mice, respectively. The densities of the first interval ( $\Delta d1-3$ ) during BL and LM (grey shaded) are compared; (b)  $*p=0.0415$  ( $\Delta d1-3$  wild-type, BL vs. LM),  $p=0.7301$  ( $\Delta d1-3$  APP/PS1, BL vs. LM); (c) all comparisons  $p>0.05$  (n.s.), two-way ANOVA. (d) Representative two-photon images of dendrites in CA1 SR of wild-type and APP/PS1 mice during test. (e f) Densities of lost (e) and gained (f) spines in wild-type and APP/PS1 mice, respectively. The densities of the second interval ( $\Delta d3-5$ ) during BL and LM (grey shaded) are compared. All comparisons  $p>0.05$  (n.s.), two-way ANOVA. Data from  $n=8$  wild-type and  $n=4$  APP/PS1 mice. Scale bar:  $2\mu\text{m}$  (a,d).

## 4. DISCUSSION

This study revealed the existence and composition of a cellular engram representing a contextual memory in the CA1 region of the hippocampus of mice. The engram of a recent memory was shown to be rather small, including just 10% of neurons that have been activated during learning. Moreover, the engram itself was intact in a mouse model of AD. Instead, aberrant CA1 network activity resembling a novelty signal was present during memory retrieval, potentially superimposing the engram and hence, causing impaired memory retrieval. Mimicking superimposition in CA1 on different scales indeed induced retrieval impairment in wild-type mice. Additionally, the importance of PV<sup>+</sup> interneurons, a subset of inhibitory neurons, was identified for learning and memory. Pathology in APP/PS1 mice was shown to have no influence on baseline CA1 network activity, measured by fosGFP expression changes. However, fosGFP intensity was decreased in the direct vicinity of A $\beta$  plaques. On the structural level, APP/PS1 mice exhibit a decreased density of spines at apical dendrites in *stratum radiatum* of CA1 pyramidal neurons. Furthermore, learning did not induce the loss of dendritic spines observed in wild-type mice, revealing an experience-dependent network malfunction on the structural level. In summary, the present study provides a novel mechanism for memory impairment in a mouse model of AD: Superimposition of the memory trace. Besides, the importance of inhibitory modulation in the hippocampus during learning and memory was stressed. Both, observed impairments in learning-dependent shaping of dendritic spines and an impaired inhibition provide potential mechanisms underlying the superimposition of the memory trace in CA1 during retrieval in APP/PS1 mice.

### 4.1. Functional and methodological aspects of fosGFP

The mRNA and protein products of immediate early genes are established markers for neurons that have been recently activated (Horn 2004). They represent one of the fastest intracellular expression changes upon neuronal activity and serve as activity footprints. A recent study already examined *Arc* expression in the extrastriate visual cortex repetitively upon visual stimulation (Rudinskiy, Hawkes et al. 2012). However, until now existing methods failed to longitudinally monitor IEG expression dynamics in the hippocampus *in vivo*. Here, we applied a chronic hippocampal window to repetitively examine the same neuronal populations with two-photon microscopy. This allowed to monitor neuronal activity for an

infinite number of points in time, thus enabling the observation of the baseline and experience-induced dynamics of fosGFP expression within the same CA1 pyramidal neurons. We demonstrated the reliability of fosGFP as a marker for endogenous Fos (**Fig. 3.1**). FosGFP visualizes neurons that had been recently activated and provides an integral of multiple calcium events. Sophisticated methods exist to visualize almost real-time activity of neurons via imaging of calcium dynamics. However, this involves either head fixation or connection to a mobile microscope, approaches that imply extensive habituation of the animal. The delay of fosGFP expression allows the separation of the behavioral experiment and the imaging session, reducing behavioral bias by the imaging procedure or vice versa. After cFC, fosGFP required around 1.5 hours to be expressed in CA1 pyramidal neurons *in vivo* (**Fig. 2.4e**). This is in line with a study examining fosGFP expression in the paraventricular nucleus upon a dehydration stimulus and subsequent water deprivation *in vivo* (Barth, Gerkin et al. 2004). Fluorescence signal decline was detectable on average six hours after onset of fosGFP expression (**Fig. 2.4e**). The chosen imaging time intervals were adapted to the fosGFP expression dynamics and were well suited to monitor daily fosGFP expression changes within the neuronal population of CA1 neurons.

## 4.2. Influence of amyloid- $\beta$ pathology on fosGFP expression

Neurons residing close ( $< 50 \mu\text{m}$ ) to MeXO4-positiv amyloid- $\beta$  ( $\text{A}\beta$ ) plaques showed a decreased fosGFP fluorescence intensity compared to neurons distant ( $> 50 \mu\text{m}$ ) to  $\text{A}\beta$  plaques, which hints at neuronal hypoactivity. To exclude random occurrence of low-fluorescent spots, the intensity distribution of fosGFP expressing neurons was examined also in wild-type mice in dependence to randomly placed virtual plaques. Here, no intensity distribution difference was observed. The finding of hypoactivity corresponds to a study performing calcium imaging in the hippocampus of AD mice. They reported an increased fraction of neurons with low activity  $< 60 \mu\text{m}$  around  $\text{A}\beta$  plaques (Busche, Chen et al. 2012). The definition of the silent population of neurons comprised those having 0 - 0.2 calcium transients per minute. The observed population of neurons with reduced fosGFP expression might represent a population with a low firing frequency caused by soluble  $\text{A}\beta$ . Possible mechanisms leading to neuronal hypoactivity are potentially driven by soluble  $\text{A}\beta$  oligomers, that were reported to form a high-concentration halo around  $\text{A}\beta$  plaques, composing a toxic microenvironment (Koffie, Meyer-Luehmann et al. 2009).  $\text{A}\beta$  plaque cores itself have been

shown to be largely inactive (Shankar, Li et al. 2008). Oligomeric A $\beta$  was shown to induce internalization of NMDA receptors (NMDARs), one of the main glutamate ionotropic receptors (Snyder, Nong et al. 2005). This can cause reduced glutamatergic transmission (Freir, Holscher et al. 2001), causing synaptic failure, which in turn can lower the input of an affected neuron, decrease its firing and consequentially cause decreased activation of the *c-fos* promoter, explaining reduced fosGFP fluorescent intensity. The internalization of NMDARs can also have a direct effect on Fos expression, since NMDAR-dependent Ca<sup>2+</sup> influx and subsequent downstream signaling mainly drive *c-fos* promoter activation. Thus, a reduction of NMDARs on neurons residing close to A $\beta$  plaques and hence, to oligomeric A $\beta$ , can account for reduced fosGFP expression. Besides neuronal hypoactivity, several studies additionally reported neuronal hyperactivity in the proximity to A $\beta$  plaques. This was assessed utilizing a calcium indicator dye in the cortex (Busche, Eichhoff et al. 2008) and hippocampus (Busche, Chen et al. 2012) of diseased mice *in vivo*. They revealed neuronal hyperactivity, defined by increased spontaneous firing frequency, to be elicited by soluble A $\beta$ . However, they also detected a fraction of hypoactive neurons in proximity to A $\beta$  plaques (Busche, Eichhoff et al. 2008). Furthermore experience-dependent *Arc* expression was found to reflect the findings obtained with Ca<sup>2+</sup>-imaging (Rudinskiy, Hawkes et al. 2012). Hyperactivity was not reflected by fosGFP expression in the present study. The different readouts can provide a possible explanation for this discrepancy. Another argument could be that the observed calcium transients were not sufficient to evoke *c-fos* promoter activation. Additionally, compensatory mechanisms might play a role in regulating the activity-dependent fosGFP expression and prevent a linear relationship between neuronal activity and promoter activation (Robertson, Kerppola et al. 1995). The density of fosGFP expressing neurons was not altered in the direct vicinity to A $\beta$  plaques. This is in accordance with previously published data, which reported neuronal loss to be moderate (Jackson, Rudinskiy et al. 2016) or not existing (Rudinskiy, Hawkes et al. 2012) in the mouse model of AD utilized in this study. Taken together, reduced fosGFP expression in APP/PS1 mice indicates an imbalance in neuronal communication potentially mediated by oligomeric A $\beta$ .

### 4.3. CA1 network dynamics

Two different populations of CA1 neurons have been identified, regarding their activity: the population with variable activity (ON and OFF) indicates that it acts as a reservoir of neurons

that easily adapt to externally induced changes like novel experiences. The continuously active population (CON) represents the major fraction and might comprise neurons that constitute the backbone of the hippocampal network necessary to provide baseline computation. The fact that the sizes of ON, OFF and CON fractions stay constant over five days reveals the enormous stability of the hippocampal network. Until the development of longitudinal activity measurements that allow the tracking of a high number of individual neurons over long time-periods *in vivo*, the dynamics of activity could not be assessed (Lütcke, Margolis et al. 2013). It is a well accepted assumption that large neuronal networks achieve a continuous trade-off between stability and flexibility, to meet the demands of mnemonic as well as adjustment tasks (Lütcke, Margolis et al. 2013). The analysis of fosGFP expression changes neglects the fate and history of a neurons activity and just counts the daily fractions of neurons being recruited to (ON), released from (OFF) or kept (CON) in the active network. This means that neurons that keep their expression from one to the other day (CON) may lose it on the next (OFF) or even gain expression again (ON) and hence, might not belong to the permanent stable subset. However, considering the average fosGFP expression duration of every individual CA1 neuron revealed that the CON fraction mainly consisted of neurons continuously expressing fosGFP. Re-examining this population three weeks later further emphasizes this robust stability. Indeed, around 60% of the initial population was still active during another five-day imaging period (**Fig. 3.3h**). Whether these neurons are active members in an oscillating network or represent a spatial component of the mice's daily environment, *i.e.* their home cage, needs to be further examined. The latter would ascribe place cell activity to this neuronal population. Long-term monitoring of place cell activity revealed that spatial information is represented by a unique neuronal population, with a daily overlap of around 15-25% (Ziv, Burns et al. 2013). However, several studies suggest that information coding is performed by a flexible pool of potential participants, that itself is constant in size but varies in the place field of individual neurons (Lütcke, Margolis et al. 2013). That would imply that the place field does not necessarily need to be represented by a particular neuron. Rather the participation of the neuron in any place field represents the stable component. It is tempting to speculate that such a pool of neurons with flexible place fields is represented by the continuously fosGFP<sup>+</sup> fraction, making up around 40% of fosGFP expressing neurons. The characterization of this population according to their spatial firing properties would need further examinations, e.g. with the expression of red-fluorescent GECIs in fosGFP mice. Moreover, this questions the spatial coding properties of the learning and

memory responsive fraction, the variable population (ON, OFF). As the potential engram belongs to this category, one would attribute it a mnemonic role. However, mnemonic coding does not necessarily exclude spatial coding. In fact, spatial firing was reported to induce LTP *in vitro* (Isaac, Buchanan et al. 2009). Likewise, to make a statement concerning spatial coding properties of fosGFP<sup>+</sup> neurons, further examination of fosGFP inducing activity is required. This will further help to classify fosGFP<sup>+</sup> neurons into different functional classes. *In vitro* electrophysiological data show *c-fos* gene expression after burst activity with 30 or more action potentials at frequencies of 10 Hz or more (Schoenenberger, Gerosa et al. 2009). This hints at Fos expression as a result of repetitive strong neuronal firing, including the possibility of a spatial component. In contrast, sub threshold oscillatory activity is thereby less likely to induce Fos expression. It is known that A $\beta$  pathology relates to profound alterations in neuronal network activity (Palop, Chin et al. 2006). Here, baseline fosGFP expression changes and the average expression duration of fosGFP were similar in wild-type and APP/PS1 mice. This either suggests that the current fosGFP mouse model combined with the applied method of analysis is inadequate to resolve changes in network activity, or that the activation of the *c-fos* promoter itself is unable to mirror pathology-induced neuronal network alterations.

#### 4.4. FosGFP expression changes during learning and memory

An increased number of ON neurons was observed after contextual fear conditioning (cFC) in wild-type and APP/PS1 mice. Increase of Fos expression after cFC was described before (Radulovic, Kammermeier et al. 1998, Tronson, Corcoran et al. 2012) and was attributed to the exploration of the yet novel context rather than to the aversive stimulus (Radulovic, Kammermeier et al. 1998, Deng, Mayford et al. 2013). Here, no difference was observed between wild-type and APP/PS1 mice indicating an intact response of CA1 neuronal activity after context exploration and hence, providing the prerequisite for contextual memory encoding. However, our method does not provide information about downstream signaling processes, leading to memory consolidation, such as strengthening of connections and concomitant structural changes. On the day after cFC the network returned to baseline state with an increased OFF fraction reducing the number of active neurons to the level observed during baseline. Memory retrieval led to a less pronounced increase of ON neurons, compared to the one induced by memory acquisition. Interestingly, the response was comparable in wild-type and APP/PS1 mice. Intact neuronal response during retrieval implies successful

encoding and consolidation. This led to the conclusion that the general network activity measured by fosGFP expression changes does not reflect the memory retrieval impairment of APP/PS1 mice on the behavioral level. Therefore, the following analysis focused on the activity of individual neurons and their fate during learning and memory.

#### 4.5. Characteristics of the reactivated neuronal ensemble

A long-standing concept is that neuronal populations active during learning will be reactivated during memory retrieval. This was shown for the amygdala and different cortical and hippocampal regions (Reijmers, Perkins et al. 2007, Deng, Mayford et al. 2013, Tayler, Tanaka et al. 2013, Denny, Kheirbek et al. 2014). The size of the reactivated ensemble strongly depends on its information content, the brain region, the time between events and, not negligible, the method for labeling neurons and defining reactivation (Josselyn, Köhler et al. 2015). The reactivated ensemble was often calculated by the overlap of active neurons in a particular brain region during two events, learning and memory test. Auditory fear conditioning followed by retrieval three days later e.g. revealed a neuronal overlap of ~13% in the basolateral amygdala (Reijmers, Perkins et al. 2007). Memory test after contextual fear conditioning induced a fraction of 40% reactivated neurons in hippocampal CA1 region. Irrespective of whether the memory test was carried out after two days (recent memory) or 14 days (remote memory) (Tayler, Tanaka et al. 2013). However, both studies used the tetracycline-dependent transactivator (tTA) system that utilizes an IEG promoter for experience-dependent tagging of neuronal populations (TetTag system). This system requires the continuous supply of doxycycline (DOX) to restrict expression to a specific DOX free time window. Nonetheless, this time-window was two to five days long, decreasing the specificity of labeled neurons due to the increased amount of labeled neurons, a phenomenon referred to as “overtagging” (Josselyn, Köhler et al. 2015). Interestingly, the data of the present study revealed about 40% of CA1 neurons in the field of view to be always active, rather than just upon stimulus. Consequentially, the size of the reactivated neuronal population was overestimated by studies just considering two time-points, neglecting the neurons activity history. This finding was confirmed using two different definitions of reactivation to analyze the present data: 70% of fosGFP<sup>+</sup> neurons during cFC also appear fosGFP<sup>+</sup> after retrieval (**Fig. 3.5b,c**). However, this population equals the size of a randomly reactivated population during baseline. Restricting the definition of reactivation to neurons that switch from fosGFP<sup>-</sup>

to fosGFP<sup>+</sup> during cFC and retrieval, revealed a reactivated fraction of 20% (**Fig. 3.5d,e**). Interestingly, the size of this fraction doubled compared to a randomly reactivated population during baseline, suggesting it to be memory-related. Hence, the potential engram was found to consist of around 10% of the initially activated neuronal population, subtracting the randomly activated fraction. This is supported by a study in rats that analyzed spatial firing of CA1 neurons during initial and repeated exposures to an environment. The authors revealed the reactivated population during re-exposure to be rather small with strong spatial tuning, a process that was determined by the initial firing during the first exposure (Karlsson and Frank 2008). This is especially interesting for evaluating the characteristics of memory retrieval, as it supports the view that retrieval is rather a reconstructive than a replicative process (Ben-Yakov, Dudai et al. 2015). This idea is further strengthened by computational approaches, as it is a far more efficient way of storing and associating information (Treves and Rolls 1994). The present study incorporated information about the activity history and fate of individual neurons and thus, provided an accurate estimation of the size of the reactivated neuronal population. The potential engram was found to consist of around 10% of the initially activated neuronal population. Corresponding with the literature, this suggests a refined population with high information content ensuring efficient mnemonic coding.

#### 4.6. Independence of cellular reactivation and memory performance

Strikingly, the current study revealed reactivated pyramidal neurons in the CA1 region of the hippocampus in wild-type and APP/PS1 mice, although their memory test performance differed. An intact engram indeed might serve as a hint for intact consolidation, at least if consolidation is the underlying process for assuring reactivation of the potential engram (Ryan, Roy et al. 2015). Recently, it was shown that the synaptic connectivity between EC-DG neuronal assemblies was impaired in the same mouse model of AD. However, direct optogenetic stimulation of DG engram neurons during retrieval was sufficient to rescue the memory deficit. Simultaneous stimulation of EC and DG engram ensembles furthermore revealed an intact connectivity between both regions. However, the connectivity was not strong enough to accomplish retrieval by natural cues (Roy, Arons et al. 2016). Furthermore it was shown that DG engram cells inherit a certain synaptic connectivity, whose strength is increased upon learning. Anisomycin treatment, a common applied protein synthase inhibitor, prevented strengthening but not the disruption of the connectivity itself (Ryan, Roy et al.

2015). Taken together, the above-mentioned studies including the present suggest a deficit in the molecular response signals regulating synaptic strength rather than deficient structural connectivity *per se*. It was found that reactivation of CA1 neurons is necessary and sufficient for memory retrieval (Goshen, Brodsky et al. 2011, Ramirez, Liu et al. 2013). Of course, one has to keep in mind that the recruitment of CA1 neurons is just one part of a brain-wide engram, possibly starting in the sensory regions of the cortex further processed by the EC that provides input to the hippocampal trisynaptic circuit and also directly to CA1. For CA3 and EC, it has been shown that their inputs on CA1 dendrites are precisely timed to induce dendritic plateau potentials that itself provide a mechanism for feature selectivity (Bittner, Grienberger et al. 2015). Monitoring those events goes beyond the temporal resolution of the model applied in the current study, as the activation of neurons *per se*, does not reveal their temporal precision. An impairment of this complex circuitry with its necessity for synchrony provides a possible mechanism for memory retrieval impairment. Hence, the cellular reactivation observed in this study might happen independent of retrieval performance, but might be just not properly timed and not strong enough to provoke successful memory retrieval.

#### 4.7. Analysis of activity patterns

FosGFP expression changes after learning and memory were shown to be comparable between wild-type and APP/PS1 mice. However, differences might occur on the level of individual neurons, hidden within the population average that itself stays constant (Lütcke, Margolis et al. 2013). Therefore an activity pattern analysis was performed taking into account each neurons' individual activity history and fate. Assuming a single neuron has two different activity states (fosGFP<sup>+</sup> and fosGFP<sup>-</sup>) and considering four imaging time-points, containing cFC and test, resulted in 16 possible patterns of activity (**Fig. 6.2a,b**). The graph depicting the relative frequencies of every pattern during the baseline period (BL, light grey) suggests no differences between wild-type and APP/PS1 mice, further confirming the finding of an intact home cage network (**Fig. 6.2c,d**). During the cFC-test period (A-A/B) the relative frequency of the reactivation pattern (pattern C) increased clearly in both genotypes, compared to BL. Remarkably, this was the only out of 15 different patterns with increased frequency in wild-type mice that successfully learned. This finding underscores that pattern C is specifically attributable to the process of memory retrieval, and further corroborates that

neurons exhibiting this activity pattern compose the memory trace. Moreover, APP/PS1 mice exposed to the conditioned context and wild-type mice exposed to a novel context shared an additional pattern that was found to be elevated. Their retrieval network contained newly recruited neurons that did not show activity before (Pattern F) (**Fig. 3.5f,g** and **Fig. 6.2d,e**). This led to the assumption that the additional activity rather than the absence of the engram itself might reflect the retrieval impairment on the cellular level.

#### 4.8. The importance of purity for the retrieval network

As the potential engram was intact in APP/PS1 mice, the behavioral differences may relate to the cellular composition of the retrieval network. Indeed, as the activity pattern data suggested before (**Fig. 3.5f,g**, **Fig. 3.6.1d**), the pattern F was found to be additionally upregulated in the retrieval network of APP/PS1 mice, comprising neurons that were present only after retrieval (retrieval-only neurons, RONLY). It was shown before that artificial brain-wide activation of a false engram during memory retrieval in the conditioned context led to impaired retrieval performance (Garner, Rowland et al. 2012). However, the current data demonstrated that superimposition of memory information by activating excitatory neurons exclusively in CA1 is sufficient to induce retrieval impairment (**Fig. 3.6.2**). Even decreasing the activated population to a more specific choice, *i.e.* context B encoding neurons, caused a decreased retrieval performance (**Fig. 3.6.3**), emphasizing the necessity of a pure engram. It is known that the response of CA1 is less pronounced during exposure to a familiar, compared to a novel environment (Karlsson and Frank 2008). This might involve a refinement of the responding population by “inverse synaptic tagging” on the synaptic scale (Morin, Guzman-Ramos et al. 2015). One of the mechanisms that provide ensemble-shaping functions is the Arc-dependent induction of LTD. As revealed by a study (Jakkamsetti, Tsai et al. 2013), activity-dependent dendritic Arc expression is involved in priming neurons activated by an experience. Re-exposure to the same environment induced LTD via an mGluR1 (group 1 metabotropic glutamate receptor)-dependent mechanism that required Arc (Jakkamsetti, Tsai et al. 2013). Further mechanisms have been described that prime neurons by changing their input receiving compartments influencing the dendrites’ spine composition (Okuno, Akashi et al. 2012) (see also **4.14.**). However, a change in spine composition can lead to a strengthening or weakening of neuronal connections and thus, to a refinement of the responding neuronal population. The presence of ensemble shaping mechanisms further

underscores the necessity for a pure engram, shaped by experience. This led to the hypothesis that the CA1 immanent, non memory-specific activity in the retrieval network of APP/PS1 mice was based on an impairment of ensemble shaping activity after learning. This further led to superimposition of the memory information and ultimately, to a memory retrieval deficit.

#### 4.9. The characteristics and regulation of potential superimposition

The data of the present study strongly suggest that the superimposing neurons encode a novelty signal. Exposing mice to a novel environment, either context A or context B, induced increased fosGFP expression, whereas exposure to a familiar environment did not increase the number of fosGFP expressing neurons. This is in line with a study examining Fos expression after both conditioning and retrieval (Radulovic, Kammermeier et al. 1998). Another study demonstrated that CA1, but not CA3 produced twice as many spikes in a novel, compared to a familiar environment (Karlsson and Frank 2008), which is further emphasized by the finding that novelty-related dopamine release in the nucleus accumbens requires hippocampal activity (Legault and Wise 2001). Taken together, this suggests that high CA1 activity provides the neuronal correlate of a novelty signal. This raises the questions how CA1 judges about novelty or familiarity of an experience, and how this mechanism is impaired under AD-like conditions. Reliably answering this questions still demands further investigations.

#### 4.10. False mismatch detection in Alzheimer's disease

The assessment of information regarding its novelty involves the comparison of expectations dependent on past experiences, with newly incoming information, a task hypothesized to be carried out by the hippocampal CA1 region (Lisman and Otmakhova 2001). The present study discovered reactivated neurons in CA1 of mice during memory test, independent of their retrieval performance (**Fig. 3.5e**). Those possibly represent the internal hippocampal representation of the past experience in context A. Data of the current study indicate that either context re-exposure (context A) or exposure to a different but similar context (context B), triggers cellular recall of related representations (here: context A). This allows CA1 to compare both inputs: If the newly incoming information equals existing memories (match), CA1 will relay just the mnemonic information leading to a learned behavioral output (wild-type A-A). If the incoming information differs from existing memories (mismatch), CA1 will broadcast a general novelty signal (Larkin, Lykken et al. 2014) that is hypothesized to

superimpose information of related memories. It is tempting to speculate that superimposition presents the output signal of false mismatch detection in CA1 during familiar context exploration in APP/PS1 mice. A mismatch-detecting property of CA1 was demonstrated before in mice and even in humans (Schacter, Curran et al. 1999, Kumaran and Maguire 2006, Duncan, Ketz et al. 2012). The increase in fosGFP expression after retrieval in the conditioned context A in APP/PS1 mice was not as pronounced as in wild-type mice exposed to a novel context B (**Fig. 3.4e-g**). However, as their freezing rates also differ, this might reflect a difference in superimposition strength. APP/PS1 mice indeed learned and showed higher freezing rates than mice exposed to a novel context, but nevertheless display impaired memory retrieval. Furthermore, the retrieval network of APP/PS1 mice shared cellular features with mice experiencing a novel environment, represented by a population of newly fosGFP<sup>+</sup> neurons (RONLY). RONLY neurons were just found elevated in the retrieval network of mice with no (wild-type A-B) or impaired memory (APP/PS1 A-A). It potentially comprises the novelty and “false” novelty encoding population in wild-type mice exposed to a novel context B and APP/PS1 mice exposed to the conditioned context A, respectively. It is still under debate, how exactly CA1 computes this comparator function. However, its multilayered structure with various multi-sensory inputs from several near and distant regions (Lee, Marchionni et al. 2014), predicts the underlying complexity of signal transformation and propagation within CA1 (Butler and Paulsen 2014). Its two main input regions provide sensory (EC layer 3, EC3) as well as mnemonic (CA3) information input, thus meeting the structural prerequisite for CA1 as comparator. An interesting study recorded local field potentials (LFPs) from several layers of CA1, CA3 and EC3, simultaneously. They found that gamma oscillatory input from EC3 and CA3 arrives precisely timed, and is coupled to distinct theta-phases at their target compartments, SLM and SR, respectively (Schomburg, Fernández-Ruiz et al. 2014). This describes a potential way of information processing within CA1 (Butler and Paulsen 2014), which both is fine-tuned and prone to disturbances and, hence, provides a possible element of the false mismatch detection observed in APP/PS1 mice in this study. Summarized, the current study strongly points to superimposition being a normal phenomenon for dealing with novel experiences mismatching expectations. The raise of activity in CA1 opens a window of increased plasticity (Lisman and Otmakhova 2001) superimposing associations of similar memories and facilitating the encoding of new information. However, the superimposing activity in CA1 of APP/PS1 mice during retrieval denotes a failure in learning-induced ensemble shaping activity, producing a weak contextual

memory. The instability of the memory causes false mismatch detection, which leads to superimposition and further weakening of the memory. Therefore, superimposition represents a disease-relevant phenomenon affecting memory under AD-like conditions.

#### 4.11. Role of PV<sup>+</sup> interneurons during learning and memory

The term “memory trace” intentionally simplifies the complexity of a neuronal network providing a brain-wide neuronal assembly that forms a memory. The focus is mainly directed on the immediate learning-mediated responses of excitatory principal neurons. However, the modulating and shaping activity of inhibitory interneurons on principal cell output must not be neglected. PV-expressing (PV<sup>+</sup>) interneurons have been shown to precisely regulate CA3 excitatory activity during learning, consolidation and memory processes (Donato, Rompani et al. 2013). In the present study it was demonstrated that PV<sup>+</sup> interneuron activity in CA1 is necessary for successful learning and retrieval. PV<sup>+</sup> interneuron inhibition during learning in wild-type mice reduced their memory retrieval performance on the next day to the level of APP/PS1 mice. This finding suggests an indispensable role of inhibitory drive during memory acquisition and hints at a possible role of PV<sup>+</sup> interneuron malfunction in APP/PS1 mice. Furthermore, inhibition of PV<sup>+</sup> interneuron impaired memory retrieval in wild-type mice. In our lab it was demonstrated that PV<sup>+</sup> interneuron inhibition in CA1 led to an increased firing rate of CA1 pyramidal neurons (data not shown). This increased activity of CA1 pyramidal neurons during retrieval might superimpose the memory information. It was hypothesized that CA1 receives constant inhibition and that new events open a temporally restricted window of increased plasticity by disinhibition (Agerskov 2016). The present study supports the hypothesis that PV<sup>+</sup> inhibitory interneurons regulate the CA1 plasticity window. Whether impaired inhibitory drive by PV<sup>+</sup> interneurons during retrieval contributes to the retrieval network impurity observed in APP/PS1 mice needs to be further examined. Finally, feedback stimulation of PV<sup>+</sup> interneurons with the aim to support and prolong exploration-dependent theta activity in APP/PS1 mice led to a rescue of their novel object recognition memory to the levels of wild-type mice (data not shown), confirming their necessity during learning in an mouse model of AD.

#### 4.12. Monitoring structural plasticity of CA1 dendrites

It was of major interest how input-receiving dendritic spines are influenced by learning and memory, and whether structural differences between wild-type and APP/PS1 mice provide evidence for underlying behavioral differences. Morphological changes in spines, which represent the postsynaptic part of potential synapses, have been shown to underlie and reflect physiological changes (Alvarez and Sabatini 2007). In the hippocampus, LTP was associated with the stabilization of existing and the growth of new spines, as revealed in hippocampal organotypic slice cultures (Engert and Bonhoeffer 1999). Long-term monitoring of baseline hippocampal structural plasticity via two-photon *in vivo* imaging has been achieved for basal (Attardo, Fitzgerald et al. 2015) as well as apical dendrites (Gu, Kleiber et al. 2014). However, learning- and memory-induced changes in the hippocampus *in vivo* have not been reported so far. In cortical regions experience-induced changes in spine number and shape were shown to occur not earlier than two days after learning *in vivo* (Lai, Franke et al. 2012). Therefore, the interval for monitoring spine changes in this study was chosen to cover two days. However, we cannot exclude that experience-induced changes on CA1 dendrites in *stratum radiatum* manifest earlier. An influence of the imaging procedure itself can be excluded, as densities and structural changes within groups showed no change over time during baseline imaging. All experience-induced structural changes have been referenced to baseline data, further avoiding a bias of data by the experimental approach. A possible influence of the imaging itself would hence be a systematic error present in all variables. Taken together, *in vivo* two-photon microscopy, combined with behavioral experiments, provide a valuable tool for monitoring experience-induced structural plasticity.

#### 4.13. Reduced spine density on CA1 pyramidal neuron dendrites

The present study revealed a reduced spine density on apical dendrites residing in SR of CA1 pyramidal neurons in APP/PS1 mice, which is in line with previous studies analyzing spine densities in the hippocampus (Bittner, Fuhrmann et al. 2010) and apical tufts of layer V pyramidal neurons in APP/PS1 mice (Zou, Montagna et al. 2015) and other rodent AD models (Shankar, Li et al. 2008, Palop and Mucke 2010). The present study extends previous results by showing that the reduction of total spines in APP/PS1 mice affects rather the stable than the transient population of dendritic spines. In the cortex, reduced spine density was attributed to a decrease in spine formation within 29 days (Zou, Montagna et al. 2015). This

raises the question whether the population of permanent spines observed in our study might also underlie a turnover, but with slower dynamics that cover not one, but several weeks. Consequentially, a reduced density in the stable spine population might also be caused by a reduction of spine formation. However, it is debatable whether spines in different brain regions have the same dynamics (Attardo, Fitzgerald et al. 2015). Thus, further investigation is necessary to clarify the question of long-term dynamics of hippocampal spines. Furthermore, the low resolution of two-photon microscopy, especially along the z-axis, might underestimate the density as well as turnover of spines, which might account for conflicting results (Attardo, Fitzgerald et al. 2015). However, in the present study wild-type and APP/PS1 mice were compared using the same imaging and analysis procedures. This might include a resolution-based systematic error, but does not exclude validity of the comparison. Many studies investigated possible mechanisms causing reduced spine densities in mouse models of AD. The presence of A $\beta$  oligomers was suggested to have a causal role in reducing spine densities. Oligomeric A $\beta$  was shown to induce internalization of NMDA receptors (NMDARs), one of the main glutamate ionotropic receptors (Snyder, Nong et al. 2005). This can cause reduced glutamatergic transmission (Freir, Holscher et al. 2001), leading to synaptic failure and hence, decreased densities of spines on hippocampal dendrites in rodents (Shankar, Li et al. 2008, Palop and Mucke 2010). Additionally, A $\beta$  oligomers were shown to alter the localization of NMDA receptors, thereby destabilizing spines (Um, Kaufman et al. 2013). It is assumed that stable spines take over mnemonic roles, in keeping life-long memories (Yang, Pan et al. 2009). The fact that exactly this population might be affected in the mouse model of AD emphasizes the severity of this structural impairment.

#### 4.14. Role of spine loss in learning

The present study demonstrated an increased density of lost spines after contextual fear conditioning (cFC) on apical dendrites of CA1 pyramidal neurons in wild-type, but not APP/PS1 mice *in vivo* (**Fig. 3.8.2b**). Previous studies demonstrated selective dendritic spine loss after fear conditioning on layer V pyramidal neurons in the frontal association cortex of mice *in vivo* (Lai, Franke et al. 2012), suggesting similar underlying mechanisms for learning-induced structural plasticity in the hippocampus and cortex. The loss of synapses was hypothesized to occur concomitant to selective strengthening of neighboring synapses, which is in line with electrophysiological data showing that learning-related LTP occurs just in a

subset of synapses (Whitlock, Heynen et al. 2006). Indeed, another study revealed spine reduction in the hippocampus that was found to be selective to active learning circuits. They hypothesized spine elimination as a mechanism to counteract the selective strengthening of learning-related synapses to retain a constant level of synaptic inputs (Sanders, Cowansage et al. 2012). Expression of the IEG Arc was described to fulfill such a refinement of synaptic connectivity. Accumulating after activity, it binds preferentially to inactive  $Ca^{2+}$ -free forms of CamKII $\beta$ , thereby mediating AMPA receptor endocytosis at silent synapses (Kim, Okuno et al. 2012). This selective elimination was named “inverse synaptic tagging” and has the potential to increase the contrast of synaptic weights (Kim, Okuno et al. 2012). Alterations in any of the participants that mediate synaptic shaping might cause alterations in mnemonic function. Indeed, the general expression of Arc was shown to be reduced in a triple transgenic mouse model of AD (Morin, Diaz-Cintra et al. 2016) and additionally revealed to be altered by A $\beta$  plaque pathology in the mouse visual cortex (Rudinskiy, Hawkes et al. 2012). The absence of this selective structural regulation of synaptic connections in APP/PS1 mice reflects their learning deficit on the structural level. The present study analyzed dendrites regardless of their vicinity to A $\beta$  plaques. Moreover, it was suggested that neural circuit impairments are A $\beta$  plaque-independent at a late-stages of pathology (Hsia, Masliah et al. 1999). However, we cannot exclude that the observed alterations in structural plasticity are even more pronounced in the direct vicinity to A $\beta$  plaques. Furthermore, the current study revealed learning-dependent changes in the transient rather than in the persistent fraction of spines in wild-type mice. The sizes of transient spine populations were comparable in wild-type and APP/PS1 mice during BL. However, the learning-dependent change was absent on dendrites of APP/PS1 mice. It is tempting to speculate that the reduction of the stable population might alter the general spine homeostasis, thus impairing experience-dependent shaping in APP/PS1 mice. However, this hypothesis needs further investigation.

## 5. CONCLUSIONS AND OPEN QUESTIONS

The current thesis identified a novel mechanism for memory impairment in a mouse model of AD. Moreover, a cellular engram of a contextual memory was detected in the CA1 region of the hippocampus. The engram was intact under AD-like conditions. However, additional neuronal activity during memory retrieval was found to superimpose the mnemonic information, impairing successful retrieval. This additional activity in CA1 resembled a novelty signal, suggesting false mismatch detection during familiar context exploration. Indeed, structural alterations of dendritic spines on CA1 pyramidal neurons and impaired inhibitory drive of PV<sup>+</sup> interneurons represented potential features underlying the alterations on the activity level. The absence of learning-dependent spine loss on apical dendrites in *stratum radiatum* of CA1 pyramidal neurons under AD-like conditions indicates malfunctioning intrinsic signaling mechanisms that interfere with the strengthening of memory-relevant connections. This provides a prerequisite for impaired input on CA1 pyramidal neurons and hence, strengthens the hypothesis of false mismatch detection. Moreover, impaired inhibition by PV<sup>+</sup> interneurons during memory acquisition and retrieval might prevent the refinement of inputs on dendrites of CA1 pyramidal neurons, necessary for successful learning and memory retrieval.

The molecular mechanisms underlying the observed malfunctioning dendritic spine remodeling and their impact on the alteration on the activity level need further examination: on the one hand, to clarify the relationship of both, on the other hand, to verify the exact role of amyloid- $\beta$  in mediating the observed impairments. This is of major importance for developing treatment strategies that aim at the prevention of synapse malfunctions induced by amyloid- $\beta$ . Besides, the deficits of PV<sup>+</sup> interneurons in refine memory traces under AD-like conditions need further investigation to draw conclusions about their involvement in dendritic spine remodeling. Moreover, the validity of the hypothesized false mismatch detection in CA1 needs to be tested. For this, electrophysiological methods as well as multi-color GECI approaches are well suited to analyze the strictly timed and compartmentalized inputs of CA3 and EC on CA1 pyramidal neurons, that are suggested to malfunction under AD-like conditions. In addition, the characterization of fosGFP signals, e.g. by recording calcium transients from the same neuronal subsets, is of major interest. This will help to further testify spatial tuning of fosGFP<sup>+</sup> neurons in general and with respect to the potential memory trace observed in this study.

## 6. APPENDIX

### 6.1. Abbreviations

<b>AAV</b>	adeno-associated virus
<b>A<math>\beta</math></b>	amyloid- $\beta$
<b>AchE</b>	acetylcholinesterase
<b>AD</b>	Alzheimer's disease
<b>APOE</b>	apolipoprotein E
<b>APP</b>	amyloid precursor protein
<b>APP/PS1</b>	APP <sup>swe</sup> /PS1 <sup>dE9</sup>
<b>APP<sup>swe</sup></b>	APP with the swedish mutation
<b>Arc</b>	activity-regulated cytoskeleton-associated protein
<b>AU</b>	arbitrary units
<b>BACE</b>	b-site APP cleavage enzyme
<b>BBB</b>	blood brain barrier
<b>BG</b>	background fluorescence
<b>BL</b>	baseline
<b>BP</b>	band pass filter
<b>BSA</b>	bovine serum albumine
<b>CA1</b>	<i>cornum ammonum 1</i>
<b>CA3</b>	<i>cornum ammonum 3</i>
<b>CamKII<math>\beta</math></b>	calcium/calmodulin-dependent protein kinase type II beta
<b>catFISH</b>	cellular compartment analysis of temporal activity by fluorescent <i>in situ</i> hybridisation
<b>CCK</b>	cholecystokinin
<b>cFC</b>	contextual fear conditioning
<b>CNO</b>	clozapine-N-oxide
<b>DG</b>	dentate gyrus
<b>DIO</b>	double floxed inverse open reading frame
<b>DMSO</b>	dimethyl sulfoxide
<b>Dox</b>	doxycycline
<b>DREADD</b>	designer receptor exclusively activated by designer drugs
<b>EC</b>	entorhinal cortex
<b>EC3</b>	EC layer 3
<b>eGFP</b>	enhanced green fluorescent protein
<b>EOAD</b>	early-onset AD
<b>ERK</b>	extracellular signal-regulated kinase
<b>FBJ</b>	Finkel-Biskis-Jinkins
<b>floxed</b>	flanked by loxP sites
<b>Fos</b>	FBJ osteosarcoma oncogene
<b>fosGFP</b>	fusion construct of Fos protein and enhanced green fluorescent protein
<b>fosGFP<sup>-/+</sup></b>	fosGFP-negative/ -positive
<b>GAD67</b>	67 kDa isoform of glutamic acid decarboxylase
<b>GECI</b>	genetically encoded calcium indicator
<b>GWAS</b>	genome-wide association studies
<b>hM3D(Gq)</b>	mutant variant of the human M3 muscarinic (hM3) receptor, engaging Gq signaling
<b>H.M.</b>	Henry Molaison
<b>i.p.</b>	intraperitoneal
<b>IEG</b>	immediate early gene
<b>ires</b>	internal ribosomal entry site
<b>ITR</b>	inverted terminal repeats

<b>LA</b>	lateral amygdala
<b>LM</b>	Learning and memory
<b>LOAD</b>	late-onset AD
<b>loxP</b>	locus of X-over P1
<b>LP</b>	long pass dichroic mirror
<b>LTD</b>	long-term depression
<b>LTP</b>	long-term potentiation
<b>MAPK</b>	mitogen-activated protein kinase
<b>MeXO4</b>	methoxy-XO4
<b>MF</b>	mossy fibers
<b>mGluR1</b>	group 1 metabotropic glutamate receptor
<b>MIP</b>	maximum intensity projection
<b>MPR</b>	massive parallel resequencing
<b>MTL</b>	medial temporal lobe
<b>NaCl</b>	sodium chloride
<b>NFT</b>	neurofibrillary tangles
<b>NMDA(R)</b>	N-methyl-D-aspartate (receptor)
<b>eNpHR</b>	modified form of halorhodopsin from <i>natronomonas</i>
<b>OFT</b>	open field test
<b>pA</b>	polyadenylation site
<b>PBS</b>	phosphate buffered saline
<b>PET</b>	positron emission tomography
<b>PFA</b>	paraformaldehyde
<b>PP</b>	perforant path
<b>PSEN1dE9</b>	mutant presenilin 1 with a deletion of exon 9
<b>PV</b>	parvalbumin
<b>PV+</b>	parvalbumin-expressing
<b>REAH</b>	fosGFP <sup>+</sup> neurons with reactivation history
<b>RH</b>	relative humidity
<b>RN</b>	retrieval network
<b>ROI</b>	region of interest
<b>RONLY</b>	neurons being fosGFP <sup>+</sup> during retrieval only
<b>rpm</b>	rounds per minute
<b>RT</b>	room temperature
<b>S-LM</b>	<i>stratum lacunosum moleculare</i>
<b>s.c.</b>	subcutaneously
<b>SC</b>	Schaffer collaterals
<b>SEM</b>	standard error of the mean
<b>SO</b>	<i>stratum oriens</i>
<b>SOM</b>	somatostatin
<b>SP</b>	<i>stratum pyramidale</i>
<b>SR</b>	<i>stratum radiatum</i>
<b>TH</b>	threshold
<b>tTA</b>	tetracycline-controlled transactivator
<b>Vglut2</b>	vesicular glutamate transporter 2
<b>WPRE</b>	woodchuck hepatitis virus posttranscriptional regulatory element
<b>YFP</b>	yellow fluorescent protein
<b>ZEN</b>	Zeiss efficient navigation

## 6.2. Supplementary data

### 6.2.1. Intra-group changes in fosGFP expression

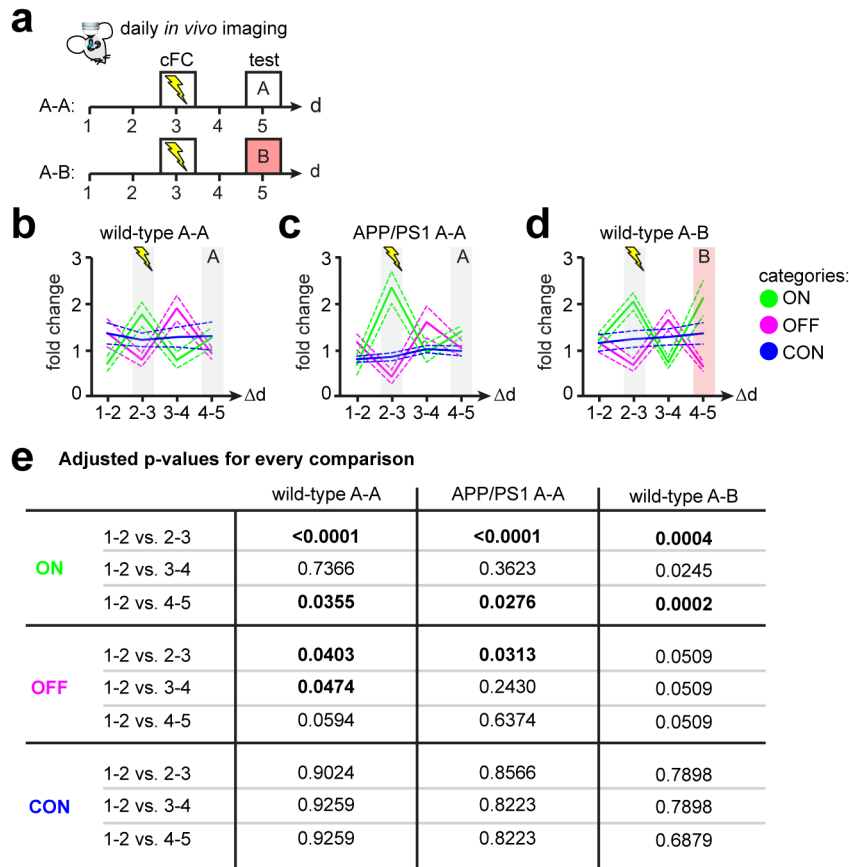


**Figure 6.1 FosGFP expression changes during learning and memory.** (a) Experimental paradigm to monitor daily fosGFP expression of mice during learning and memory. (b-d) Fold changes of fosGFP expression changes in wild-type A-A (b), APP/PS1 A-A (c) and wild-type A-B mice (d). FosGFP expression changes are visualized green (ON, switch on), magenta (OFF, switch off) and blue (CON, continue expression). Data are presented as mean (continuous line)  $\pm$  SEM (dashed lines). (e) Adjusted p-values for every comparison of intra-group expression changes corresponding to graphs (b) to (d). Data from n=8 wild-type A-A mice (4775 neurons), n=6 APP/PS1 A-A mice (3776 neurons) and n=6 wild-type A-B mice (5099 neurons); two-way ANOVA with Holm-Sidak's correction for multiple comparisons.

## 6.2.2. Relative pattern frequencies

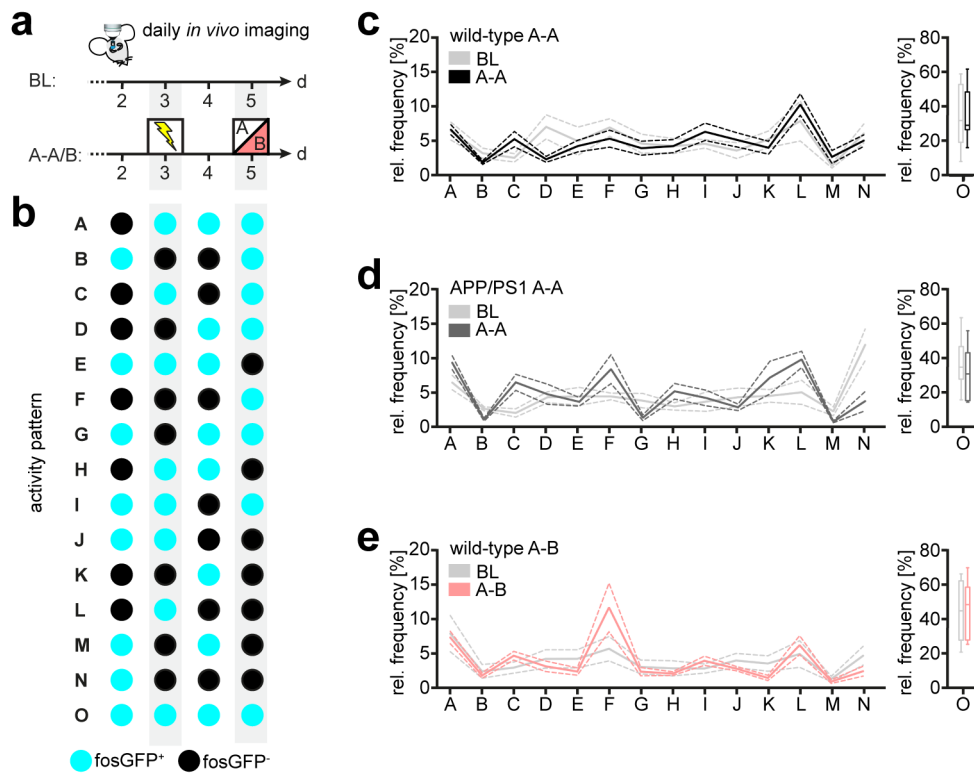


**Figure 6.2 Activity pattern analysis.** (a) Experimental timeline to monitor daily fosGFP expression of mice during learning and memory. (b) Scheme illustrating every possible activity pattern an individual neuron can show during four days of imaging (d2 to d5). Cyan and black circles represent fosGFP<sup>+</sup> and fosGFP<sup>-</sup> neurons, respectively. Individual activity patterns were randomly assigned capital letters ranging from A to O. (c-e) Relative frequency of an individual pattern during baseline (BL) and learning and memory period (A-A/B) in wild-type A-A (c), APP/PS1 A-A (d) and wild-type A-B mice (e), respectively. Data are presented in mean (continuous line)  $\pm$  SEM (dashed lines). Data from n=8 wild-type A-A mice (4775 neurons), n=6 APP/PS1 A-A mice (3776 neurons) and n=6 wild-type A-B mice (5099 neurons).

## 6.2.3. Cellular and structural data

	Statistical n [mice]	Samples/n	No. of neurons or spines
<b>Figure 3.1d</b>	3 wild-type	4-5 unilateral brain slices/mouse	333 Fos <sup>+</sup> , 39 GAD67 <sup>+</sup> , 4 double <sup>+</sup>
<b>Figure 3.1f</b>	3 wild-type, 3 APP/PS1	4-5 unilateral brain slices/mouse	276 fosGFP <sup>+</sup> (wild-type), 516 fosGFP <sup>+</sup> (APP/PS1)
<b>Figure 3.2e,f,h,i</b>	8 wild-type, 6 APP/PS1	1-3 ROIs/mouse	2874 fosGFP <sup>+</sup> (wild-type), 2092 fosGFP <sup>+</sup> (APP/PS1)
<b>Figure 3.3c-e</b>	8 wild-type, 6 APP/PS1	1-3 ROIs/mouse	4134 fosGFP <sup>+</sup> (wild-type), 2993 fosGFP <sup>+</sup> (APP/PS1)
<b>Figure 3.3g</b>	8 wild-type, 6 APP/PS1	1-3 ROIs/mouse	2956 fosGFP <sup>+</sup> at d1 (wild-type), 2198 fosGFP <sup>+</sup> at d1 (APP/PS1)

<b>Figure 3.3h</b>	8 wild-type, 6 APP/PS1	1-3 ROIs/mouse	1541 fosGFP <sup>+</sup> d1 to d5 (wild-type), 1064 d1 to d5 (APP/PS1)
<b>Figure 3.4g-i, Figure 3.5c,e,g, Figure 3.6.1</b>	8 wild-type A-A, 6 APP/PS1 A-A, 6 wild-type A-B	1-3 ROIs/mouse	4775 fosGFP <sup>+</sup> (wild-type A-A), 3776 fosGFP <sup>+</sup> (APP/PS1 A-B), 5099 fosGFP <sup>+</sup> (wild-type A-B)
<b>Figure 3.6.2e</b>	5 CNO-treated, 4 placebo-treated	4 unilateral brain slices/mouse	1379 Fos <sup>+</sup> (CNO-treated), 229 Fos <sup>+</sup> (placebo-treated)
<b>Figure 3.6.3f</b>	8 CNO-treated, 7 placebo-treated, 5 non-labeled	4 or 1 (non-labeled) unilateral brain slice(s)/mouse	1090 Fos <sup>+</sup> (CNO-treated), 648 Fos <sup>+</sup> (placebo-treated), 98 Fos <sup>+</sup> (non-labeled)
<b>Figure 3.8.1h-j</b>	8 wild-type, 4 APP/PS1	2-6 dendrites/mouse	1459 spines* (wild-type), 403 spines* (APP/PS1)
<b>Figure 3.8.2b,c,e,f</b>	8 wild-type, 4 APP/PS1	2-6 dendrites/mouse	516 transient spines (wild-type), 164 transient spines (APP/PS1)

\*sum of spines on every dendrite at BL d1 (see **Figure 3.8.1b**).

#### 6.2.4. Behavioral data

	<b>Statistical n [mice]</b>	<b>Analyzed time interval</b>
<b>Figure 3.4b</b>	16 wild-type A-A, 14 APP/PS1 A-A, 10 wild-type A-B	First 4 minutes
<b>Figure 3.4c</b>	16 wild-type A-A, 14 APP/PS1 A-A, 10 wild-type A-B	First minute
<b>Figure 3.6.2f</b>	5 CNO-treated, 4 placebo-treated	First 4 minutes
<b>Figure 3.6.3g</b>	8 CNO-treated, 7 placebo-treated	First 4 minutes
<b>Figure 3.7e</b>	7 wild-type sham, 11 wild-type NpHR, 5 APP/PS1 sham, 7 APP/PS1 NpHR	First 3 minutes, fiber-attached
<b>Figure 3.7f-h</b>	7 wild-type sham, 11 wild-type NpHR, 5 APP/PS1 sham, 7 APP/PS1 NpHR	First 3 minutes, fiber-attached
<b>Figure 3.8.1c</b>	10 wild-type, 8 APP/PS1	First 3 minutes
<b>Figure 3.8.1d</b>	10 wild-type, 8 APP/PS1	First minute

### 6.3. List of figures

Figure 1.1 CA1 within the hippocampal circuitry .....	3
Figure 1.2 Activation of the <i>c-fos</i> promoter in fosGFP mice .....	8
Figure 1.3 Processing of APP .....	10
Figure 2.1 Hippocampal window .....	17
Figure 2.2 Behavioral setups .....	19
Figure 2.3 TetTag-system for activity-dependent labelling within a specified time window .....	21
Figure 2.4 Definition of fosGFP expressing neurons .....	26
Figure 3.1 Immunohistochemical validation of fosGFP .....	28
Figure 3.2 Reduced fosGFP expression in A $\beta$ plaque vicinity .....	29
Figure 3.3 FosGFP baseline dynamics revealed two distinct neuronal populations .....	31
Figure 3.4 CA1 network activity revealed to be intact in APP/PS1 mice .....	32
Figure 3.5 Reactivated ensemble emerged independent of memory retrieval .....	34
Figure 3.6.1 Superimposition as determinant of retrieval performance .....	36
Figure 3.6.2 Artificial superimposition in CA1 impaired retrieval performance .....	37
Figure 3.6.3 Superimposition by false context information in CA1 impaired retrieval performance .....	38
Figure 3.7 PV <sup>+</sup> interneurons were crucial for memory encoding and retrieval .....	40
Figure 3.8.1 Altered structural plasticity in CA1 of APP/PS1 mice .....	42
Figure 3.8.2 Learning-induced spine loss was absent in APP/PS1 mice .....	43
Figure 6.1 FosGFP expression changes during learning and memory .....	62
Figure 6.2 Activity pattern analysis .....	63

## 6.4. Consumables

### 6.4.1. Surgery

<b>Designation</b>	<b>Product no.</b>	<b>Company</b>
<b>Cyano Fast</b>	152261	Hager Werken (Duisburg, Germany)
<b>Cyano Veneer® Anmischblock</b>	152270	Hager Werken (Duisburg, Germany)
<b>Cyano Veneer® Einwegpinsel</b>	152266	Hager Werken (Duisburg, Germany)
<b>Cyano Veneer® Pinselhalter</b>	152267	Hager Werken (Duisburg, Germany)
<b>Cyano Veneer® Pulver</b>	152255	Hager Werken (Duisburg, Germany)
<b>Disposable scalpels, sterile</b>	0505	Swann-Morton (Sheffield, England)
<b>Drill head</b>	H71.104.004	Gebr. Basseler (Lemgo, Germany)
<b>EUROTUBO®, sterile collection swabs</b>	300202	DeltaLab (Barcelona, Spain)
<b>GRADIA® DIRECT Flo BW</b>	2358	GC (Leuven, Belgium)
<b>Norland Optical Adhesive 81</b>	NOA 81	Norland Products (Cranbury, New Jersey)
<b>OptiBond™ FL, two-component bonding agent</b>	26684 E	Kerr (Salerno, Italy)
<b>Pasteur-pipette, disposable</b>	211C	COPAN (Brescia, Italy)
<b>Pattex, instant adhesive, liquid</b>	n/a	Henkel (Düsseldorf, Germany)
<b>Standard Biopsy Punch, 3 mm</b>	48301	pfm medical (Cologne, Germany)
<b>Sterican® cannula, BL/LB, 27G x 3/4"</b>	4657705	B Braun (Melsungen, Germany)
<b>Sterican® cannula, blunt, 21G x 7/8"</b>	9180109	B Braun (Melsungen, Germany)
<b>Sterican® cannula, blunt, 27G x 1"</b>	9180117	B Braun (Melsungen, Germany)
<b>Sugi®Eyespear</b>	30601	Kettenbach (Eschenburg, Germany)
<b>Suture, coated VICRYL®</b>	MPV490H	Ethicon (New Jersey, USA)
<b>TERUMO® Tuberculin Syringes</b>	SS-01T1	Terumo (Tokyo)

## 6.4.2. Behavior

Designation	Product no.	Company
Hygienic paper	n/a	Unigloves (Troisdorf, germany)

## 6.5. Reagents

## 6.5.1. Anaesthesia and medication

Designation	Product no.	Company
<b>Bepanthen® Augen- und Nasensalbe (ointment)</b>	n/a	Bayer (Leverkusen, Germany)
<b>Betaisodona® (Povidon-iodine)</b>	10074524	Mundipharma (Limburg, Germany)
<b>Dexamethasone 21-phosphate disodium salt</b>	D1159-500MG	Sigma (Darmstadt, Germany)
<b>Glucose 5%</b>	11383011	B Braun (Melsungen, Germany)
<b>Isofluran</b>	07253744	Actavis (New Jersey, USA)
<b>Ketavet® (Ketaminhydrochlorid) 100mg.mL</b>	D3821-07	Pfizer (New York, USA)
<b>Rompun® (Xylazinhydrochloride) 2%</b>	KP09X0L	Bayer (Leverkusen, Germany)
<b>Temgesic® (Buprenorphinhydrochloride, 0.324 mg)</b>	n/a	Reckitt Benckiser Healthcare (UK)

## 6.5.2. Adeno-associated viruses (AAVs)

Designation	Supplier	Titer [vg/ml]
AAV2/1-Fos-tTA	VCF, University of Bonn	n/a
AAV2/1-PTRE-tight-hM3D(Gq)-mCherry	VCF, University of Bonn	n/a
AAV1-EF1a-DIO-eNpHR-eYFP-WPRE-hGH	PennVectors	1.53E+13
AAV2-FLEX-tdTomato	UNC Vector Core	4.70E+12
AAV2-hSyn-DIO-hM3D(Gq)-mCherry	UNC Vector Core	6.10E+12

## 6.5.3. Immunohistochemistry

<b>Designation</b>	<b>Product no.</b>	<b>Company</b>
<b>10% normal goat serum</b>	50062Z	Life technologies (Carlsbad, USA)
<b>Alexa Fluor® 488 goat anti-rabbit</b>	A11008	Life technologies (Carlsbad, USA)
<b>Alexa Fluor® 647 goat anti-mouse</b>	A21235	Life technologies (Carlsbad, USA)
<b>anti-Fos, rabbit</b>	sc-52	Santa Cruz (Dallas, USA)
<b>anti-GAD67, mouse</b>	MAB5406	Millipore/Merck (Darmstadt, Germany)
<b>anti-PV</b>	PV27	Swant (Marly, Switzerland)
<b>Bovine serum albumine</b>	0163	Roth (Karlsruhe, Germany)
<b>Fluorescence mounting medium</b>	S3023	Dako/Agilent Technologies (Santa Clara, USA)
<b>NeuroTrace® 435/455 Nissl stain</b>	N21479	Life technologies (Carlsbad, USA)
<b>Phosphate buffered saline</b>	A0964	AppliChem (Darmstadt, Germany)
<b>Triton™-X100</b>	A1388	Sigma-Aldrich (St. Louis, USA)

## 6.6. Equipment

### 6.6.1. Microscopes

<b>Designation</b>	<b>Product no.</b>	<b>Company</b>
<b>Multiphoton microscope LSM7MP</b>	n/a	Carl Zeiss GmbH (Oberkochen, Germany)
<b>Detectors LSM BiG</b>	n/a	s.a.
<b>Filter-set 1 (BP 450/60, Dichroic 490, BP 525/50)</b>	1756-083	s.a.
<b>Filter-set 2 (BP 525/50, Dichroic 555, BP 592.5/35)</b>	1756-085	s.a.
<b>Objective 16x (Water)</b>	CFI75 LWD 16XW	Nikon Corp. (Tokio, Japan)
<b>Chameleon Ultra II Laser</b>	n/a	Coherent, Inc. (Santa Clara, USA)
<b>Multiphoton microscope Trim Scope II</b>	n/a	La Vision Biotech (Bielefeld, Germany)
<b>Detectors</b>	H7422-40, H6780-20	Hamamatsu Photonics K.K. (Hamamatsu, Japan)
<b>BP460/80 BrightLine HC</b>	n/a	Semrock Inc. (Rochester, USA)
<b>LP500</b>	FF-1-500/LP-25	Semrock Inc. (Rochester, USA)
<b>LP525</b>	ET525lp	Chroma Technology Corp. (Bellevue, USA)
<b>LP585</b>	T585lpxr	Chroma Technology Corp. (Bellevue, USA)
<b>BP555/55</b>	n/a	Chroma Technology Corp. (Bellevue, USA)
<b>Confocal microscope LSM700</b>	n/a	Carl Zeiss GmbH (Oberkochen, Germany)
<b>Fixation frame for mouse <i>in vivo</i> imaging</b>	n/a	custom build

## 6.6.2. Surgery

<b>Designation</b>	<b>Product no.</b>	<b>Company</b>
<b>Auxiliary ear bars</b>	EB-5N	Narishige international ltd. (London, UK)
<b>Control system SM7</b>	200-100 900 7411	Luigs and Neumann (Ratingen, Germany)
<b>Dental drill</b>	A755983	Schick (Schemmerhofen, Germany)
<b>Fixation frame for mice</b>	n/a	custom build
<b>Head holding adapter</b>	MA-6N	Narishige international ltd. (London, UK)
<b>Heating pad</b>	21061-90	Fine Science Tools GmbH (Heidelberg, Germany)
<b>LED light source</b>	KL1500 LED	Schott (Mainz, Germany)
<b>Light-curing device, LED smart (420nm-480nm, 1000 W/cm<sup>2</sup>)</b>	14012119	Kohlschein-Dental GmbH & Co. KG (Altenberge, Germany)
<b>LN Junior RE/LE (3 axes)</b>	210- 100000070- RE/LE	Luigs and Neumann (Ratingen, Germany)
<b>Micro4 Micro Syringe Pump Controller</b>	SYS-MICRO4	World Precision Instruments (Sarasota, USA)
<b>NanoFil Syringe 10 µL</b>	NANOFIL	World Precision Instruments (Sarasota, USA)
<b>Peri-Star Pro, peristaltic pump</b>	PERIPRO-4LS	World Precision Instruments (Sarasota, USA)
<b>Pipette holder</b>	UPN-1	Narishige (Tokyo, Japan)
<b>Pipette holder</b>	UPN-2	Narishige (Tokyo, Japan)
<b>Remote Control SM-7</b>	200-100 900 9050	Luigs and Neumann (Ratingen, Germany)
<b>Stereomicroscope SZ 51</b>	19320	Olympus (Tokyo, Japan)
<b>Sterilizer, Steri 250</b>	031100	Keller (Burgdorf, Switzerland)
<b>UMP3 Ultra Micro Pump</b>	UMP3	World Precision Instruments (Sarasota, USA)

## 6.6.3. Behavior

<b>Designation</b>	<b>Product no.</b>	<b>Company</b>
<b>Camcorder, DV-883.IR</b>	PX-8262-675	Somikon (Pearl.GmbH, Buggingen, Germany)
<b>Context B chamber</b>	n/a	custom build
<b>Fear conditioning chamber</b>	n/a	custom build
<b>Open field box</b>	n/a	custom build
<b>Quick disconnect grid harness</b>	ENV-307W-QD	Med Associates (Fairfax, Vermont)
<b>Shock output cable 10'</b>	SG-219G-10 DB-9	Med Associates (Fairfax, Vermont)
<b>Stainless steel grid floor, mouse</b>	ENV-307W- GFW	Med Associates (Fairfax, Vermont)
<b>Stand alone shocker/scrambler (230V)</b>	ENV-414SA	Med Associates (Fairfax, Vermont)
<b>Webcam, USB-Design</b>	971975 - 62	Conrad Electronics SE (Hirschau, Germany)

## 6.6.4. Optogenetics

<b>Designation</b>	<b>Product. No (customized)</b>	<b>Company</b>
<b>Fiberoptic Rotary Joint</b>	FRJ_1x2i_FC-2M3	Doric Lenses (Ville de Québec, Canada)
<b>Mono Fiberoptic Cannula</b>	MFC_300/370- 0.22_2.5mm_RMR_A45	s.a.
<b>Mono Fiberoptic Patchchords</b>	MFP_300/330/900- 0.22_0.5m_CM3-RMC	s.a.
<b>OBIS Laser, 100mW</b>	34-233	Coherent, Inc. (Santa Clara, USA)
<b>Two-ferrules Cannula</b>	TFC_300/370- 0.22_2.5_TM3_FLT	Doric Lenses (Ville de Québec, Canada)

## 6.6.5. Miscellaneous

<b>Designation</b>	<b>Product no.</b>	<b>Company</b>
<b>Automated Vibatome</b>	VT1200 S	Leica (Nussloch, Germany)
<b>Eppendorf Research® plus pipettes</b>	31200000XX	Eppendorf (Hamburg, Germany)
<b>Titramax 100, shaker</b>	544-11200-00	Heidolph (Schwabach, Germany)
<b>Vet Equip anesthesia system</b>	800-466-6463	KF Technology (Rome, Italy)

## 6.6.6. Software

<b>Designation</b>	<b>Company</b>
<b>Adobe Illustrator CS5, Version 15.0.1</b>	Adobe Systems Inc., USA
<b>Adobe Photoshop CS5, Version 12.1</b>	Adobe Systems Inc., USA
<b>EthoVision XT11.5</b>	Noldus, NL
<b>Fiji/ImageJ 2.0.0</b>	Wayne Rasband, NIH, USA
<b>GraphPad Prism 5 &amp; 6</b>	GraphPad Software, Inc., USA
<b>ImSpector Pro</b>	LaVision BioTec GmbH, DE
<b>Microsoft Excel Mac 2008</b>	Microsoft Corp., USA
<b>Microsoft Word Mac 2011</b>	Microsoft Corp., USA
<b>ZEN 2010</b>	Carl Zeiss AG, DE

## 6.7. Contributions and remarks

Julia Steffen conducted the genotyping for fosGFP, YFP-H, APP/PS1, PV-Cre transgenic mice. She further supported with perfusions during the DREADD experiment (**Fig. 3.6.2**) and performed immunohistochemical stainings of PV-Cre mice with optical fiber implantations (**Fig. 3.7c**).

Walker S. Jackson provided the Vglut2-ires-cre line.

Lioba Dammer and Susanne Schoch produced and provided the AAVs composing the TetTag-System, namely AAV2/1-cfos-rtTA and AAV2/1-PTREtight-hM3D(Gq)-mCherry via their viral core facility (VCF) at the university of Bonn.

Boris Schmidt produced and provided the A $\beta$  plaque staining compound Methoxy-XO4.

Manuel Mittag conducted the PV<sup>+</sup> interneuron inhibition and Eleonora Ambrad performed the feedback stimulation of PV<sup>+</sup> interneurons in APP/PS1 mice mentioned on page 55 (section 4.11).

Parts of the current thesis compose a manuscript that was submitted for publication in NEURON (sections 3.1. to 3.6. and parts of 2.1. to 2.3., 2.5.2., 2.5.4., 2.6.2., 2.6.3., 2.7., and 2.8. are included). The manuscript with the title “Memory trace superimposition impairs recall in a mouse model of AD” is currently under peer-review. Concomitant, it is accessible via the platform Cell Press Sneak Peek that hosts manuscripts under consideration at all Cell Press Journals.

## 7. REFERENCES

- Agerskov, C. (2016). "Vector Symbolic Spiking Neural Network Model of Hippocampal Subarea CA1 Novelty Detection Functionality." *Neural Comput* **28**(4): 613-628.
- Alvarez, V. A. and B. L. Sabatini (2007). "Anatomical and physiological plasticity of dendritic spines." *Annu Rev Neurosci* **30**: 79-97.
- Andersen, P. M., Richard; Amaral, David; Bliss, Tim; O'Keefe, John (2007). *The hippocampus book*, Oxford university press.
- Attardo, A., J. E. Fitzgerald and M. J. Schnitzer (2015). "Impermanence of dendritic spines in live adult CA1 hippocampus." *Nature* **523**(7562): 592-596.
- Bailey, C. H. and E. R. Kandel (1993). "Structural changes accompanying memory storage." *Annu Rev Physiol* **55**: 397-426.
- Ballatore, C., V. M. Lee and J. Q. Trojanowski (2007). "Tau-mediated neurodegeneration in Alzheimer's disease and related disorders." *Nat Rev Neurosci* **8**(9): 663-672.
- Barth, A. L., R. C. Gerkin and K. L. Dean (2004). "Alteration of neuronal firing properties after in vivo experience in a FosGFP transgenic mouse." *J Neurosci* **24**(29): 6466-6475.
- Basu, J., K. V. Srinivas, S. K. Cheung, H. Taniguchi, Z. J. Huang and S. A. Siegelbaum (2013). "A cortico-hippocampal learning rule shapes inhibitory microcircuit activity to enhance hippocampal information flow." *Neuron* **79**(6): 1208-1221.
- Bear, M. F. C., Barry W.; Paradiso, Michael A. (2007). *Neuroscience - exploring the brain*, Lippincott Williams & Wilkins.
- Ben-Yakov, A., Y. Dudai and M. R. Mayford (2015). "Memory Retrieval in Mice and Men." *Cold Spring Harb Perspect Biol* **7**(12).
- Bittner, K. C., C. Grienberger, S. P. Vaidya, A. D. Milstein, J. J. Macklin, J. Suh, S. Tonegawa and J. C. Magee (2015). "Conjunctive input processing drives feature selectivity in hippocampal CA1 neurons." *Nat Neurosci* **18**(8): 1133-1142.
- Bittner, T., M. Fuhrmann, S. Burgold, S. M. Ochs, N. Hoffmann, G. Mitteregger, H. Kretschmar, F. M. LaFerla and J. Herms (2010). "Multiple events lead to dendritic spine loss in triple transgenic Alzheimer's disease mice." *PLoS One* **5**(11): e15477.
- Blanchard, R. J. and D. C. Blanchard (1969). "Crouching as an index of fear." *J Comp Physiol Psychol* **67**(3): 370-375.
- Bliss, T. V. and T. Lomo (1973). "Long-lasting potentiation of synaptic transmission in the dentate area of the anaesthetized rabbit following stimulation of the perforant path." *J Physiol* **232**(2): 331-356.
- Braak, H. and E. Braak (1991). "Demonstration of amyloid deposits and neurofibrillary changes in whole brain sections." *Brain Pathol* **1**(3): 213-216.
- Buee, L., T. Bussiere, V. Buee-Scherrer, A. Delacourte and P. R. Hof (2000). "Tau protein isoforms, phosphorylation and role in neurodegenerative disorders." *Brain Res Brain Res Rev* **33**(1): 95-130.
- Burgold, S., T. Bittner, M. M. Dorostkar, D. Kieser, M. Fuhrmann, G. Mitteregger, H. Kretschmar, B. Schmidt and J. Herms (2011). "In vivo multiphoton imaging reveals gradual growth of newborn amyloid plaques over weeks." *Acta Neuropathol* **121**(3): 327-335.

- Busche, M. A., X. Chen, H. A. Henning, J. Reichwald, M. Staufenbiel, B. Sakmann and A. Konnerth (2012). "Critical role of soluble amyloid-beta for early hippocampal hyperactivity in a mouse model of Alzheimer's disease." *Proc Natl Acad Sci U S A* **109**(22): 8740-8745.
- Busche, M. A., G. Eichhoff, H. Adelsberger, D. Abramowski, K. H. Wiederhold, C. Haass, M. Staufenbiel, A. Konnerth and O. Garaschuk (2008). "Clusters of hyperactive neurons near amyloid plaques in a mouse model of Alzheimer's disease." *Science* **321**(5896): 1686-1689.
- Butler, J. L. and O. Paulsen (2014). "The hippocampal cacophony: multiple layers of communication." *Neuron* **84**(2): 251-253.
- Buzsaki, G. (1984). "Feed-forward inhibition in the hippocampal formation." *Prog Neurobiol* **22**(2): 131-153.
- Cajal, S. R. (1894). "La fine structure des centres nerveux." *Proc. R. Soc. Lond.*(55): 444-468.
- Caroni, P. (2015). "Regulation of Parvalbumin Basket cell plasticity in rule learning." *Biochemical and biophysical research communications* **460**: 100-103.
- Cingolani, L. A. and Y. Goda (2008). "Actin in action: the interplay between the actin cytoskeleton and synaptic efficacy." *Nat Rev Neurosci* **9**(5): 344-356.
- Cohen, S. and M. E. Greenberg (2008). "Communication between the synapse and the nucleus in neuronal development, plasticity, and disease." *Annual review of cell and developmental biology* **24**: 183-209.
- Corder, E. H., A. M. Saunders, W. J. Strittmatter, D. E. Schmechel, P. C. Gaskell, G. W. Small, A. D. Roses, J. L. Haines and M. A. Pericak-Vance (1993). "Gene dose of apolipoprotein E type 4 allele and the risk of Alzheimer's disease in late onset families." *Science* **261**(5123): 921-923.
- Cowansage, Kiriana K., T. Shuman, Blythe C. Dillingham, A. Chang, P. Golshani and M. Mayford (2014). "Direct Reactivation of a Coherent Neocortical Memory of Context." *Neuron* **84**: 432-441.
- Cruz, F. C., E. Koya, D. H. Guez-Barber, J. M. Bossert, C. R. Lupica, Y. Shaham and B. T. Hope (2013). "New technologies for examining the role of neuronal ensembles in drug addiction and fear." *Nature reviews. Neuroscience* **14**: 743-754.
- Cummings, J. L. (2004). "Alzheimer's disease." *N Engl J Med* **351**(1): 56-67.
- Curran, T. (1991). "Coupling in the nervous system: involvement of the inducible proto-oncogenes."
- De Oca, B. M., J. P. DeCola, S. Maren and M. S. Fanselow (1998). "Distinct regions of the periaqueductal gray are involved in the acquisition and expression of defensive responses." *J Neurosci* **18**(9): 3426-3432.
- De Strooper, B., R. Vassar and T. Golde (2010). "The secretases: enzymes with therapeutic potential in Alzheimer disease." *Nat Rev Neurol* **6**(2): 99-107.
- Deng, W., M. Mayford and F. H. Gage (2013). "Selection of distinct populations of dentate granule cells in response to inputs as a mechanism for pattern separation in mice." *eLife* **2**: e00312.
- Denny, C. a., M. a. Kheirbek, E. L. Alba, K. F. Tanaka, R. a. Brachman, K. B. Laughman, N. K. Tomm, G. F. Turi, A. Losonczy and R. Hen (2014). "Hippocampal memory traces are differentially modulated by experience, time, and adult neurogenesis." *Neuron* **83**: 189-201.
- Donato, F., S. B. Rompani and P. Caroni (2013). "Parvalbumin-expressing basket-cell network plasticity induced by experience regulates adult learning." *Nature* **504**(7479): 272-276.
- Duncan, K., N. Ketz, S. J. Inati and L. Davachi (2012). "Evidence for area CA1 as a match/mismatch detector: a high-resolution fMRI study of the human hippocampus." *Hippocampus* **22**(3): 389-398.

- Eguchi, M. and S. Yamaguchi (2009). "In vivo and in vitro visualization of gene expression dynamics over extensive areas of the brain." *Neuroimage* **44**(4): 1274-1283.
- Engert, F. and T. Bonhoeffer (1999). "Dendritic spine changes associated with hippocampal long-term synaptic plasticity." *Nature* **399**(6731): 66-70.
- Fleischmann, A., O. Hvalby, V. Jensen, T. Strelakova, C. Zacher, L. E. Layer, A. Kvello, M. Reschke, R. Spanagel, R. Sprengel, E. F. Wagner and P. Gass (2003). "Impaired long-term memory and NR2A-type NMDA receptor-dependent synaptic plasticity in mice lacking c-Fos in the CNS." *J Neurosci* **23**(27): 9116-9122.
- Frankland, P. W. and B. Bontempi (2005). "The organization of recent and remote memories." *Nature reviews. Neuroscience* **6**: 119-130.
- Freir, D. B., C. Holscher and C. E. Herron (2001). "Blockade of long-term potentiation by beta-amyloid peptides in the CA1 region of the rat hippocampus in vivo." *J Neurophysiol* **85**(2): 708-713.
- Games, D., D. Adams, R. Alessandrini, R. Barbour, P. Berthelette, C. Blackwell, T. Carr, J. Clemens, T. Donaldson, F. Gillespie and et al. (1995). "Alzheimer-type neuropathology in transgenic mice overexpressing V717F beta-amyloid precursor protein." *Nature* **373**(6514): 523-527.
- Ganguly, K. and M. M. Poo (2013). "Activity-dependent neural plasticity from bench to bedside." *Neuron* **80**(3): 729-741.
- Garner, A. R., D. C. Rowland, S. Y. Hwang, K. Baumgaertel, B. L. Roth, C. Kentros and M. Mayford (2012). "Generation of a synthetic memory trace." *Science (New York, N.Y.)* **335**: 1513-1516.
- Gilman, S., M. Koller, R. S. Black, L. Jenkins, S. G. Griffith, N. C. Fox, L. Eisner, L. Kirby, M. B. Rovira, F. Forette, J. M. Orgogozo and A. N. S. Team (2005). "Clinical effects of Abeta immunization (AN1792) in patients with AD in an interrupted trial." *Neurology* **64**(9): 1553-1562.
- Glenner, G. G. and C. W. Wong (1984). "Alzheimer's disease: initial report of the purification and characterization of a novel cerebrovascular amyloid protein." *Biochem Biophys Res Commun* **120**(3): 885-890.
- Goate, A., M. C. Chartier-Harlin, M. Mullan, J. Brown, F. Crawford, L. Fidani, L. Giuffra, A. Haynes, N. Irving, L. James and et al. (1991). "Segregation of a missense mutation in the amyloid precursor protein gene with familial Alzheimer's disease." *Nature* **349**(6311): 704-706.
- Gong, Y., L. Chang, K. L. Viola, P. N. Lacor, M. P. Lambert, C. E. Finch, G. A. Krafft and W. L. Klein (2003). "Alzheimer's disease-affected brain: presence of oligomeric A beta ligands (ADDLs) suggests a molecular basis for reversible memory loss." *Proc Natl Acad Sci U S A* **100**(18): 10417-10422.
- Goshen, I., M. Brodsky, R. Prakash, J. Wallace, V. Gradinaru, C. Ramakrishnan and K. Deisseroth (2011). "Dynamics of retrieval strategies for remote memories." *Cell* **147**: 678-689.
- Gotz, J., A. Schild, F. Hoernkli and L. Pennanen (2004). "Amyloid-induced neurofibrillary tangle formation in Alzheimer's disease: insight from transgenic mouse and tissue-culture models." *Int J Dev Neurosci* **22**(7): 453-465.
- Grundke-Iqbal, I., K. Iqbal, M. Quinlan, Y. C. Tung, M. S. Zaidi and H. M. Wisniewski (1986). "Microtubule-associated protein tau. A component of Alzheimer paired helical filaments." *J Biol Chem* **261**(13): 6084-6089.
- Gu, L., S. Kleiber, L. Schmid, F. Nebeling, M. Chamoun, J. Steffen, J. Wagner and M. Fuhrmann (2014). "Long-term in vivo imaging of dendritic spines in the hippocampus reveals structural plasticity." *The Journal of neuroscience : the official journal of the Society for Neuroscience* **34**: 13948-13953.
- Guzowski, J. F. and J. L. McGaugh (1997). "Antisense oligodeoxynucleotide-mediated disruption of hippocampal cAMP response element binding protein levels impairs consolidation of memory for water maze training." *Proc Natl Acad Sci U S A* **94**(6): 2693-2698.

- Guzowski, J. F., B. L. McNaughton, C. A. Barnes and P. F. Worley (1999). "Environment-specific expression of the immediate-early gene *Arc* in hippocampal neuronal ensembles." *Nat Neurosci* **2**(12): 1120-1124.
- Haass, C. (2004). "Take five--BACE and the gamma-secretase quartet conduct Alzheimer's amyloid beta-peptide generation." *EMBO J* **23**(3): 483-488.
- Haass, C. and D. J. Selkoe (2007). "Soluble protein oligomers in neurodegeneration: lessons from the Alzheimer's amyloid beta-peptide." *Nat Rev Mol Cell Biol* **8**(2): 101-112.
- Hardy, J. (1997). "Amyloid, the presenilins and Alzheimer's disease." *Trends Neurosci* **20**(4): 154-159.
- Harkany, T., S. O'Mahony, J. P. Kelly, K. Soos, I. Toro, B. Penke, P. G. Luiten, C. Nyakas, K. Gulya and B. E. Leonard (1998). "Beta-amyloid(Phe(SO<sub>3</sub>H)<sub>24</sub>)<sub>25-35</sub> in rat nucleus basalis induces behavioral dysfunctions, impairs learning and memory and disrupts cortical cholinergic innervation." *Behav Brain Res* **90**(2): 133-145.
- Hebb, D. O. (1949). "The organization of behavior: a neuropsychological theory." (NY: Wiley).
- Helmchen, F. and W. Denk (2005). "Deep tissue two-photon microscopy." *Nat Methods* **2**(12): 932-940.
- Hippenmeyer, S., E. Vrieseling, M. Sigrist, T. Portmann, C. Laengle, D. R. Ladle and S. Arber (2005). "A developmental switch in the response of DRG neurons to ETS transcription factor signaling." *PLoS Biol* **3**(5): e159.
- Hippius, H. and G. Neundorfer (2003). "The discovery of Alzheimer's disease." *Dialogues Clin Neurosci* **5**(1): 101-108.
- Holtmaat, A. and P. Caroni (2016). "Functional and structural underpinnings of neuronal assembly formation in learning." *Nat Neurosci*.
- Honkura, N., M. Matsuzaki, J. Noguchi, G. C. Ellis-Davies and H. Kasai (2008). "The subspine organization of actin fibers regulates the structure and plasticity of dendritic spines." *Neuron* **57**(5): 719-729.
- Horn, G. (2004). "Pathways of the past: the imprint of memory." *Nat Rev Neurosci* **5**(2): 108-120.
- Hsia, A. Y., E. Masliah, L. McConlogue, G. Q. Yu, G. Tatsuno, K. Hu, D. Kholodenko, R. C. Malenka, R. A. Nicoll and L. Mucke (1999). "Plaque-independent disruption of neural circuits in Alzheimer's disease mouse models." *Proc Natl Acad Sci U S A* **96**(6): 3228-3233.
- Hsiao, K., P. Chapman, S. Nilsen, C. Eckman, Y. Harigaya, S. Younkin, F. Yang and G. Cole (1996). "Correlative memory deficits, A $\beta$  elevation, and amyloid plaques in transgenic mice." *Science* **274**(5284): 99-102.
- Huang, Y. and L. Mucke (2012). "Alzheimer mechanisms and therapeutic strategies." *Cell* **148**(6): 1204-1222.
- Hubener, M. and T. Bonhoeffer (2010). "Searching for engrams." *Neuron* **67**(3): 363-371.
- Isaac, J. T., K. A. Buchanan, R. U. Muller and J. R. Mellor (2009). "Hippocampal place cell firing patterns can induce long-term synaptic plasticity in vitro." *J Neurosci* **29**(21): 6840-6850.
- Ito, M. (2001). "Cerebellar long-term depression: characterization, signal transduction, and functional roles." *Physiol Rev* **81**(3): 1143-1195.
- Iwatsubo, T., A. Odaka, N. Suzuki, H. Mizusawa, N. Nukina and Y. Ihara (1994). "Visualization of A $\beta$  42(43) and A $\beta$  40 in senile plaques with end-specific A $\beta$  monoclonals: evidence that an initially deposited species is A $\beta$  42(43)." *Neuron* **13**(1): 45-53.
- Jackson, R. J., N. Rudinskiy, A. G. Herrmann, S. Croft, J. M. Kim, V. Petrova, J. J. Ramos-Rodriguez, R. Pitstick, S. Wegmann, M. Garcia-Alloza, G. A. Carlson, B. T. Hyman and T. L. Spires-Jones (2016). "Human

- tau increases amyloid beta plaque size but not amyloid beta-mediated synapse loss in a novel mouse model of Alzheimer's disease." *Eur J Neurosci* **44**(12): 3056-3066.
- Jakkamsetti, V., N. P. Tsai, C. Gross, G. Molinaro, K. A. Collins, F. Nicoletti, K. H. Wang, P. Osten, G. J. Bassell, J. R. Gibson and K. M. Huber (2013). "Experience-induced Arc/Arg3.1 primes CA1 pyramidal neurons for metabotropic glutamate receptor-dependent long-term synaptic depression." *Neuron* **80**(1): 72-79.
- Jankowsky, J. L., D. J. Fadale, J. Anderson, G. M. Xu, V. Gonzales, N. A. Jenkins, N. G. Copeland, M. K. Lee, L. H. Younkin, S. L. Wagner, S. G. Younkin and D. R. Borchelt (2004). "Mutant presenilins specifically elevate the levels of the 42 residue beta-amyloid peptide in vivo: evidence for augmentation of a 42-specific gamma secretase." *Hum Mol Genet* **13**(2): 159-170.
- Jarrett, J. T., E. P. Berger and P. T. Lansbury, Jr. (1993). "The carboxy terminus of the beta amyloid protein is critical for the seeding of amyloid formation: implications for the pathogenesis of Alzheimer's disease." *Biochemistry* **32**(18): 4693-4697.
- Johnson, K. A., N. C. Fox, R. A. Sperling and W. E. Klunk (2012). "Brain imaging in Alzheimer disease." *Cold Spring Harb Perspect Med* **2**(4): a006213.
- Josselyn, S. a., S. Köhler and P. W. Frankland (2015). "Finding the engram." *Nature Reviews Neuroscience* **16**: 521-534.
- Jouhanneau, J. S., L. Ferrarese, L. Estebanez, N. J. Audette, M. Brecht, A. L. Barth and J. F. Poulet (2014). "Cortical fosGFP expression reveals broad receptive field excitatory neurons targeted by P0m." *Neuron* **84**(5): 1065-1078.
- Kandel, E. R., Y. Dudai and M. R. Mayford (2014). "The molecular and systems biology of memory." *Cell* **157**: 163-186.
- Karlsson, M. P. and L. M. Frank (2008). "Network dynamics underlying the formation of sparse, informative representations in the hippocampus." *J Neurosci* **28**(52): 14271-14281.
- Katzman, R. (1976). "Editorial: The prevalence and malignancy of Alzheimer disease. A major killer." *Arch Neurol* **33**(4): 217-218.
- Kentros, C., E. Hargreaves, R. D. Hawkins, E. R. Kandel, M. Shapiro and R. V. Muller (1998). "Abolition of long-term stability of new hippocampal place cell maps by NMDA receptor blockade." *Science* **280**(5372): 2121-2126.
- Kilgore, M., C. a. Miller, D. M. Fass, K. M. Hennig, S. J. Haggarty, J. D. Sweatt and G. Rumbaugh (2010). "Inhibitors of class 1 histone deacetylases reverse contextual memory deficits in a mouse model of Alzheimer's disease." *Neuropsychopharmacology : official publication of the American College of Neuropsychopharmacology* **35**: 870-880.
- Kim, J., J. T. Kwon, H. S. Kim, S. A. Josselyn and J. H. Han (2014). "Memory recall and modifications by activating neurons with elevated CREB." *Nat Neurosci* **17**(1): 65-72.
- Kim, R., H. Okuno and H. Bito (2012). "Deciphering the molecular rules governing synaptic targeting of the memory-related protein Arc." *Commun Integr Biol* **5**(5): 496-498.
- Knierim, J. J. (2015). "The hippocampus." *Curr Biol* **25**(23): R1116-1121.
- Knight, R. (1996). "Contribution of human hippocampal region to novelty detection." *Nature* **383**(6597): 256-259.
- Koffie, R. M., T. Hashimoto, H. C. Tai, K. R. Kay, A. Serrano-Pozo, D. Joyner, S. Hou, K. J. Kopeikina, M. P. Frosch, V. M. Lee, D. M. Holtzman, B. T. Hyman and T. L. Spire-Jones (2012). "Apolipoprotein E4 effects in Alzheimer's disease are mediated by synaptotoxic oligomeric amyloid-beta." *Brain* **135**(Pt 7): 2155-2168.

- Koffie, R. M., M. Meyer-Luehmann, T. Hashimoto, K. W. Adams, M. L. Mielke, M. Garcia-Alloza, K. D. Micheva, S. J. Smith, M. L. Kim, V. M. Lee, B. T. Hyman and T. L. Spires-Jones (2009). "Oligomeric amyloid beta associates with postsynaptic densities and correlates with excitatory synapse loss near senile plaques." Proc Natl Acad Sci U S A **106**(10): 4012-4017.
- Konorski, J. (1948). "Conditioned reflexes and neuronal organization." (New York: Cambridge University Press).
- Kubik, S., T. Miyashita and J. F. Guzowski (2007). "Using immediate-early genes to map hippocampal subregional functions." Learn Mem **14**(11): 758-770.
- Kumaran, D. and E. A. Maguire (2006). "An unexpected sequence of events: mismatch detection in the human hippocampus." PLoS Biol **4**(12): e424.
- LaFerla, F. M. (2002). "Calcium dyshomeostasis and intracellular signalling in Alzheimer's disease." Nat Rev Neurosci **3**(11): 862-872.
- LaFerla, F. M. and K. N. Green (2012). "Animal models of Alzheimer disease." Cold Spring Harb Perspect Med **2**(11).
- LaFerla, F. M., K. N. Green and S. Oddo (2007). "Intracellular amyloid-beta in Alzheimer's disease." Nat Rev Neurosci **8**(7): 499-509.
- Lai, C. S. W., T. F. Franke and W.-B. Gan (2012). "Opposite effects of fear conditioning and extinction on dendritic spine remodelling." Nature **483**: 87-91.
- Lanahan, A. and P. Worley (1998). "Immediate-early genes and synaptic function." Neurobiol Learn Mem **70**(1-2): 37-43.
- Larkin, M. C., C. Lykken, L. D. Tye, J. G. Wickelgren and L. M. Frank (2014). "Hippocampal output area CA1 broadcasts a generalized novelty signal during an object-place recognition task." Hippocampus **24**(7): 773-783.
- Lee, S. H., I. Marchionni, M. Bezaire, C. Varga, N. Danielson, M. Lovett-Barron, A. Losonczy and I. Soltesz (2014). "Parvalbumin-positive basket cells differentiate among hippocampal pyramidal cells." Neuron **82**(5): 1129-1144.
- Legault, M. and R. A. Wise (2001). "Novelty-evoked elevations of nucleus accumbens dopamine: dependence on impulse flow from the ventral subiculum and glutamatergic neurotransmission in the ventral tegmental area." Eur J Neurosci **13**(4): 819-828.
- Lisman, J. E. and N. A. Otmakhova (2001). "Storage, recall, and novelty detection of sequences by the hippocampus: elaborating on the SOCRATIC model to account for normal and aberrant effects of dopamine." Hippocampus **11**(5): 551-568.
- Lopes da Silva, F. H., M. P. Witter, P. H. Boeijinga and A. H. Lohman (1990). "Anatomic organization and physiology of the limbic cortex." Physiol Rev **70**(2): 453-511.
- Lovett-Barron, M., P. Kaifosh, M. A. Kheirbek, N. Danielson, J. D. Zaremba, T. R. Reardon, G. F. Turi, R. Hen, B. V. Zemelman and A. Losonczy (2014). "Dendritic inhibition in the hippocampus supports fear learning." Science **343**(6173): 857-863.
- Lütcke, H., D. J. Margolis and F. Helmchen (2013). "Steady or changing? Long-term monitoring of neuronal population activity." Trends in neurosciences **36**: 375-384.
- Maren, S., G. Aharonov and M. S. Fanselow (1997). "Neurotoxic lesions of the dorsal hippocampus and Pavlovian fear conditioning in rats." Behav Brain Res **88**(2): 261-274.
- Matsuzaki, M., N. Honkura, G. C. Ellis-Davies and H. Kasai (2004). "Structural basis of long-term potentiation in single dendritic spines." Nature **429**(6993): 761-766.

- Mayford, M., S. A. Siegelbaum and E. R. Kandel (2012). "Synapses and memory storage." Cold Spring Harb Perspect Biol **4**(6).
- Morgan, J. I. and T. Curran (1986). "Role of ion flux in the control of c-fos expression." Nature **322**(6079): 552-555.
- Morin, J. P., S. Diaz-Cintra, F. Bermudez-Rattoni and I. Delint-Ramirez (2016). "Decreased levels of NMDA but not AMPA receptors in the lipid-raft fraction of 3xTg-AD model of Alzheimer's disease: Relation to Arc/Arg3.1 protein expression." Neurochem Int **100**: 159-163.
- Morin, J. P., K. Guzman-Ramos and F. Bermudez-Rattoni (2015). "New Insights on Retrieval-Induced and Ongoing Memory Consolidation: Lessons from Arc." Neural Plast **2015**: 184083.
- Mucke, L. (2009). "Neuroscience: Alzheimer's disease." Nature **461**(7266): 895-897.
- Mullan, M., F. Crawford, K. Axelman, H. Houlden, L. Lilius, B. Winblad and L. Lannfelt (1992). "A pathogenic mutation for probable Alzheimer's disease in the APP gene at the N-terminus of beta-amyloid." Nat Genet **1**(5): 345-347.
- Nabavi, S., R. Fox, C. D. Proulx, J. Y. Lin, R. Y. Tsien and R. Malinow (2014). "Engineering a memory with LTD and LTP." Nature **511**(7509): 348-352.
- Nadel, L. (2007). Consolidation: The demise of the fixed trace. Science of Memory: Concepts. H. L. D. Y. F. Roediger, S.M., Oxford university press.
- Nakazawa, K., T. J. McHugh, M. A. Wilson and S. Tonegawa (2004). "NMDA receptors, place cells and hippocampal spatial memory." Nat Rev Neurosci **5**(5): 361-372.
- O'Keefe (1971). "The hippocampus as a spatial map. Preliminary evidence from unit activity in the freely-moving rat."
- Okuno, H., K. Akashi, Y. Ishii, N. Yagishita-Kyo, K. Suzuki, M. Nonaka, T. Kawashima, H. Fujii, S. Takemoto-Kimura, M. Abe, R. Natsume, S. Chowdhury, K. Sakimura, P. F. Worley and H. Bito (2012). "Inverse synaptic tagging of inactive synapses via dynamic interaction of Arc/Arg3.1 with CaMKIIbeta." Cell **149**(4): 886-898.
- Palop, J. J., J. Chin and L. Mucke (2006). "A network dysfunction perspective on neurodegenerative diseases." Nature **443**(7113): 768-773.
- Palop, J. J., J. Chin, E. D. Roberson, J. Wang, M. T. Thwin, N. Bien-Ly, J. Yoo, K. O. Ho, G.-Q. Yu, A. Kreitzer, S. Finkbeiner, J. L. Noebels and L. Mucke (2007). "Aberrant Excitatory Neuronal Activity and Compensatory Remodeling of Inhibitory Hippocampal Circuits in Mouse Models of Alzheimer's Disease." Neuron **55**: 697-711.
- Palop, J. J. and L. Mucke (2009). "Epilepsy and cognitive impairments in Alzheimer disease." Arch Neurol **66**(4): 435-440.
- Palop, J. J. and L. Mucke (2010). "Amyloid-beta-induced neuronal dysfunction in Alzheimer's disease: from synapses toward neural networks." Nature neuroscience **13**: 812-818.
- Prince, M. W., Anders; Guerchet, Maelenn; Ali, Gemma-Claire, Wu, Yu-Tzu; Prina, Matthew (2015). The global impact of dementia - an analysis of prevalence, incidence, cost and trends. World Alzheimer's report 2015. A. s. d. international.
- Radde, R., C. Duma, M. Goedert and M. Jucker (2008). "The value of incomplete mouse models of Alzheimer's disease." Eur J Nucl Med Mol Imaging **35 Suppl 1**: S70-74.
- Radulovic, J., J. Kammermeier and J. Spiess (1998). "Relationship between Fos Production and Classical Fear Conditioning: Effects of Novelty, Latent Inhibition, and Unconditioned Stimulus Preexposure." The Journal of neuroscience : the official journal of the Society for Neuroscience **18**: 7452-7461.

- Ramirez, S., X. Liu, P. A. Lin, J. Suh, M. Pignatelli, R. L. Redondo, T. J. Ryan and S. Tonegawa (2013). "Creating a false memory in the hippocampus." *Science* **341**(6144): 387-391.
- Reijmers, L. G., B. L. Perkins, N. Matsuo and M. Mayford (2007). "Localization of a Stable Neural Correlate of Associative Memory." *Science* **317**: 1230-1233.
- Robertson, L. M., T. K. Kerppola, M. Vendrell, D. Luk, R. J. Smeyne, C. Bocchiaro, J. I. Morgan and T. Curran (1995). "Regulation of *c-fos* expression in transgenic mice requires multiple interdependent transcription control elements." *Neuron* **14**(2): 241-252.
- Rocheftort, N. L. and A. Konnerth (2012). "Dendritic spines: from structure to in vivo function." *EMBO Rep* **13**(8): 699-708.
- Rodriguez-Ortiz, C. J. and F. Bermudez-Rattoni (2007). *Memory Reconsolidation or Updating Consolidation? Neural Plasticity and Memory: From Genes to Brain Imaging*. F. Bermudez-Rattoni. Boca Raton (FL).
- Roux, L. and G. Buzsaki (2015). "Tasks for inhibitory interneurons in intact brain circuits." *Neuropharmacology* **88**: 10-23.
- Roy, D. S., A. Arons, T. I. Mitchell, M. Pignatelli, T. J. Ryan and S. Tonegawa (2016). "Memory retrieval by activating engram cells in mouse models of early Alzheimer's disease." *Nature* **531**(7595): 508-512.
- Roy, S., B. Zhang, V. M. Lee and J. Q. Trojanowski (2005). "Axonal transport defects: a common theme in neurodegenerative diseases." *Acta Neuropathol* **109**(1): 5-13.
- Rudinskiy, N., J. M. Hawkes, R. a. Betensky, M. Eguchi, S. Yamaguchi, T. L. Spires-Jones and B. T. Hyman (2012). "Orchestrated experience-driven Arc responses are disrupted in a mouse model of Alzheimer's disease." *Nature neuroscience* **15**: 1422-1429.
- Ruediger, S., C. Vittori, E. Bednarek, C. Genoud, P. Strata, B. Sacchetti and P. Caroni (2011). "Learning-related feedforward inhibitory connectivity growth required for memory precision." *Nature* **473**(7348): 514-518.
- Ryan, T. J., D. S. Roy, M. Pignatelli, A. Arons and S. M. Toggas (2015). "Engram cells retain memory under retrograde amnesia." *Science* **348**(6238): 1007-1013.
- Sagar, S. M., F. R. Sharp and T. Curran (1988). "Expression of *c-fos* Protein in Brain : Metabolic Mapping at the Cellular Level." *Science* **240**: 5-8.
- Sanders, J., K. Cowansage, K. Baumgärtel and M. Mayford (2012). "Elimination of dendritic spines with long-term memory is specific to active circuits." *The Journal of neuroscience : the official journal of the Society for Neuroscience* **32**: 12570-12578.
- Schacter, D. L., T. Curran, E. M. Reiman, K. Chen, D. J. Bandy and J. T. Frost (1999). "Medial temporal lobe activation during episodic encoding and retrieval: a PET study." *Hippocampus* **9**(5): 575-581.
- Schaffer, K. (1892). "Beitrag zur Histologie der Ammon's horn formation." *Archiv für Mikroskopische Anatomie*(39): 611-632.
- Schmid, L. C., M. Mittag, S. Poll, J. Steffen, J. Wagner, H. R. Geis, I. Schwarz, B. Schmidt, M. K. Schwarz, S. Remy and M. Fuhrmann (2016). "Dysfunction of Somatostatin-Positive Interneurons Associated with Memory Deficits in an Alzheimer's Disease Model." *Neuron* **92**(1): 114-125.
- Schoenenberger, P., D. Gerosa and T. G. Oertner (2009). "Temporal control of immediate early gene induction by light." *PLoS One* **4**(12): e8185.
- Schomburg, Erik W., A. Fernández-Ruiz, K. Mizuseki, A. Berényi, Costas A. Anastassiou, C. Koch and G. Buzsáki (2014). "Theta Phase Segregation of Input-Specific Gamma Patterns in Entorhinal-Hippocampal Networks." *Neuron*.

- Schor, N. F. (2011). "What the halted phase III gamma-secretase inhibitor trial may (or may not) be telling us." *Ann Neurol* **69**(2): 237-239.
- Scoville, W. B. and B. Milner (1957). "Loss of recent memory after bilateral hippocampal lesions."
- Selkoe, D. J. (2002). "Alzheimer's disease is a synaptic failure." *Science* **298**(5594): 789-791.
- Semon, R. (1921). "The Mneme." (*G.Allen & Unwin*).
- Seubert, P., C. Vigo-Pelfrey, F. Esch, M. Lee, H. Dovey, D. Davis, S. Sinha, M. Schlossmacher, J. Whaley, C. Swindlehurst and et al. (1992). "Isolation and quantification of soluble Alzheimer's beta-peptide from biological fluids." *Nature* **359**(6393): 325-327.
- Shankar, G. M., S. Li, T. H. Mehta, A. Garcia-Munoz, N. E. Shepardson, I. Smith, F. M. Brett, M. A. Farrell, M. J. Rowan, C. A. Lemere, C. M. Regan, D. M. Walsh, B. L. Sabatini and D. J. Selkoe (2008). "Amyloid-beta protein dimers isolated directly from Alzheimer's brains impair synaptic plasticity and memory." *Nat Med* **14**(8): 837-842.
- Sheng, M. and M. E. Greenberg (1990). "The regulation and function of c-fos and other immediate early genes in the nervous system." *Neuron* **4**(4): 477-485.
- Sherrington, R., E. I. Rogaev, Y. Liang, E. A. Rogaeva, G. Levesque, M. Ikeda, H. Chi, C. Lin, G. Li, K. Holman, T. Tsuda, L. Mar, J. F. Foncin, A. C. Bruni, M. P. Montesi, S. Sorbi, I. Rainero, L. Pinessi, L. Nee, I. Chumakov, D. Pollen, A. Brookes, P. Sanseau, R. J. Polinsky, W. Wasco, H. A. Da Silva, J. L. Haines, M. A. Pericak-Vance, R. E. Tanzi, A. D. Roses, P. E. Fraser, J. M. Rommens and P. H. St George-Hyslop (1995). "Cloning of a gene bearing missense mutations in early-onset familial Alzheimer's disease." *Nature* **375**(6534): 754-760.
- Shull, S., N. H. Heintz, M. Periasamy, M. Manohar, Y. M. Janssen, J. P. Marsh and B. T. Mossman (1991). "Differential regulation of antioxidant enzymes in response to oxidants." *J Biol Chem* **266**(36): 24398-24403.
- Small, S. A. and K. Duff (2008). "Linking Abeta and tau in late-onset Alzheimer's disease: a dual pathway hypothesis." *Neuron* **60**(4): 534-542.
- Snyder, E. M., Y. Nong, C. G. Almeida, S. Paul, T. Moran, E. Y. Choi, A. C. Nairn, M. W. Salter, P. J. Lombroso, G. K. Gouras and P. Greengard (2005). "Regulation of NMDA receptor trafficking by amyloid-beta." *Nat Neurosci* **8**(8): 1051-1058.
- Spruston, N. (2008). "Pyramidal neurons: dendritic structure and synaptic integration." *Nat Rev Neurosci* **9**(3): 206-221.
- Squire, L. R., C. E. Stark and R. E. Clark (2004). "The medial temporal lobe." *Annu Rev Neurosci* **27**: 279-306.
- Sturchler-Pierrat, C., D. Abramowski, M. Duke, K. H. Wiederhold, C. Mistl, S. Rothacher, B. Ledermann, K. Burki, P. Frey, P. A. Paganetti, C. Waridel, M. E. Calhoun, M. Jucker, A. Probst, M. Staufenbiel and B. Sommer (1997). "Two amyloid precursor protein transgenic mouse models with Alzheimer disease-like pathology." *Proc Natl Acad Sci U S A* **94**(24): 13287-13292.
- Svoboda, K. and R. Yasuda (2006). "Principles of two-photon excitation microscopy and its applications to neuroscience." *Neuron* **50**(6): 823-839.
- Taylor, K. K., E. Lowry, K. Tanaka, B. Levy, L. G. Reijmers, M. Mayford and B. J. Wiltgen (2011). "Characterization of NMDAR-independent learning in the hippocampus." *Frontiers in behavioral neuroscience* **5**: 28.
- Taylor, K. K., K. Z. Tanaka, L. G. Reijmers and B. J. Wiltgen (2013). "Reactivation of neural ensembles during the retrieval of recent and remote memory." *Current Biology* **23**: 99-106.

- Thevenaz, P., U. E. Ruttimann and M. Unser (1998). "A pyramid approach to subpixel registration based on intensity." *IEEE Trans Image Process* **7**(1): 27-41.
- Treves, A. and E. T. Rolls (1994). "Computational analysis of the role of the hippocampus in memory." *Hippocampus* **4**(3): 374-391.
- Trojanowski, J. Q., A. B. Smith, D. Hurn and V. M. Lee (2005). "Microtubule-stabilising drugs for therapy of Alzheimer's disease and other neurodegenerative disorders with axonal transport impairments." *Expert Opin Pharmacother* **6**(5): 683-686.
- Tronson, N. C., K. a. Corcoran, V. Jovasevic and J. Radulovic (2012). "Fear conditioning and extinction: emotional states encoded by distinct signaling pathways." *Trends in neurosciences* **35**: 145-155.
- Um, J. W., A. C. Kaufman, M. Kostylev, J. K. Heiss, M. Stagi, H. Takahashi, M. E. Kerrisk, A. Vortmeyer, T. Wisniewski, A. J. Koleske, E. C. Gunther, H. B. Nygaard and S. M. Strittmatter (2013). "Metabotropic glutamate receptor 5 is a coreceptor for Alzheimer abeta oligomer bound to cellular prion protein." *Neuron* **79**(5): 887-902.
- Van Cauwenberghe, C., C. Van Broeckhoven and K. Sleegers (2016). "The genetic landscape of Alzheimer disease: clinical implications and perspectives." *Genet Med* **18**(5): 421-430.
- Van Dam, D. and P. P. De Deyn (2006). "Drug discovery in dementia: the role of rodent models." *Nat Rev Drug Discov* **5**(11): 956-970.
- Vassar, R., B. D. Bennett, S. Babu-Khan, S. Kahn, E. A. Mendiáz, P. Denis, D. B. Teplow, S. Ross, P. Amarante, R. Loeloff, Y. Luo, S. Fisher, J. Fuller, S. Edenson, J. Lile, M. A. Jarosinski, A. L. Biere, E. Curran, T. Burgess, J. C. Louis, F. Collins, J. Treanor, G. Rogers and M. Citron (1999). "Beta-secretase cleavage of Alzheimer's amyloid precursor protein by the transmembrane aspartic protease BACE." *Science* **286**(5440): 735-741.
- Verret, L., E. O. Mann, G. B. Hang, A. M. Barth, I. Cobos, K. Ho, N. Devidze, E. Masliah, A. C. Kreitzer, I. Mody, L. Mucke and J. J. Palop (2012). "Inhibitory interneuron deficit links altered network activity and cognitive dysfunction in Alzheimer model." *Cell* **149**(3): 708-721.
- Vinogradova, O. S. (2001). "Hippocampus as comparator: role of the two input and two output systems of the hippocampus in selection and registration of information." *Hippocampus* **11**(5): 578-598.
- Walsh, D. M., I. Klyubin, J. V. Fadeeva, W. K. Cullen, R. Anwyl, M. S. Wolfe, M. J. Rowan and D. J. Selkoe (2002). "Naturally secreted oligomers of amyloid beta protein potently inhibit hippocampal long-term potentiation in vivo." *Nature* **416**(6880): 535-539.
- Weidemann, A., G. König, D. Bunke, P. Fischer, J. M. Salbaum, C. L. Masters and K. Beyreuther (1989). "Identification, biogenesis, and localization of precursors of Alzheimer's disease A4 amyloid protein." *Cell* **57**(1): 115-126.
- Whitlock, J. R., A. J. Heynen, M. G. Shuler and M. F. Bear (2006). "Learning induces long-term potentiation in the hippocampus." *Science* **313**(5790): 1093-1097.
- Wisniewski, T. and U. Konietzko (2008). "Amyloid-beta immunisation for Alzheimer's disease." *Lancet Neurol* **7**(9): 805-811.
- Yamada, M., T. Chiba, J. Sasabe, M. Nawa, H. Tajima, T. Niikura, K. Terashita, S. Aiso, Y. Kita, M. Matsuoka and I. Nishimoto (2005). "Implanted cannula-mediated repetitive administration of Abeta25-35 into the mouse cerebral ventricle effectively impairs spatial working memory." *Behav Brain Res* **164**(2): 139-146.
- Yang, G., F. Pan and W. B. Gan (2009). "Stably maintained dendritic spines are associated with lifelong memories." *Nature* **462**(7275): 920-924.

- Yassin, L., B. L. Benedetti, J. S. Jouhanneau, J. A. Wen, J. F. Poulet and A. L. Barth (2010). "An embedded subnetwork of highly active neurons in the neocortex." *Neuron* **68**(6): 1043-1050.
- Yiu, Adelaide P., V. Mercaldo, C. Yan, B. Richards, Asim J. Rashid, H.-Lin L. Hsiang, J. Pressey, V. Mahadevan, Matthew M. Tran, Steven A. Kushner, Melanie A. Woodin, Paul W. Frankland and Sheena A. Josselyn (2014). "Neurons Are Recruited to a Memory Trace Based on Relative Neuronal Excitability Immediately before Training." *Neuron* **83**: 722-735.
- Zhang, Z., V. Ferretti, I. Guntan, A. Moro, E. A. Steinberg, Z. Ye, A. Y. Zecharia, X. Yu, A. L. Vysotski, S. G. Brickley, R. Yustos, Z. E. Pillidge, E. C. Harding, W. Wisden and N. P. Franks (2015). "Neuronal ensembles sufficient for recovery sleep and the sedative actions of alpha2 adrenergic agonists." *Nat Neurosci* **18**(4): 553-561.
- Zhu, P., M. I. Aller, U. Baron, S. Cambridge, M. Bausen, J. Herb, J. Sawinski, A. Cetin, P. Osten, M. L. Nelson, S. Kugler, P. H. Seeburg, R. Sprengel and M. T. Hasan (2007). "Silencing and un-silencing of tetracycline-controlled genes in neurons." *PLoS One* **2**(6): e533.
- Ziv, Y., L. D. Burns, E. D. Cocker, E. O. Hamel, K. K. Ghosh, L. J. Kitch, A. El Gamal and M. J. Schnitzer (2013). "Long-term dynamics of CA1 hippocampal place codes." *Nat Neurosci* **16**(3): 264-266.
- Zou, C., E. Montagna, Y. Shi, F. Peters, L. Blazquez-Llorca, S. Shi, S. Filser, M. M. Dorostkar and J. Herms (2015). "Intraneuronal APP and extracellular Abeta independently cause dendritic spine pathology in transgenic mouse models of Alzheimer's disease." *Acta Neuropathol* **129**(6): 909-920.

## DANKSAGUNG

Ich danke herzlichst meinem Betreuer Dr. Martin Fuhrmann für seine Unterstützung, sein Vertrauen in meine Arbeit, für zahlreiche anregende Diskussionen und für seine unglaubliche Art für Wissenschaft zu begeistern. Weiterhin danke ich Prof. Dr. Stefan Remy für seine Fähigkeit Arbeitsgruppen-übergreifend Motivation zu streuen und seine Bereitschaft meine Doktorarbeit als Erstgutachter zu bewerten. Meinem Zweitgutachter Prof. Dr. Michael Pankratz möchte ich sehr für seine Zeit zu Beginn meiner Promotion und auch für seine Flexibilität in Bezug auf die Ausrichtung meiner Doktorarbeit danken. Ebenfalls gilt mein Dank Prof. Dr. Susanne Schoch, sowohl für Ihre Bereitschaft sich meiner Doktorarbeit anzunehmen, als auch für die Bereitstellung der Viren, die mir ein grandioses Experiment ermöglicht haben. Weiterhin geht mein Dank an Prof. Dr. Ulrich Kubitscheck für seine Bereitschaft sich meiner Arbeit zu widmen.

Ich danke auch der gesamten Arbeitsgruppe Fuhrmann; für ein kreatives, angenehmes und freundschaftliches Arbeitsklima: Ich danke der lieben Julia Steffen für ihre stete Unterstützung in jeder Angelegenheit. Lena Schmid und Manuel Mittag möchte ich für die erfrischenden Reisen zwischendurch danken.

Ein großes Dankeschön geht an Martin Fuhrmann, Manuel Mittag, Eleonora Ambrad und Monika Müller, für die Muße und Sorgfalt die alle beim wissenschaftlichen Korrekturlesen meiner Doktorarbeit investiert haben. Weiterhin danke ich meiner Schwägerin, Farhana Poll für die Zeit, die sie in die sprachliche Korrektur meiner Arbeit investiert hat. Ich bin all den Menschen zu großem Dank verpflichtet, die mir den Weg bis hierhin geebnet haben, vor Allem meiner Familie und Cornelia Noeske.

Zu guter Letzt danke ich meiner geliebten Frau Vivian Poll, für ihre bedingungslose Unterstützung, ihre Geduld, das gemeinsame Frönen der „Science nights“ und die unzähligen anregenden Gespräche, die mir so einige Male dabei halfen nach vorne zu schauen und Optimismus zu leben.